NASA Technical Paper 1062

Prelaunch Testing of the Laser Geodynamic Satellite (LAGEOS)

M. W. Fitzmaurice, P. O. Minott,
J. B. Abshire, and H. E. Rowe

OCTOBER 1977

NASA

NASA Technical Paper 1062

Prelaunch Testing of the Laser Geodynamic Satellite (LAGEOS)

M. W. Fitzmaurice, P. O. Minott,
J. B. Abshire, and H. E. Rowe
Goddard Space Flight Center
Greenbelt, Maryland

National Aeronautics
and Space Administration

**Scientific and Technical
Information Office**

1977

This document makes use of international metric units according to the Systeme International d'Unites (SI). In certain cases, utility requires the retention of other systems of units in addition to the SI units. The conventional units stated in parentheses following the computed SI equivalents are the basis of the measurements and calculations reported.

CONTENTS

Page

INTRODUCTION 1

TARGET SIGNATURE TESTS 3

LIDAR CROSS-SECTION TESTS 26

SUMMARY OF TEST RESULTS 41

ACKNOWLEDGMENTS 55

REFERENCES 57

APPENDIX A—ANALYSIS OF LAGEOS USING RETRO PROGRAM A-1

APPENDIX B—A SECOND METHOD OF MEASURING THE RANGE CORRECTION B-1

PRELAUNCH TESTING OF THE LASER GEODYNAMIC SATELLITE (LAGEOS)

M. W. Fitzmaurice, P. O. Minott,
J. B. Abshire, and H. E. Rowe
Goddard Space Flight Center
Greenbelt, Maryland

INTRODUCTION

The Laser Geodynamic Satellite (Lageos) was launched from the Western Test Range on May 3, 1976, and achieved its planned orbit. Although there are several other satellites that are used as targets by ground-based laser ranging systems, this is the first satellite devoted *exclusively* to laser ranging. As such, the Lageos plays a key role in the National Aeronautics and Space Administration's (NASA's) Earth and Ocean Dynamics Application Program (EODAP), as well as the increasing international effort in laser measurement systems for geophysics investigations (Reference 1). Lageos is expected to have a lifetime that may well span several decades, and will be tracked by the several types of existing lasers as well as the next generation systems. To maximize the usefulness of the data to be gathered by existing systems and to guide the development of the next generation ranging systems, Lageos underwent extensive prelaunch testing at the Goddard Space Flight Center (GSFC) in December 1975 and January 1976. These tests represent the most thorough evaluation of satellite-borne laser reflectors yet carried out and are the subject of this document.

The Lageos

This satellite was designed as a passive long-lived target with a stable well-defined orbit. As such, it functions as a reference point in inertial space and by ranging to it, sets of ground-based laser systems may recover their internal geometry, or their position with respect to the Earth's center of mass, or their position with respect to an inertial reference. The geophysical investigations to be carried out in conjunction with Lageos require that the ranging measurements be made with an accuracy of about 2 cm. Several error sources contribute to the total error in such systems (Reference 2), and at the 2-cm level, each must be carefully scrutinized. In this case, the error contributed by the satellite itself cannot be allowed to exceed 5 millimeters (mm) if the overall 2-cm system accuracy is to be achieved. Lageos is shown during testing at GSFC in figure 1.

In order to enhance its reflectivity as a laser target, the satellite is covered with optical cube corners which retrodirect any incident optical signal. There are a total of 426 cube corner reflectors (CCR's); 422 of these are made of fused silica. These operate throughout the visible and near infrared portions of the spectrum. The remaining 4 are of germanium which is

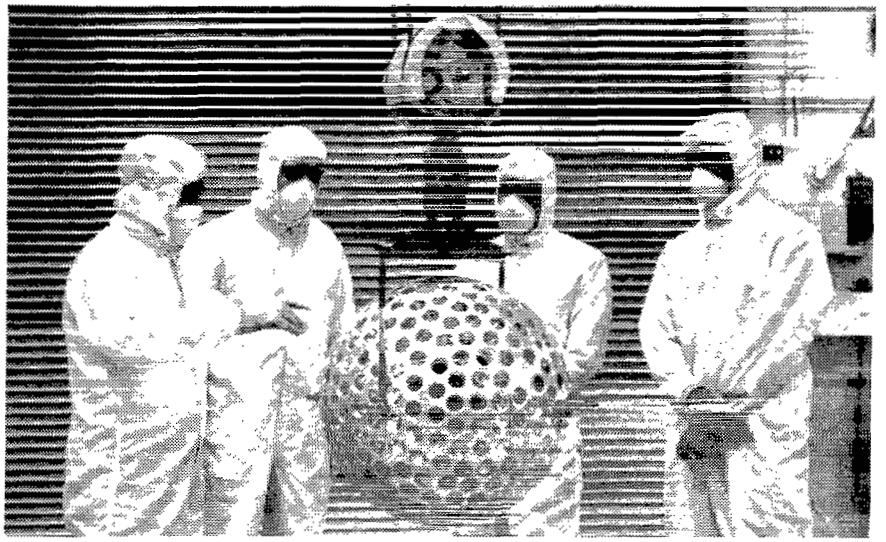

Figure 1. Lageos shown during test at GSFC.

effective in the middle infrared (10-micrometer) region. These germanium CCR's were not installed on the satellite at the time of the GSFC test, and no tests were conducted on these units at GSFC. The fused silica CCR's on Lageos are unique in that the back faces are uncoated so as to ensure very long life; all other CCR's flown on NASA satellites have had reflective coatings on the back faces.

The primary orbit and satellite characteristics are listed as follows:

Altitude	5900 km
Inclination	110 degrees
Eccentricity	0
Diameter of Satellite	60 cm
Weight	411 kg
Number of Retroreflectors	422 fused silica
	4 germanium

Purpose and Scope of GSFC Tests

The Lageos tests can be subdivided into two major parts: target-signature tests and lidar cross-section tests. A discussion of each follows.

Target Signature

Target-signature tests concentrate on the spreading, distortion, and delay induced on a very short laser pulse by the satellite reflectors. The design of optimal transmitters and receivers for laser-ranging systems is heavily impacted by these considerations, and therefore these data become essential for both the existing laser tracking network as well as the evolving next generation systems. In addition to the spreading and distortion effects, pulses reflected by the satellite emerge from points near the surface of the satellite (since the CCR's are located

near the outer surface). However, in most geophysical applications, it is desirable to "correct" the range measurement so that it can be related to the center of gravity of the target, since it is this point whose motion through the Earth's geopotential field can be precisely calculated. In general, this "correction" is a function of the attitude of the satellite with respect to the incident pulse. Because Lageos is a completely unstabilized target and because no information will be available on its attitude, it is important to: (1) measure the value of the range correction and (2) measure the amount of variation in this correction as a function of attitude. Attitude-dependent variations represent a noise source in the ranging system which may not be reducible through data averaging.

Lidar Cross Section

The lidar cross section (σ) is the single parameter which quantifies the ability of a target to reflect incident energy in a specified direction (Reference 3). Because Lageos is in an orbit which is substantially higher than most of the other CCR-equipped satellites (5900 km versus a typical 1000-km orbit), the radar link is much more difficult, making the absolute value of the lidar cross section extremely important. As discussed in Reference 3, σ is a function of the characteristics of the incident signal (wavelength, polarization, and angle of incidence) and the direction of interest in the far field of the reflected signal. All these factors were modeled during the design phase of the Lageos CCR's (Reference 4), but it was widely recognized that variations in the properties of individual cube corners due to material inhomogeneity and manufacturing tolerances could be substantial (Reference 5), and that the overall performance of an array consisting of several hundred of these reflectors could be significantly different than the computer model. With this motivation, extensive tests of the cross-section value and the far-field pattern of reflected signals from Lageos were carried out during this program.

TARGET SIGNATURE TESTS

The target signature tests were divided into three parts. The first part addresses the average spreading that is imposed on reflected laser pulses by the satellite reflectors. The second part consisted of measurements of the range corrections so that range measurements can be referenced to the satellite center of mass; the third part addresses the pulse-to-pulse waveform variations which result from coherent interference between the individual satellite reflectors. The tests are described in this order in the sections that follow.

Pulse Spreading

Physical Mechanism

The mechanism of pulse spreading can be understood by reference to figure 2. When a transmitted laser pulse illuminates the satellite, all the cube corners within approximately ±25° of the pulse propagation direction reflect significant energy back to the transmitter (Reference 5). Because these CCR's are on the surface of a sphere, they are at different distances from the transmitter, and the pulses reflected back to the transmitter will be displaced in time (as

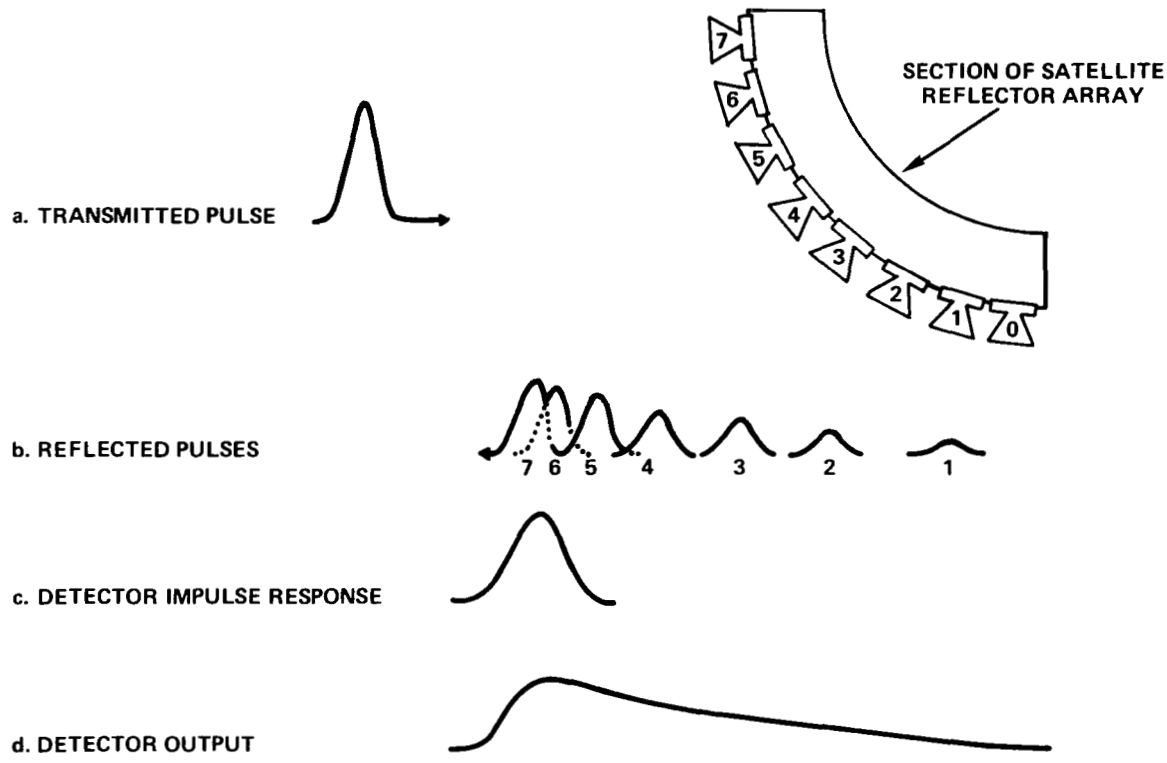

Figure 2. Array-induced pulse spreading.

shown in figure 2b). Generally, the receiver is collocated with the transmitter, and its output signal (figure 2d) is given by the convolution of its impulse response (figure 2c) with the received pulse train;* this pulse can be significantly broadened as compared with the return from a single CCR or a flat array of CCR's aligned normal to the transmitted pulse (which would produce a detector output given by the convolution of figures 2a and 2c).

It should be noted that in those cases where the reflected pulses overlap in time (for example, pulses 5, 6, and 7 of figure 2), the resultant waveform is dependent on the relative phases of the optical fields of the respective pulses;† the impact of these coherent interactions on pulse spreading is discussed in the section, "Pulse Shape Variations due to Coherency Effects." However, for average pulse-spreading considerations, these coherent effects can be neglected, and net reflected signal can be obtained by addition of pulse energies.

*In the more general case of separated transmitter and receiver stations, the effect is no different.

†In a rigorous sense, this is true only for the case of very high optical signal-to-noise (SNR) ratios. At low signal levels, the randomness induced by poissonian photoemission causes another degree of randomization of the output waveform (Reference 6). The data to be reported here result from averaged waveforms built up using large numbers of optical pulses (typical 10^4). This averaging is equivalent to operating at very high SNR.

Instrumentation and Measurement Technique

The electro-optical system used for the target signature tests is shown in figure 3. A continuous wave (CW) lamp pumped Nd:YAG* laser was mode-locked at 200 MHz using an acousto-optic loss modulator. The laser was operated in the lowest order spatial mode (TEM_{00}), with approximately 0.3 watt of average 1.06-μm power, and produced a 200-MHz train of short pulses where each pulse typically had the shape shown in figure 4a. The 1.06-μm pulse train was focused into a 5-mm cube of barium sodium niobate for second-harmonic generation; about 10 mW of 0.53-μm radiation was generated. This 0.53-μm pulse train became the transmitter signal for all target signature tests. No direct measurement of the 0.53-μm pulse shape was possible because of the extremely short rise times involved, but an accurate calculation of the pulse can be made based on the 1.06-μm pulse shape and the well-known quadratic dependence of second harmonic-power generation on fundamental power. The results of this calculation are shown in figure 4b; this indicates that a 0.53-μm pulse width of about 60 ps full width at half-maximum (FWHM) was transmitted to Lageos during those tests. The 1.06-μm pulse train was separated from the second harmonic by a polarization beam splitter† (figure 3).

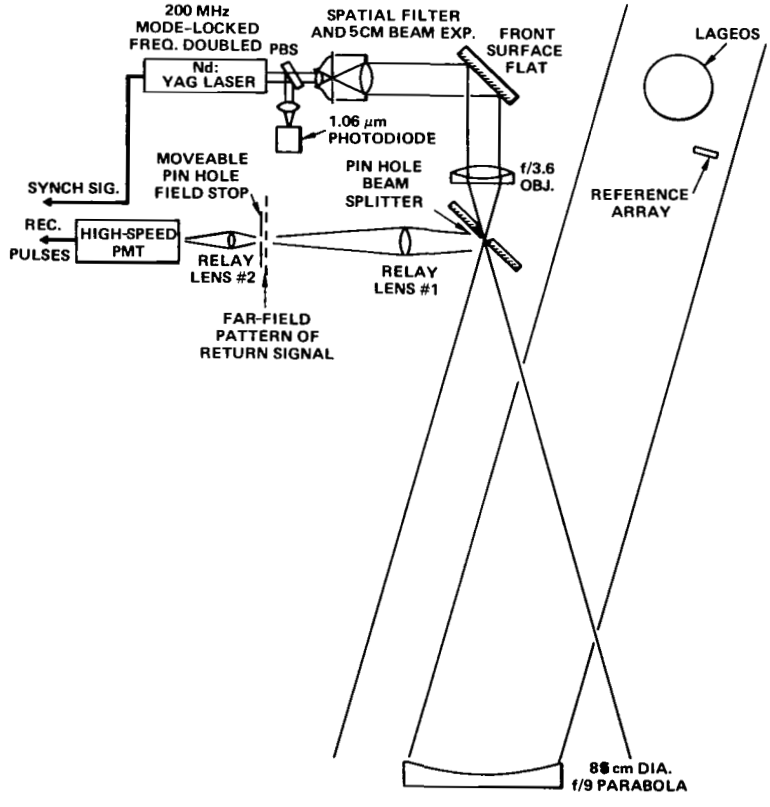

Figure 3. Optical system for Lageos pulse-spreading tests.

*Neodymium yttrium aluminum garnet.

†When BaNaNio is used as a type 1 frequency doubler, the fundamental and second harmonic beams are orthogonally polarized.

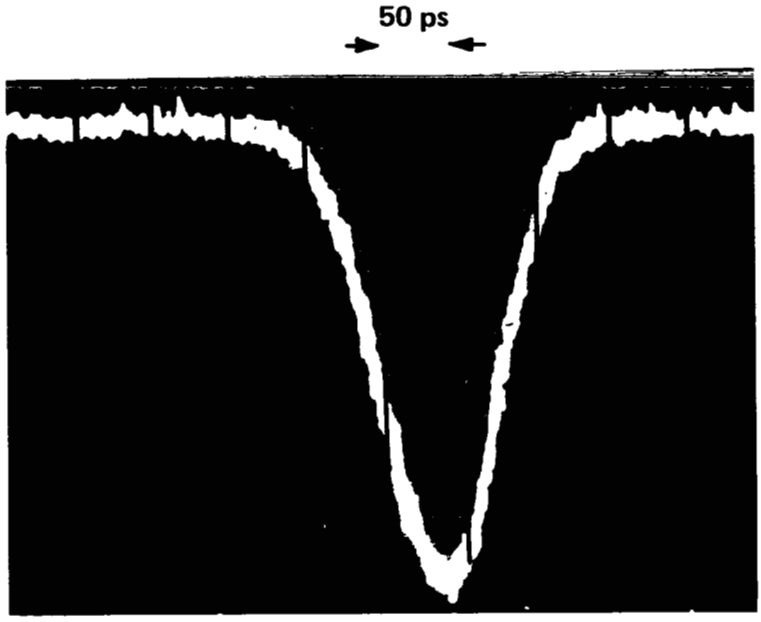

λ = 1.06 MICROMETERS
FULL WIDTH AT HALF MAXIMUM: 90 ps
PULSE MEASURED BY GaAsSb PHOTODIODE

Figure 4a. Nd:YAG laser mode-locked pulse.

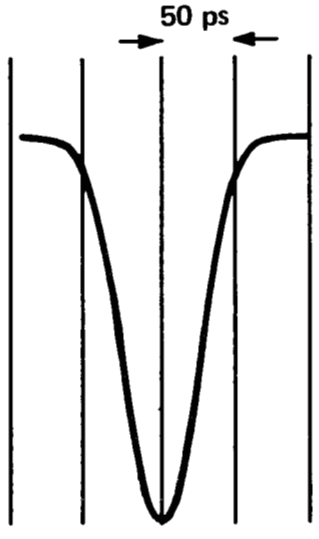

λ = 0.53 MICROMETERS
FULL WIDTH AT HALF MAXIMUM: 60 ps

Figure 4b. Frequency doubled mode-locked pulse (calculated).

These pulses were detected by a fast photodiode so as to monitor laser amplitude and wave-shape stability. The 0.53-μm beam was directed into a beam expander/spatial filter telescope (Tropel Catalog No. 280-50) to minimize spatial amplitude variations in the beam cross section. After reflection by a front-surface flat mirror, the beam was brought to focus by the f/3.6 objective at the front surface of the pin hole beam splitter. This splitter was a flat mirror which had a drilled conical hole of an apex diameter 180 μm. The position where the f/3.6 objective focused the outgoing beam was located precisely at the focal plane of the large (80-cm diameter) parabola, so the outgoing beam, afer passing through focus, expanded* and was collimated by the parabola. This collimated beam illuminated the Lageos as well as a flat reference array of CCR's which were used throughout these tests for calibration purposes. A photograph of the satellite in its handling fixture and the reference array is shown in figure 5.

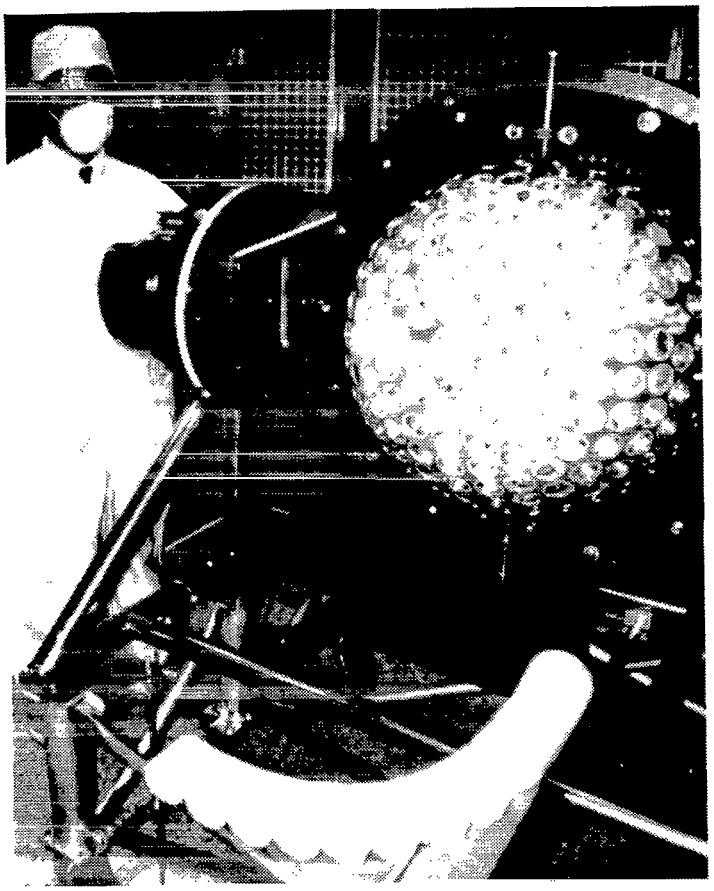

Figure 5. The satellite in its handling fixture and reference array.

*As is apparent from figure 3, the expanding beam substantially overfilled the parabola so that only the central portion of the beam (which had very little amplitude taper) was used to illuminate the satellite.

The return signal from the satellite and reference array traverses the exact same path as the transmitted signal (due to the retrodirective property of cube corners) and is brought to a focus at the front surface of the pin-hole beam splitter. This pin-hole beam splitter serves to separate the transmitted and received signals, while maintaining excellent imaging quality throughout the receiver system.* The transmitter beam, when focused by the f/3.6 objective, has an essentially diffraction-limited spot size of about 3 μm, and can therefore easily pass through the 180-μm hole in the splitter. The return beam from the satellite (and/or reference array) has an angular spread of about $\pm$ 45 microradians (μr), that results in a spot size of about 800 μm when focused by the large collimating parabola onto the front surface of the splitter. The central 180 μm of this image is lost, but the remainder is reflected by the splitter to a relay lens that magnifies the image and establishes the desired image plane scaling. A photograph of the f/3.6 objective, beam splitter, and relay lens is shown in figure 6. The portion of the image that is lost is of no consequence because it subtends only about the central 20 μr of the reflected beam. The velocity aberration effect (Reference 3) causes ground-based receivers to be located 35 to 38 μr off the axis of the return beam, and all target signature measurements were made in this part of the far-field

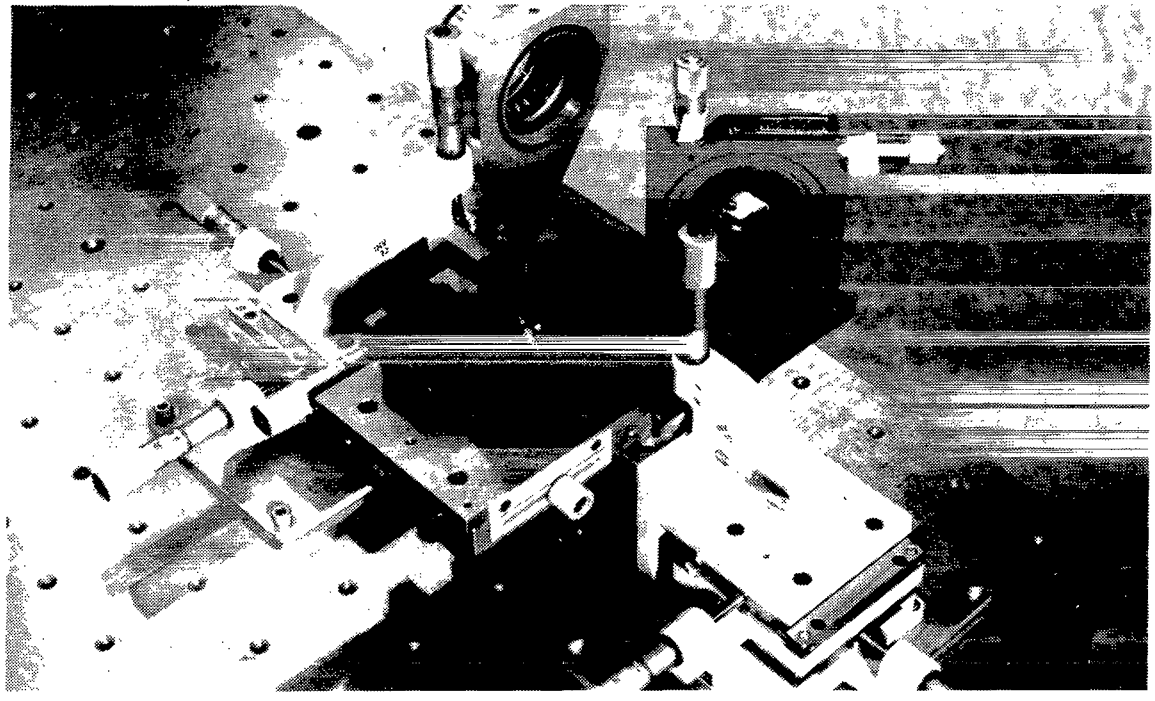

Figure 6. The f/3.6 beam splitter and relay lens.

*Alternate techniques for transmitter-receiver isolation such as partially silvered beam splitters were not acceptable because of the depolarizing effects and multiple images generated.

pattern. Two types of field stops were used during these tests: (1) a small circular aperture of 0.18-mm diameter and (2) an annulus of 3-mm inner radius and 4-mm outer radius. With a receiver system focal length of 100 m, this corresponds to an angular subtense of 1.8 μr for the circular aperture and a transmission ring of 30 to 40 μr for the annulus. The energy passing through the field stop was collected by a relay lens and focused through an interference filter onto the photocathode of a high-speed photomultiplier (Varian Catalog No. 154). A photograph of the detector assembly is shown in figure 7. The manufacturer's performance specifications for this detector are given in the following list:

Designator	Description
Photocathode/Window Material	S-20/Sapphire
Cathode Diameter	5.08 mm (0.2 in)
Cathode Quantum Efficiency	10 Percent Typical at 5300 Angstrom (Å)
Gain	10^5 Typical
Number of Stages	6
Dynode Material	Becu Alloy
Anode Dark Current	3×10^{-9} Typical at 20°C
Output Current	250-Microamps (μA) Maximum Continuous
Bandwidth, 0 to -3 Decibel (db)	Direct Current (dc) to 2.5 Gigahertz (GHz)
Anode Rise Time (10% to 90%)	150 Picoseconds (ps)
Output Coupler	50-Ohm Coaxial OSM
Dimensions, Housed with Magnets	8.25 cm (3.25 in) × 6.68 cm (2.63 in) 15.87 cm (6.25 in)
Weight	1.81 kg (4 lb)

The photomultiplier output signal as well as a synchronized trigger signal from the laser were sent to the data system shown in figure 8. The sampled analog waveforms that were developed by the sampling system were digitized by a Tektronix R7912 and stored in the computer. The R7912 supplied waveforms to the computer at a rate of approximately 10 per second. Typically, for a given set of test parameters, 100 waveforms were input to the computer, averaged by the computer, and the resultant waveform delivered to one of the output devices. Following the data taking, the averaged waveforms were recalled from storage and hardcopy generated. The waveforms were analyzed graphically to recover pulse shape characteristics and interpulse spacing. A photographic overview of the entire test area (with only the large collimator outside the frame) is shown in figure 9.

Results

The received waveforms that were analyzed during the target signature tests are shown schematically in figure 10. To make full use of the precision available from the time axis of the R7912, the pulse pair shown in the figure was recorded for each of target signature tests. This reference-array pulse and the Lageos pulse differ only because of the planar and nonplanar characteristics of their respective cube corner arrays, and this fact was used to measure the pulse spreading induced on the laser pulse by the Lageos.

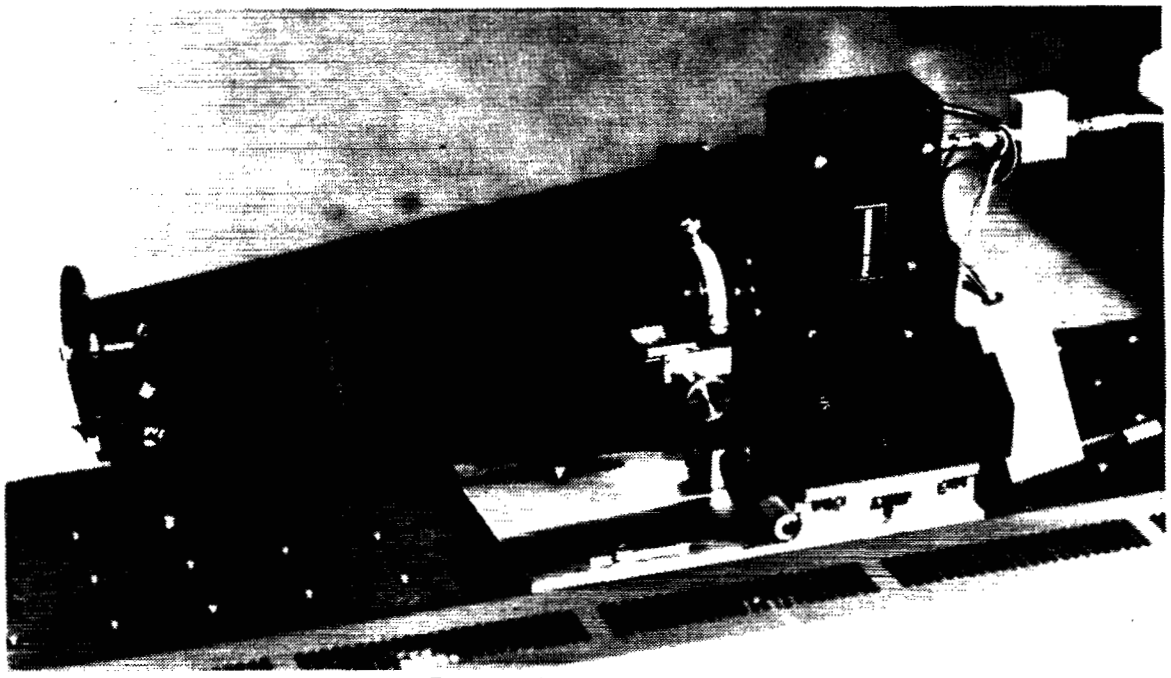

Figure 7. Detector assembly.

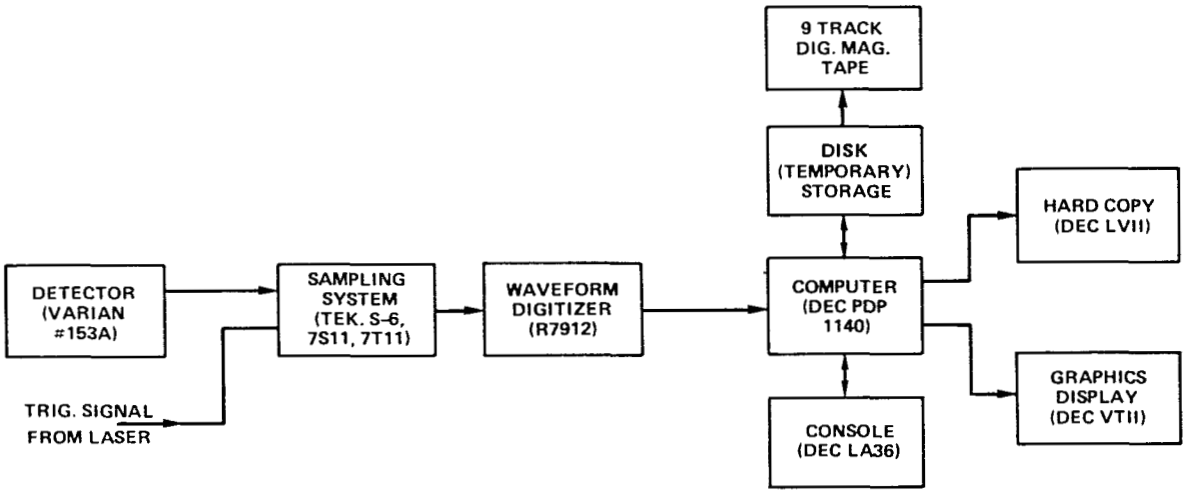

Figure 8. Data processing system.

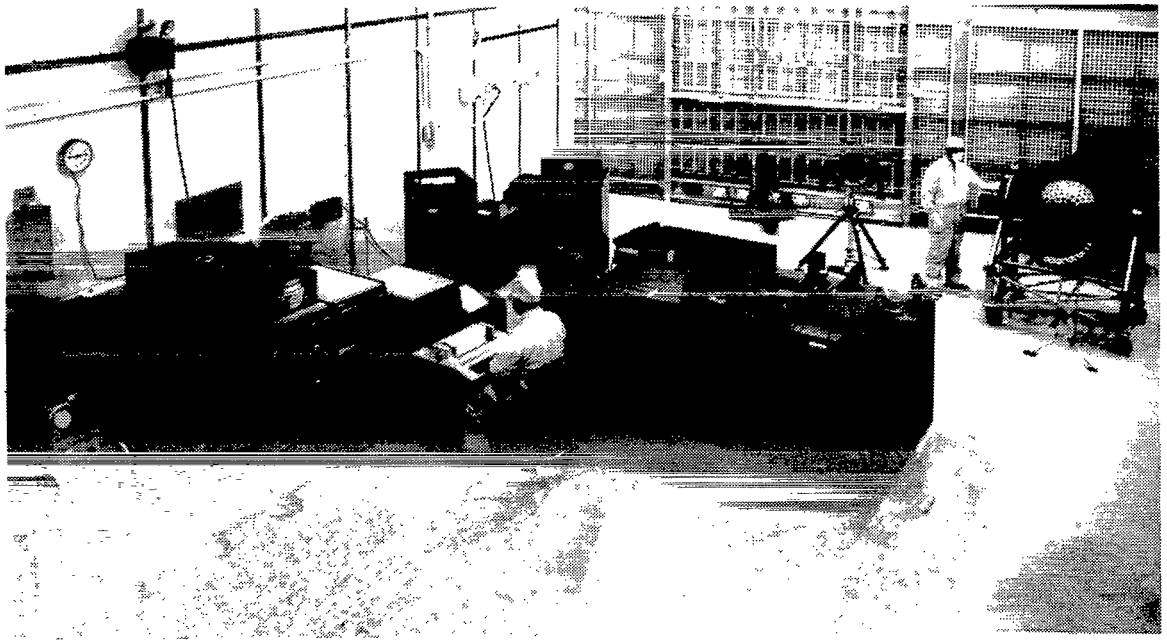

Figure 9. The test area.

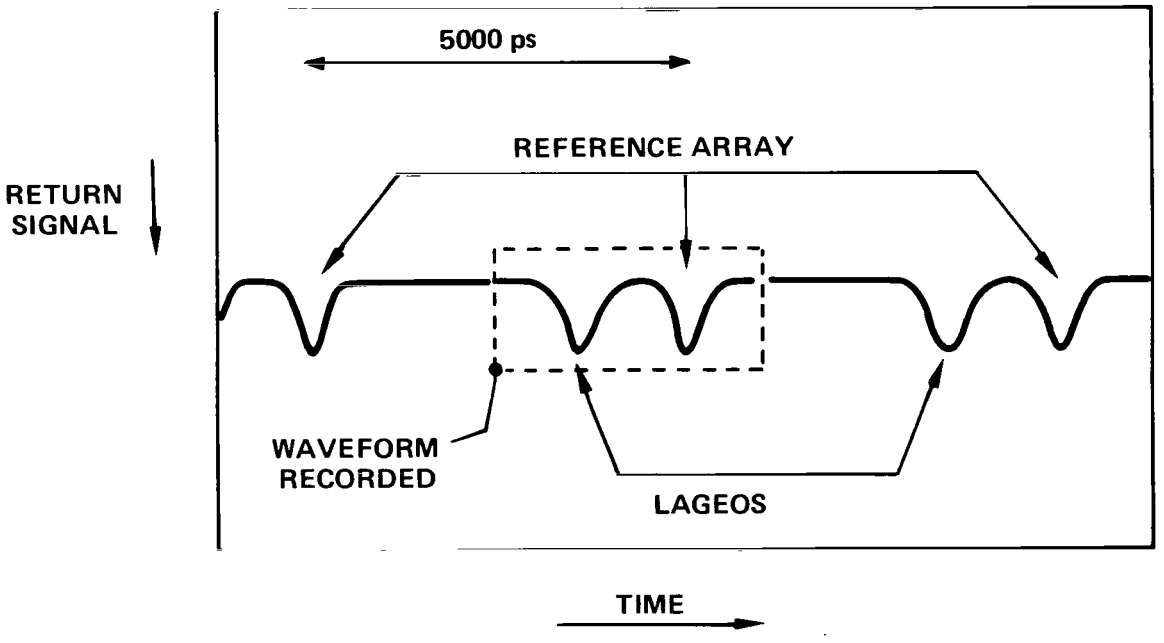

Figure 10. Received waveform schematic.

The results of the pulse-spreading tests are shown in figure 11. The measured values vary from 210 ps to 260 ps depending on the orientation of Lageos with respect to the incident pulse. The satellite was rotated with respect to the incident pulse by the handling fixture shown in figure 5; however, the reference array was not changed and remained normal to the incident pulse throughout the tests.

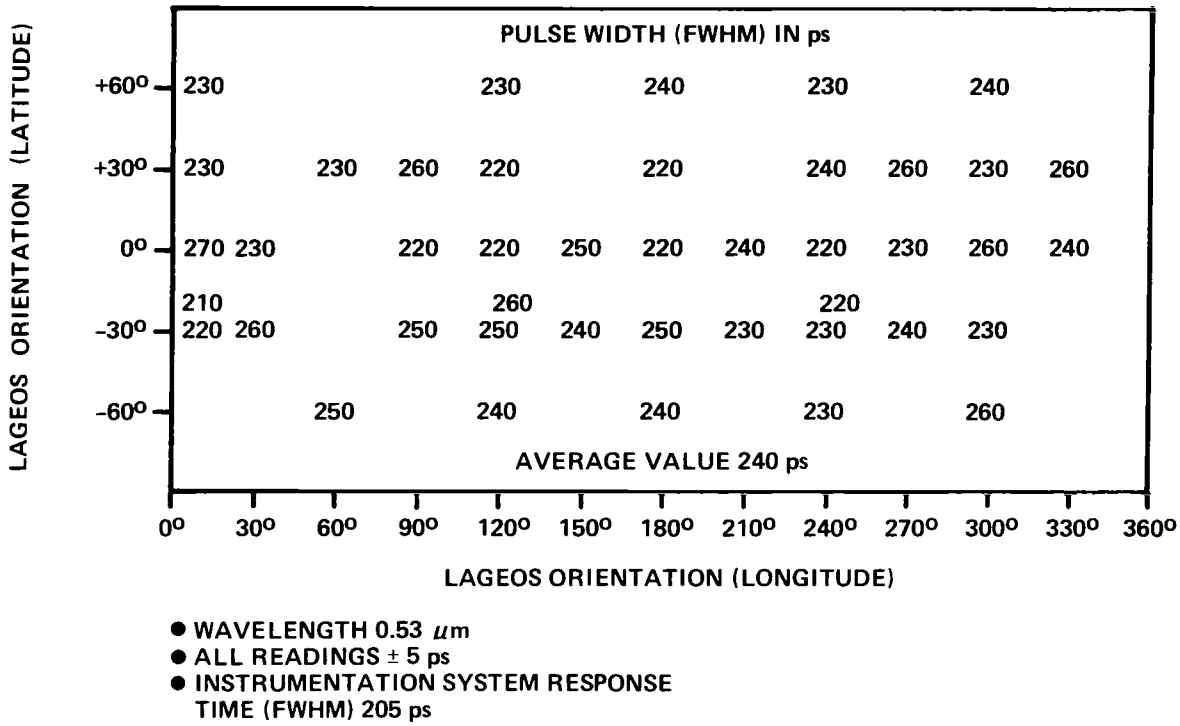

Figure 11. Pulse width of reflected signals from Lageos.

Because CCR's as much as 25° off-normal contribute to the return signal, a data point such as +60° latitude and 0° longitude, in fact, samples the satellite over the ranges of +35° to +85° latitude and 335° to 25° longitude. As shown in figure 11, the average pulse width of the received signal was 240 ps. A sample of the measured waveforms is shown in figure 12.

The temporal resolution of the instrumentation system (as measured by the returned from the flat reference array) was 205 ps, so the instrumentation system (especially the photomultiplier) contributed significantly to the measured pulse width. The relative contributions of satellite and instrumentation system to the total pulse width can be evaluated to first order by assuming Gaussian waveshapes for both the reference array and Lageos signals. In this case, the pulse widths add in quadrature and the Lageos contribution can be easily evaluated. These results are listed in figure 13 and can be used to estimate the width of the reflected pulse from Lageos for arbitrary transmitter/receiver systems by carrying through the root-sum-squares (RSS) calculation.

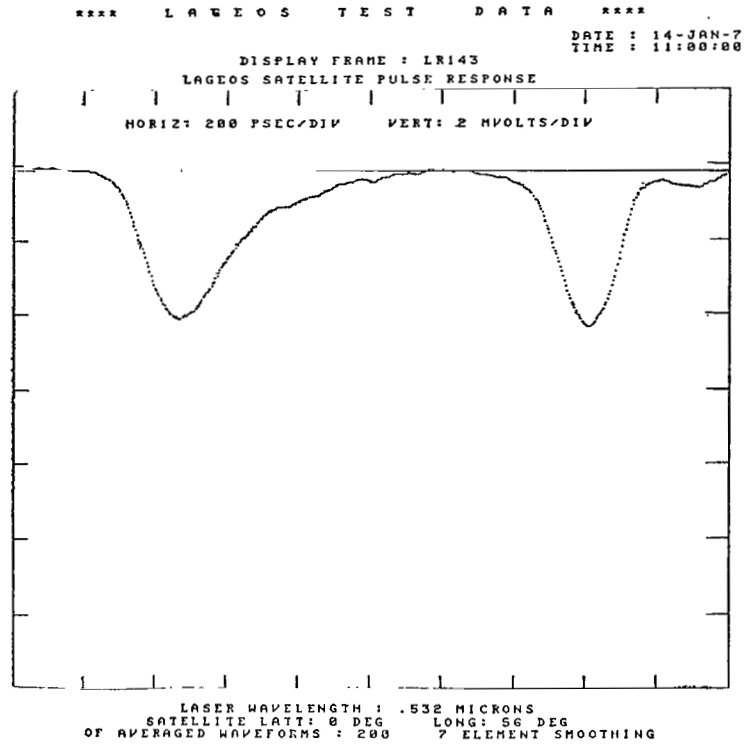

Figure 12. A sample of the measured waveforms.

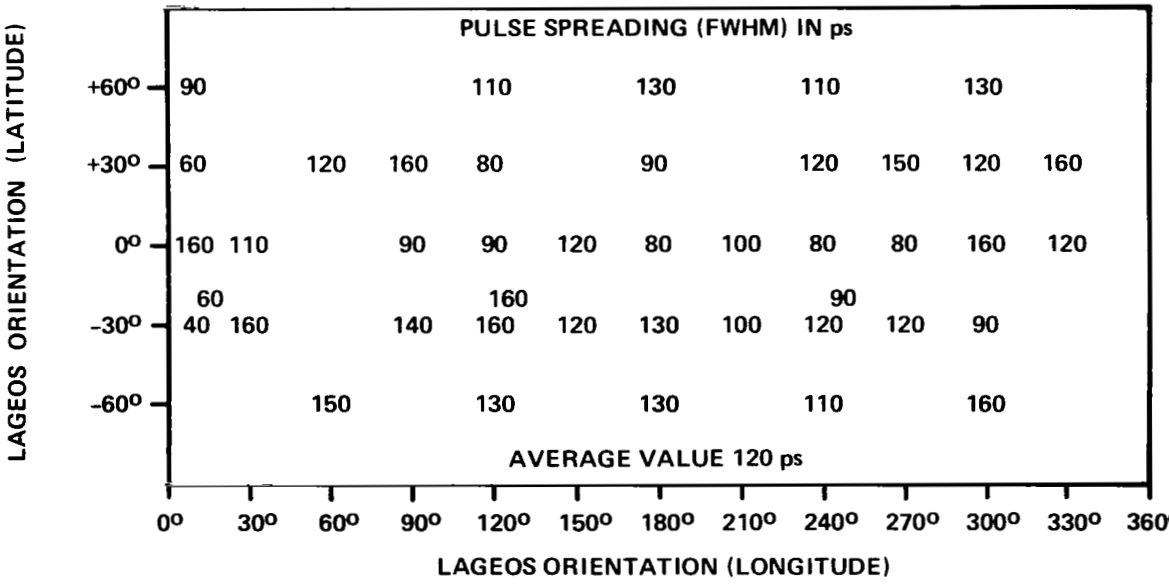

- WAVELENGTH 0.53 μm
- ALL READINGS ± 5 ps

Figure 13. Pulse spreading induced by Lageos.

A motion picture camera was installed in the received optical system (figure 3) and relay lens No. 1 was repositioned, so that an image of the rotating satellite (rather than the far-field pattern of the return beam) was recorded on film. Four of these frames are shown in figure 14. The brightness of the individual CCR is proportional to the total energy reflected by each. The arc of CCR's in the lower right-hand corner is the reference array; each of the cubes in this array was normal to the incident beam, and therefore no brightness variation exists. Figure 14a shows a localized cluster of CCR's dominating the return signal, and therefore very little pulse spreading would be expected at this satellite attitude. Figure 14b shows Lageos with its north pole aligned with the incident beam. The black spot in the center is the location of one of the germanium CCR's. These CCR's were not installed at the time of the tests, but even if they were in place, the results would not be different because germanium is opaque at visible wavelengths. Figure 14c shows the north pole again, but in an off-axis condition. Figure 14d is another orientation where significant pulse spreading can be expected. The amount of pulse spreading contributed by off-axis CCR's can be estimated using the geometry of figure 15.* Inspection of these values and the frames of figure 14 show the reason for the pulse spreading variations listed in figure 11.

Analysis of the waveforms from the reference and satellite arrays shows that the Lageos-induced broadening is primarily an increase in pulse fall time, with pulse rise time changes too small to be measured. The data reported in this section were taken with a "point" aperture (0.9-μr radius) positioned 35-μr off-axis in the far-field pattern of the reflected beam. During an actual satellite pass, the ground-based receiver will change position in the far field, although always remaining 35- to 38-μr off-axis. Accordingly, during these tests, data were taken with the "point" receiver at different locations in the 35- to 38-μr annular region. No significant difference from the data of figure 11 was noted. Data were also taken with the "point" aperture replaced by a 30- to 40-μr annular aperture. These data are effectively an average of the pulse shapes over the entire far-field region of interest. Again, no significant difference from the data of figure 11 was noted. In conclusion, the data of figure 11 are an accurate measure of the pulse-spreading characteristics of the Lageos, and this characteristic is not a sensitive function of receiver position in the far field.

Center-of-Gravity Correction

The range measurements from a ground station to Lageos during a typical satellite pass are, in fact, distance measurements from a well-defined point on the ground to a point approximately 5 cm inside the surface of the Lageos. The geophysical applications for which Lageos was launched require that the range measurements be "corrected" so that they can be interpreted as distance measurements to the center of mass of the satellite. To do this, it is necessary, to first define precisely the location of the equivalent reflection point within the satellite, and, secondly, to measure the variability of this point with satellite attitude, because this represents a potentially irreducible error source in the overall ranging system.

*An accurate calculation must take into account not only the energy reflected by each CCR but also the antenna pattern associated with each CCR return.

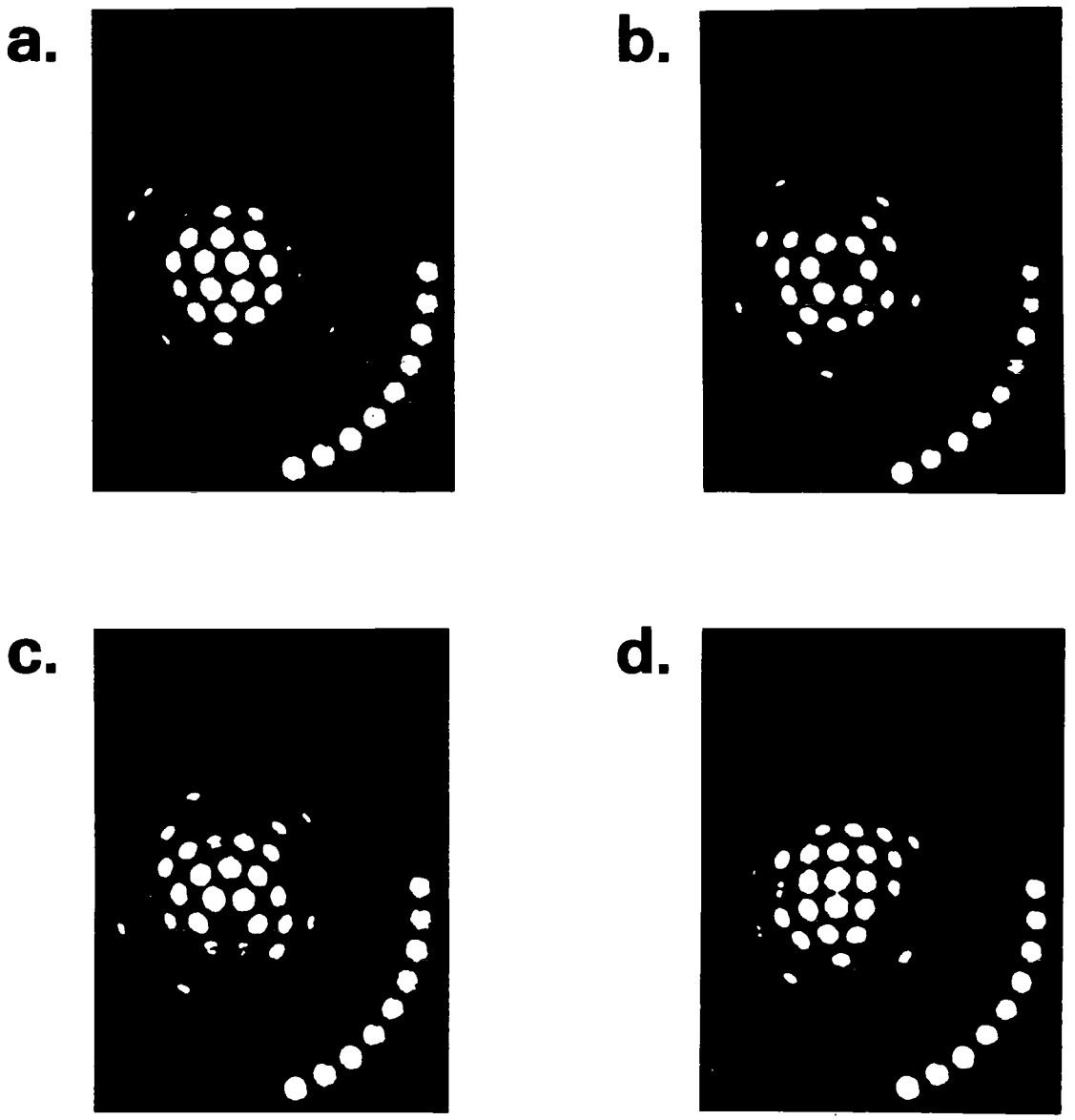

Figure 14. Lageos images for various orientations.

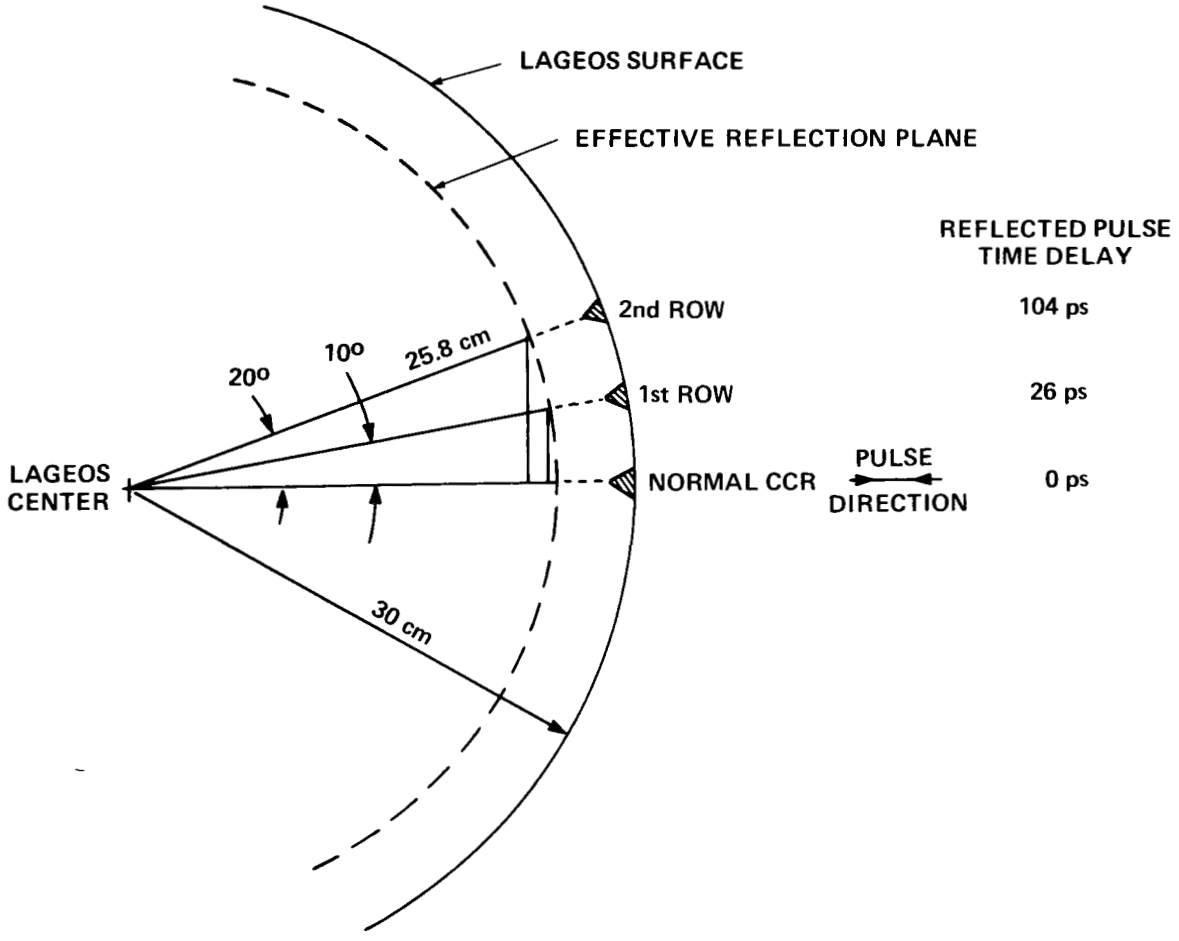

Figure 15. Effect of off-axis CCR's on pulse spreading.

Physical Mechanism

The equivalent reflection point for a solid cube corner is given by

$$\Delta R = L\sqrt{n^2 - \sin^2 \theta} \qquad (1)$$

where

- ΔR is measured from the center of the front face of the cube corner to the reflection point
- L is the vertex to front-face dimension
- n is the refractive index of the material
- θ is the angle of incidence

Using this equation and the geometry of figure 15, it follows that the reflection planes for the first and second rows are 3.6 mm and 14.5 mm further into the satellite than that of the normal CCR. The total signal detected at the receiver station is the sum of the contributions from the individual CCR's; therefore, with proper weighting, the received waveform could be calculated and the equivalent reflection plane, precisely defined. There are two difficulties which prevent this analytic treatment from being entirely adequate.

First, the proper weighting to apply to each of the CCR reflections is not known better than approximately ±3 dB due to material and manufacturing variations inherent in high-gain CCR's. Secondly, the geometry of figure 15 is merely one particular orientation of the satellite with respect to the incident pulse, and a shift of just 5° of the (unstabilized) satellite would significantly change the relative positions of the individual CCR reflection planes. It is clear from the photographs of figure 14 that significant variations and asymmetries in the cluster of active Lageos CCR's exist for different satellite attitudes.

The optical system that was used for the range-correction measurements and is shown in figure 16, was nearly the same as that used for the pulse-spreading tests (figure 3). The two differences are: (1) the insertion of a polarization rotator in the 0.53-μm beam just before the entry into the spatial filter-beam expander telescope assembly and (2) the insertion of a mask with a clear aperture equal to 1 cube corner diameter in front of the satellite. The data processing system was the same as described in the section, "Instrumentation and Measurement Technique" under "Pulse Spreading" and illustrated in figure 8.

Instrumentation and Measurement Technique

The measurement technique can be explained with the aid of figure 17. At the top of this figure, the Lageos is shown behind a mask which allows only the cube corner normal to the incident beam to be illuminated. This results in a signal $S_0(t)$ at the output of the receiver, where R refers to the pulses from the flat reference array in front of the mask, and the Lageos single cube corner signal is as shown. The mechanical design of the Lageos places the front face of each of the CCR's at a distance of 298.1 mm from the center of the satellite. Therefore, by using equation (2), the point within the satellite from which the single CCR pulse is reflected can be defined precisely in terms of its relation to the satellite center of mass; similarly, by measuring the Δ_0 value of $S_0(t)$, the position of the reference array, with respect to the satellite center, can be defined precisely. Having recorded the $S_0(t)$ signal, the mask was then removed, and the entire satellite was illuminated by the pulse train. This results in the signal $S_1(t)$ at the receiver output. The range correction, ΔR, for satellite orientation 1 can then be computed from

$$\Delta R_1 = 298.1 - (L)(n) - \frac{ct_1}{2} \quad (mm) \qquad (2)$$

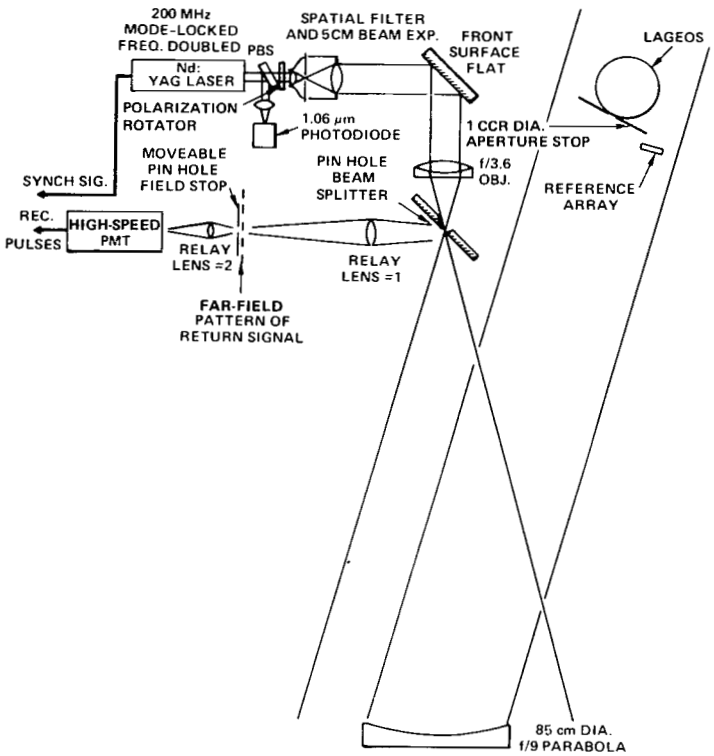

Figure 16. Optical system for Lageos range correction measurements.

where

L = 27.8 mm

n = 1.455

$$t_1 = \Delta_1 - \Delta_0 \text{ (s)} \tag{3}$$

This measurement sequence was repeated for a sufficient number of Lageos orientations so that the entire satellite was mapped. The numerical values for the range correction are slightly different depending on whether leading edge (half maximum) or peak detection is used in the receiver. Both sets of values were computed and are reported under "Results."

Calibration

The instrumentation system used in these tests was evaluated in terms of its precision (or resolution) and absolute accuracy of time-interval measurement. The precision test consisted of illuminating the reference array and Lageos as in figure 17 (with mask removed), recording the received waveshape, measuring the time interval between the reference array and Lageos pulses, and repeating this measurement a number of times without any changes to the system.

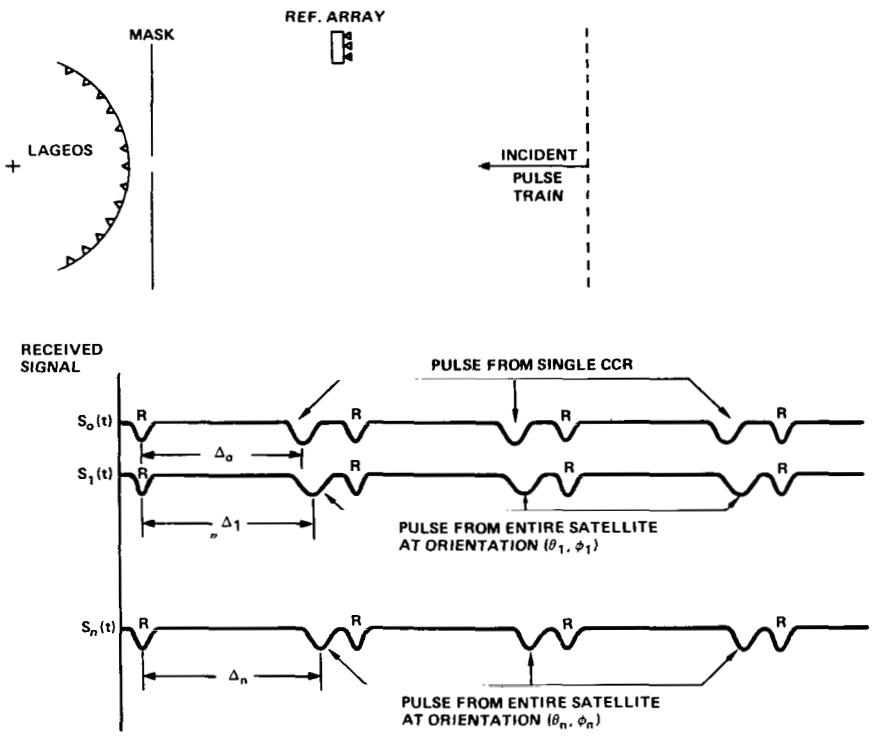

Figure 17. Measurement technique for Lageos.

The statistics of the time-interval measurement were computed, and the standard deviation of the measurement was defined as the system precision. One typical set of measurements is listed in table 1.

Precision checks were run several times during the course of the Lageos testing, and the results listed in table 1 are typical. To measure accuracy, the Lageos was removed from the collimated beam, and an additional flat array of CCR's was installed in front of (and to the side of) the reference array. The distance between the two arrays was measured with a caliper, and then the two arrays were illuminated by the laser pulses. The received pulses were recorded, and the time differential between the reflections from the two arrays was measured. This measurement of array spacing was then compared with the caliper measurement to evaluate absolute accuracy. The results of this test are listed as follows:

File No.	Spacing (ps)
LR 5811	1248
LR 5812	1250
LR 5813	1264
LR 5814	1248

File No.	Spacing (ps)
LR 5815	1262
LR 5816	1247
LR 5819	1243
LR 5820	1252

Predicted Pulse Spacing (Based on Caliper Measurement) = 1255 ps
Average Difference (Measured–Predicted) = 3 ps (0.5 mm)

Table 1
Instrumentation System Precision

File No.	Time Interval (ps) (Half Max. to Half Max.)	Time Interval (ps) (Peak to Peak)
LR 1429	1140	1131
LR 1430	1143	1120
LR 1431	1143	1117
LR 1432	1152	1137
LR 1434	1143	1114
LR 1435	1143	1120
LR 1436	1137	1137
LR 1438	1143	1134
LR 1439	1134	1131

Standard Deviation (Half Maximum) = 3.8 ps (0.6 mm)
Standard Deviation (Peak) = 8.9 ps (1.3 mm)

Based on these precision and accuracy tests, it is estimated that the pulse measurements are correct to within ±1 mm (or ±7 ps).

Results

The range correction measurements for Lageos using the criterion of leading edge/half-maximum detection are given in figure 18. The average value is 251 mm with a variability of standard deviation 1.3 mm. The data points at locations -27° latitude and 7° longitude and -27° latitude and 123° longitude and at the north pole correspond to germanium CCR positions. Some reduction in range correction at these locations is apparent as would be expected.

A similar range-correction map is shown in figure 19 for the case of peak detection at the receiver. The average correction is slightly less at 249 mm and has a variability with a standard

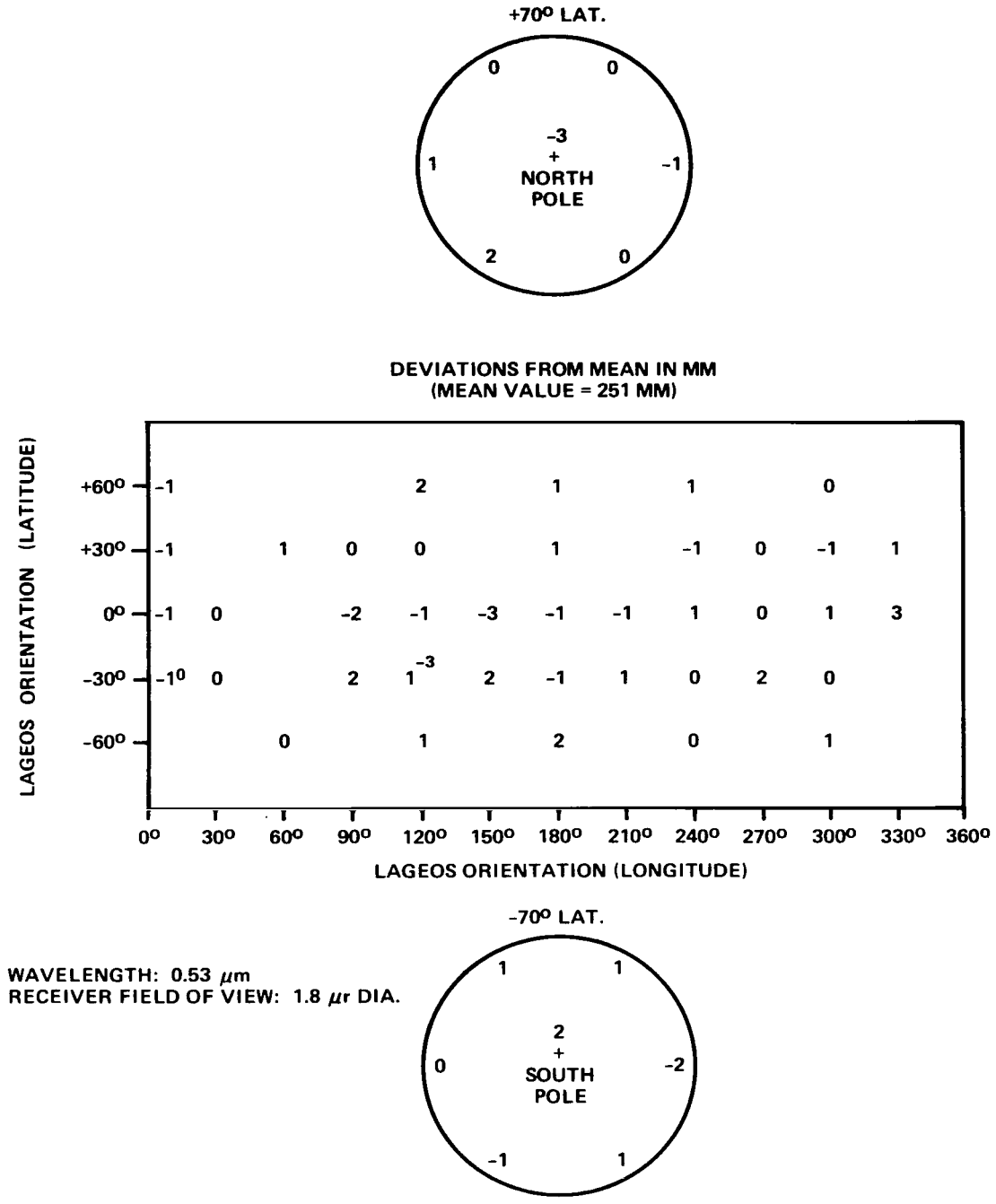

Figure 18. Lageos range-correction map—half-maximum detection.

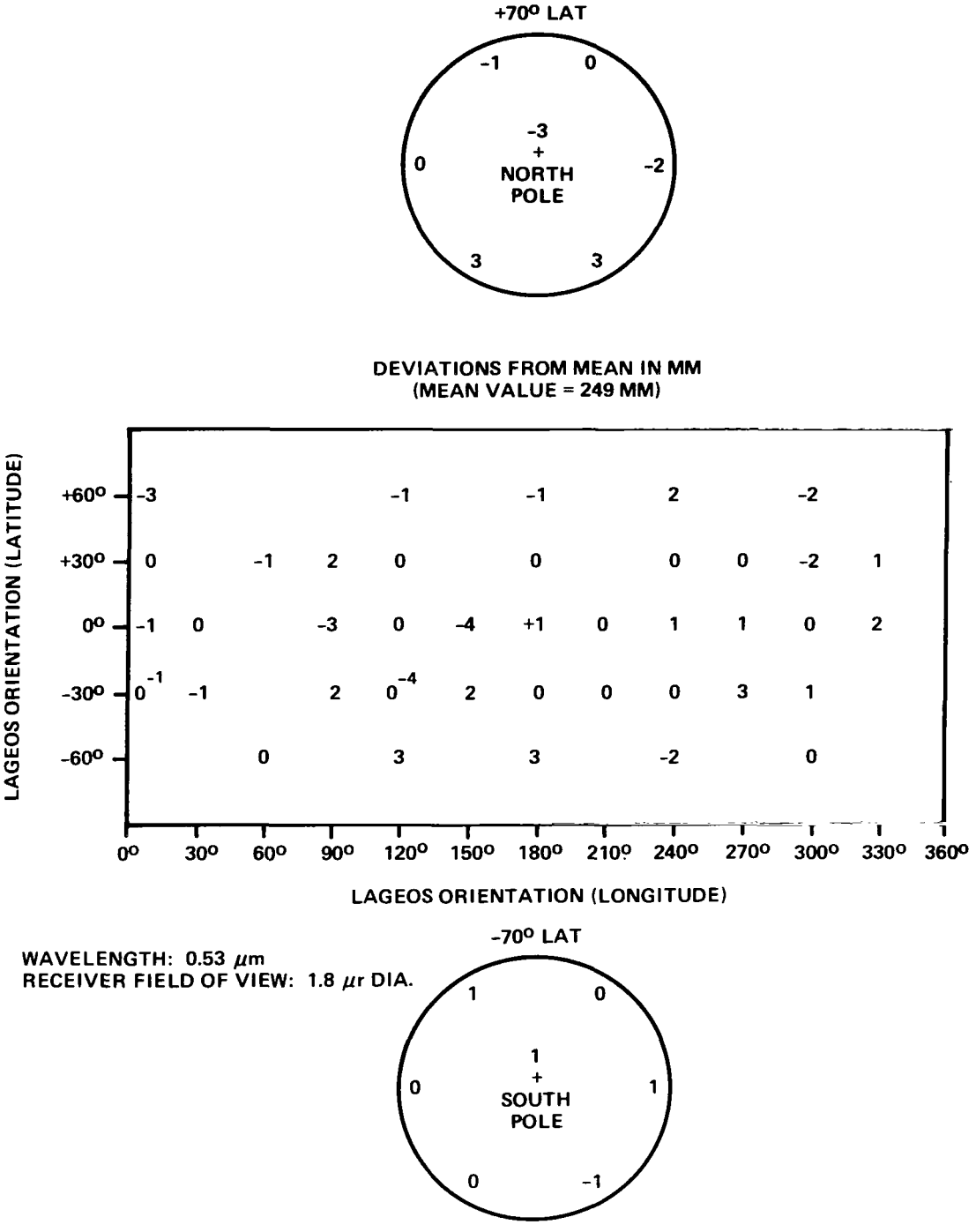

Figure 19. Lageos range-correction map—peak detection.

deviation of 1.7 mm. The range-correction variations for both the half-maximum and peak detection cases are significantly less than the 5-mm systems specification.

The data of figures 18 and 19 were taken with a 1.8-μr receiver field stop-positioned 35 μr off the center line of the return beam. Additional measurements were taken to determine if the location of the receiver in the far-field pattern would have any effect on the range correction.* The receiver was positioned at four different locations (separated by 90°) in the far field and reference array/Lageos pulse spacing measured. No significant variations were found; peak deviations in the range correction were approximately 2 mm.

Range-correction measurements were also taken with the annular-field stop in the receiver system; this essentially averages out any position-dependent variations which do exist. These results are shown in figure 20, where the listing at the top refers to leading edge half-maximum detection and the values at the bottom are for peak detection. As expected, the variations are somewhat less, with the half-maximum values having a standard deviation of 0.2 mm and the peak detection values having a standard deviation of 1.3 mm.

The effects of transmitter polarization on range correction were also investigated. The satellite was illuminated with a circularly polarized beam, as well as three different linear polarizations; the range correction was measured for each case. No statistically significant differences were observed.

Pulse Shape Variations Due to Coherency Effects

As noted in the section, "Physical Mechanism" under "Pulse Spreading" and figure 2, the laser pulses returned by the individual retroreflectors on the satellite often overlap in time, and therefore the net field strength at the photodetector is determined by the coherent addition of the fields from the individual pulses. These optical fields have phases that are not predictable, and therefore the detected pulse shape can be expected to show some amount of randomness. Since the time-of-flight measurement is referenced to some point on the return signal waveform, this variation in received wave shape will introduce some amount of error in the range measurement.

No direct measurements of single-shot Lageos reflected signals which had sufficient bandwidth to show coherent fading were made during this test program. The technology to perform such measurements is available,† but is very complex and could not be fitted into the very tight prelaunch schedule.

However, computer calculations were carried out which provide a good estimate of the magnitude of this effect. The program for these calculations (Retro-Lageos) was developed by one of the authors (P. O. Minott) and can be used for cube corner arrays of arbitrary geometry.

*This is important because in typical ground station-orbiting satellite geometries, the receiver position in the far field of the return beam moves nearly 180° around the annulus from beginning to end of a pass.

†Streak tubes have sufficient bandwidth and sensitivity to make single shot measurements.

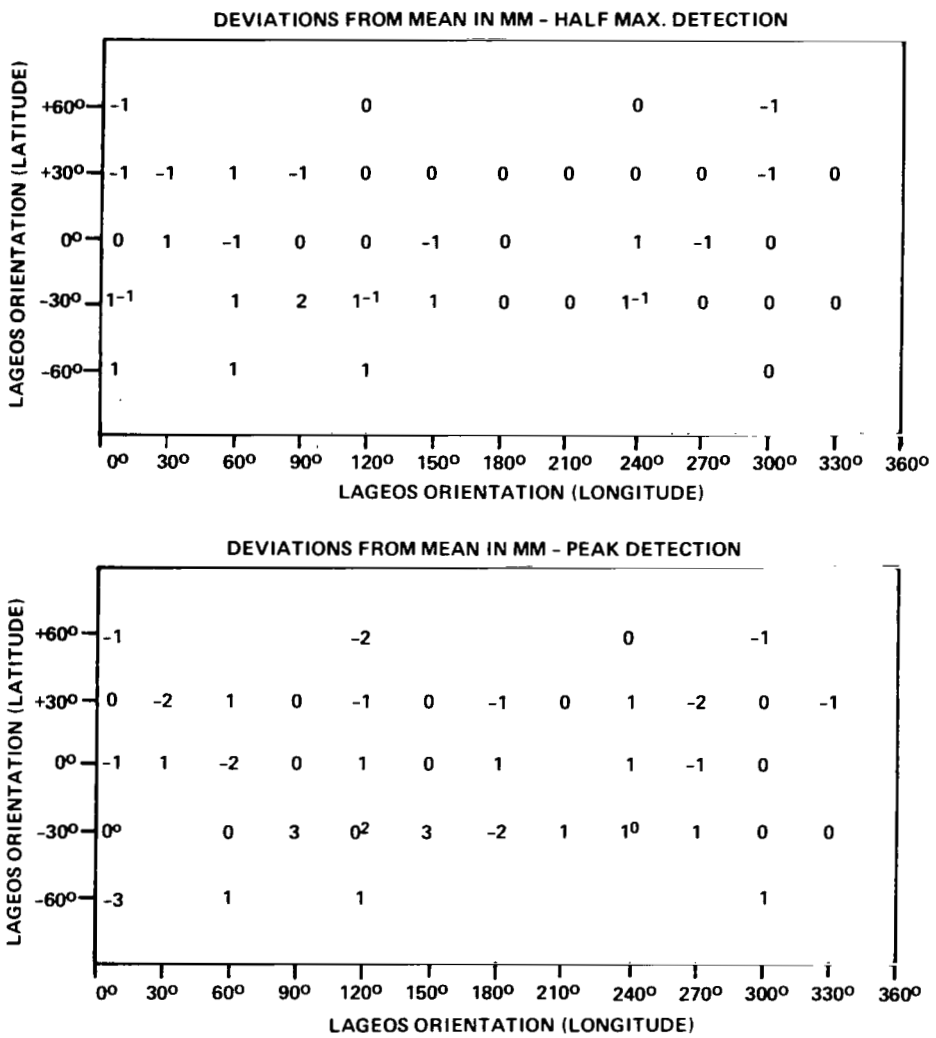

Figure 20. Range-correction measurements taken with annular-field stop in receiver system.

The calculation procedure for Lageos was as follows:

1. The satellite orientation with respect to the incident pulse was specified. In this case, the face of the south-pole cube corner was normal to the incident beam..
2. The satellite was illuminated with a plane wave of specified wavelength, polarization, and shape; in this case wavelength was 0.53 μm, polarization was vertical, and pulse shape was Gaussian with a 63-ps standard deviation.
3. Each of the participating retroreflectors reflects back a signal whose magnitude is proportional to the lidar cross section of the retroreflector and whose phase depends upon its position.
4. To determine the magnitude of the pulse from each retroreflector, the program calculates a far-field-diffraction pattern (FFDP), computes the position of the receiver (including velocity aberration effects), and assigns the value corresponding to this point as the energy of the reflected pulse.
5. Each cube corner produces a pulse with identical temporal width but with differing peak positions due to the different distances of the individual retroreflectors from the laser source. The program accounts for this by calculating the optical line-of-sight distance from the reflection point of each cube corner to the satellite center of gravity (CG). This is converted to a temporal delay of each cube corner pulse referenced to the spacecraft CG.
6. When the pulses returned from each cube corner are known, both from a magnitude and temporal delay standpoint, the pulses are summed to obtain the net array pulse. However, a simple summing of the wave forms from all the retroreflectors would produce only the incoherent wave shape. Therefore, the square root of each pulse magnitude is taken to convert to a term proportional to the optical field strength, and a random number generator is used to assign phases between 0 and 2π radians. The resultant pulses are then summed to obtain the coherent field strength pulse shape of the array. To convert back to signal strength, the resultant pulse magnitude is then squared.
7. At this point, a single coherent pulse shape has been generated. To determine the statistics of the pulse centroid position, the process is repeated several hundred times, and a histogram of the pulse centroid position is developed.

Figure 21 gives the results of these calculations for Lageos. Even with all other system parameters fixed, it is apparent that the centroid of the reflected pulse can undergo peak-to-peak excursions of several hundred ps. The standard deviation of the received pulse is calculated to be 77 ps. Taking into account that each measurement is a two-way (or double pass) range measurement, this standard deviation becomes 1.15 cm in range.

Clearly, an error source of this magnitude is very significant for Lageos tracking. However, the pulse shape variations that cause this should be essentially uncorrelated over time intervals of

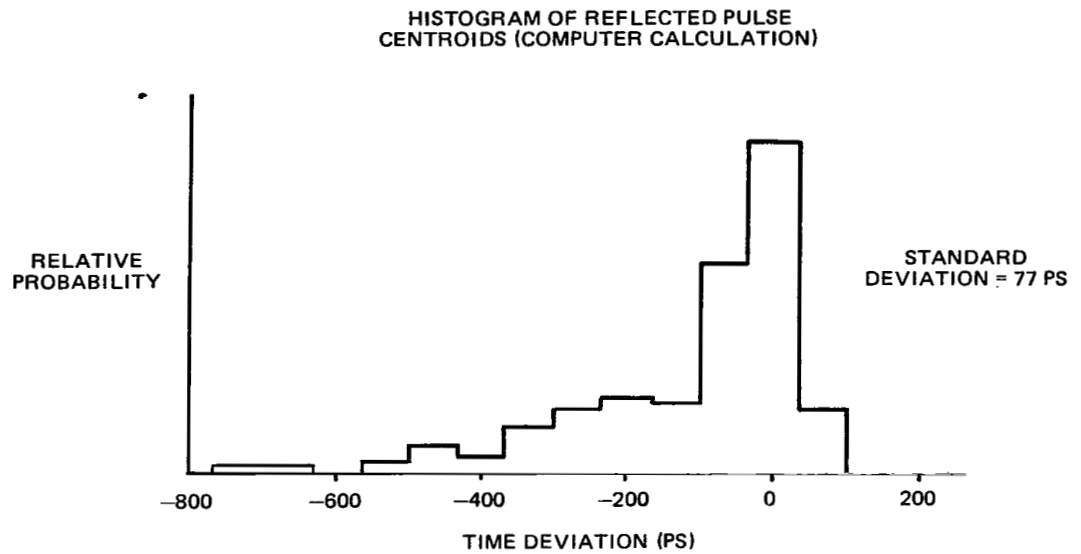

Figure 21. Lageos pulse shape variations due to coherent fading.

approximately 1 second (which is the typical spacing of range measurements), and therefore data averaging over measurement sets of 10 would effectively reduce this error source to approximately 4 mm.

LIDAR CROSS-SECTION TESTS

Introduction

The major reason for a careful analysis of the Lidar cross section is shown in figure 22. This figure shows the expected signal levels from Lageos, using a cross-section value of 7.0 million square meters, and the parameters of the present Stationary Laser (Stalas) tracking station. Table 2 shows the parameters of the existing laser tracking stations. The last column labeled station parameter (P_S) gives the figure for each existing station computed as follows

$$P_S = \frac{32\pi^2 \eta \tau_O \tau_P E_T}{N_{C_\cdot}(h\upsilon)} \left(\frac{D}{\theta_T}\right)^2 \qquad (4)$$

where η = quantum efficiency of receiver phototube

τ_O = optical efficiency of transmitter/receiver combination

τ_P = tracking error loss

E_T = energy transmitted by laser

D = receiver diameter

N_C = number of photoelectrons required for an acceptable range measurement

$h\upsilon$ = energy of a photon at the laser wavelength

θ_T = transmitter divergence to the $1/e^2$ intensity points (Gaussian profile assumed)

In this table, N_C has been set at 1.

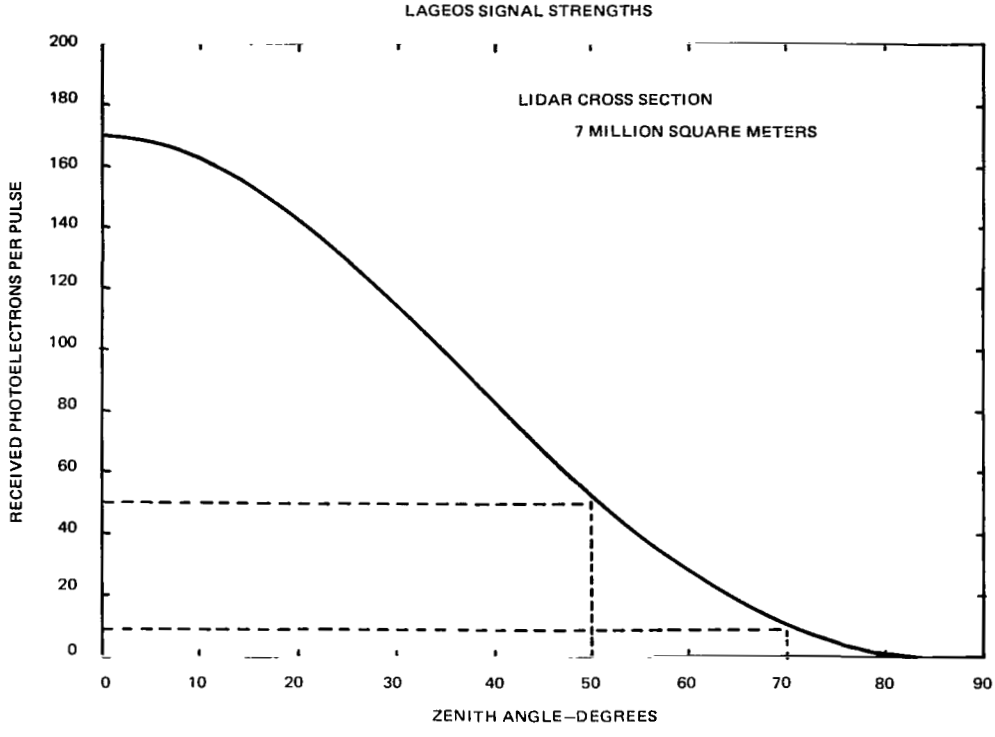

Figure 22. Lidar cross-section analysis.

From figure 22, it can be seen that at 70° zenith angle only 9 photoelectrons are received, while at 50° zenith angle only 50 photoelectrons are received. Figure 23 shows the root-mean-square range error to be expected for various signal levels. Clearly, the accuracy of Lageos ranging is severely limited at present and for the near future by the small cross section of the satellite. However, because Lageos is expected to have a useful lifetime of several decades, improvements in ground-station technology should reduce this problem. As shown in figure 23, an increase of 10 to 20 times in ground-station effectiveness will be required to fully utilize the accuracy inherent in the Lageos array.

Because of the very weak signal levels, it was decided that a careful analysis of the Lidar cross section was necessary. The results of this analysis shown in the following sections indicate that while the average cross section is approximately 70 percent of its design value (10 million

Table 2
Parameters of Existing and Proposed
Laser Tracking Stations

Tracking Station	(Å)	E_T (joules)	η (%)	D_R (cm)	τ_O (%)	Θ_T (mrad)	τ_P	P_S ($M^2 \times 10^{25}$)
SAO 1	6943	0.50	3.0	51	34	0.6	0.5	0.20
SAO 2	6943	0.50	3.0	51	34	0.6	0.5	0.20
SAO 3	6943	0.50	3.0	51	34	0.6	0.5	0.20
MOBLAS 2	6943	0.25	2.5	51	15	0.25	0.5	0.22
MOBLAS 1	6943	0.80	2.5	41	15	0.15	0.5	1.24
MOBLAS 3	6943	0.80	2.5	51	15	0.15	0.5	1.91
MOBLAS 4*	5320	0.25	10.0	75	26	0.20	0.5	3.86
MOBLAS 5*	5320	0.25	10.0	75	26	0.20	0.5	3.86
MOBLAS 6*	5320	0.25	10.0	75	26	0.20	0.5	3.86
MOBLAS 7*	5320	0.25	10.0	75	26	0.20	0.5	3.86
MOBLAS 8*	5320	0.25	10.0	75	26	0.20	0.5	3.86
STALAS	5320	0.25	10.0	61	0.15	0.10	0.5	5.90

*Under development

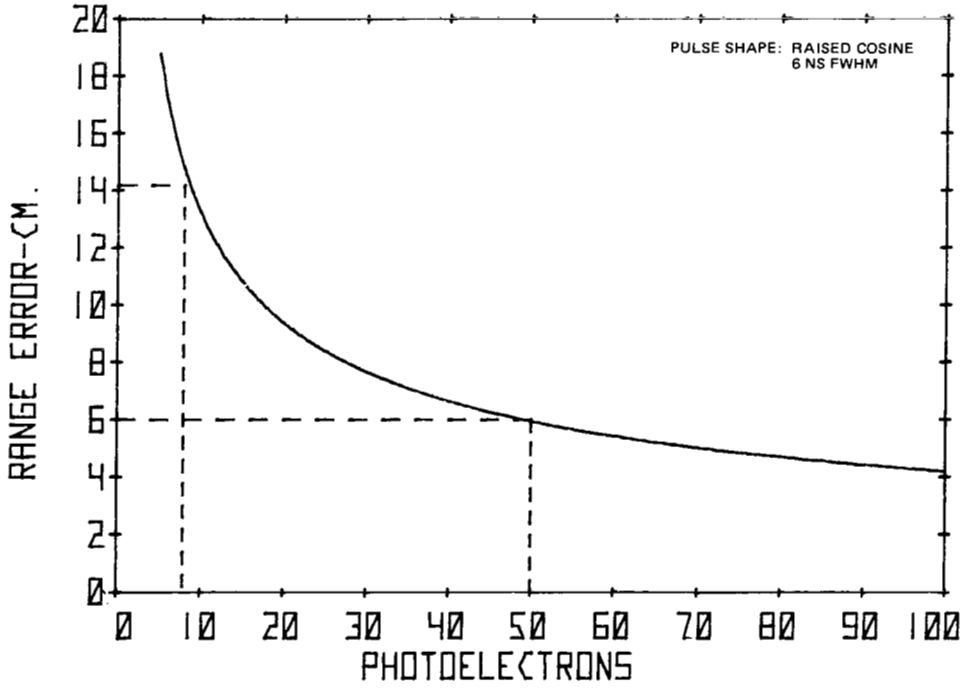

Figure 23. Range error versus signals.

square meters (m^2)), for certain conditions it drops by nearly an order of magnitude. The effects noted are expected to result in considerable changes in the method of operation of the ground tracking networks.

Instrumentation

Description of Test Equipment

In the following paragraphs, the design parameters of the test equipment used for the Lageos FFDP tests are discussed.

The FFDP test setup is shown in figure 24. A laser projects radiation into a polarization rotator which controls the orientation of the laser radiation. The beam is then spatially filtered, expanded, and condensed by a pair of refractive objectives and passed through a hole-coupling beam splitter. The hole-coupling beam splitter is at the focus of an 85-cm diameter parabola of 900-cm focal length, which produces an 85-cm collimated beam to illuminate Lageos when coupled to the previous optical system. Radiation reflected by Lageos is focused by the parabola on the hole-coupling beam splitter, which deflects it into an 11:1 relay lens, which, in turn, produces an expanded image of the FFDP on the optical data digitizer.

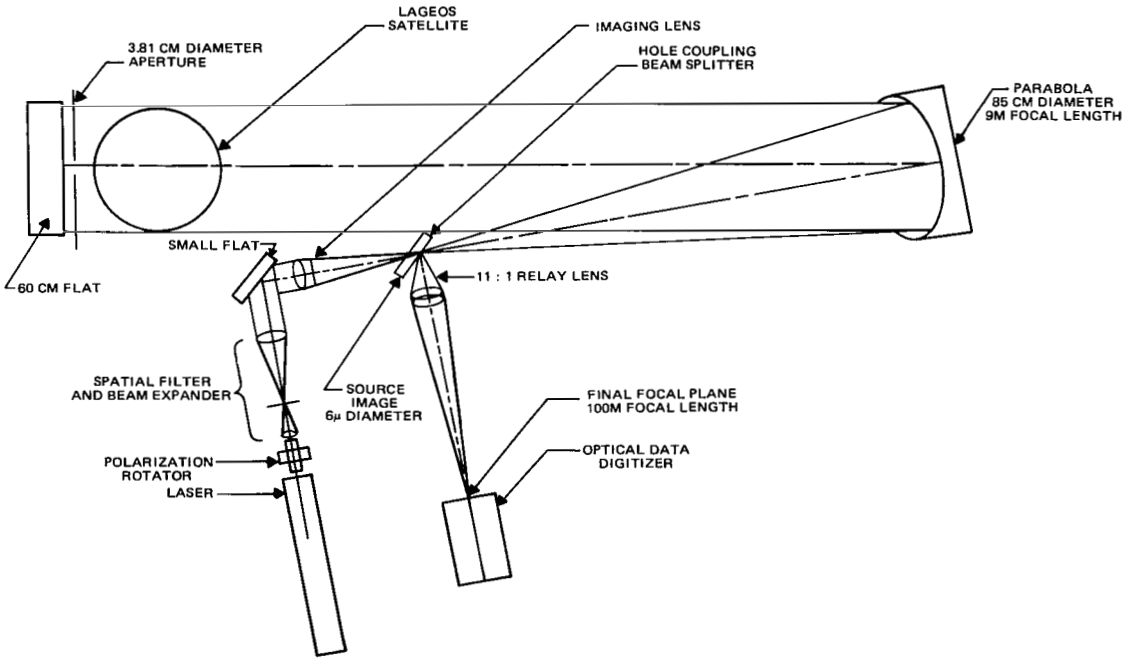

Figure 24. Lageos FFDP optical test setup.

Several lasers were used in the FFDP tests to evaluate the performance of Lageos at different wavelengths. The parameters of these lasers are shown in table 3.

Table 3
Laser Parameters

Characteristic	Laser Type			
	HeCd	HeNe	Nd:YAG	
Wavelength (μm)	0.4416	0.6328	1.064	0.532
Average Output (ω)	0.017	0.010	0.350	0.010
Transverse Mode Structure	TEM_{00}	TEM_{00}	TEM_{00}	TEM_{00}
Amplitude Stability	±5%	±3%	±5%	±10%
Polarization	Linear	Linear	Linear	Linear
Polarization Purity	1000:1	> 100:1	> 50:1	> 50:1

The polarization rotator consists of a Gaertner Babinet-Soleil compensator, which acts as a $\lambda/4$ plate to produce circularly polarized radiation. This is followed by a Nichol prism, which selects the desired polarization when a plane polarized beam is desired. The Nichol prism is removed from the system on all tests denoted as circularly polarized. The adjustable nature of the Babinet-Soleil compensator allows it to be adjusted to $\lambda/4$ for any desired wavelength. Tests confirmed a better than 100:1 extinction ratio for the cross polarization when in the plane-polarized mode.

A Spectra Physics Model 331/332 beam expander/spatial filter was used to expand the laser beams to 50 mm and to spatially filter the laser beams. This was followed by a second Model 331 collimating objective, which focuses the beam on a hole-coupling beam splitter.

The hole-coupling beam splitter consists of a 25.4-mm (1-in.) diameter, 2.99-mm (0.118-in.) thick fused silica flat inclined at 45° to the axis of the transmitted beam. At the center of this flat, a cone-shaped hole (f/3.0) is drilled from the back, through the flat, along the axis of the transmitted beam. The hole in the front reflective face of the flat is a 45° ellipse with a 180-μm minor diameter. The reflective face is flat to a tolerance of 1/4 wave and aluminized and overcoated with SiO. Because this flat is the only polarization sensitive element in the system, its reflectivity was checked as a function of polarization orientation and was found to be constant within 5 percent.

The parabola is a 900-cm focal length, 85-cm aperture aluminized fused silica element. Its full aperture resolution is on the order of 50 μr, but it is diffraction-limited over any 3.81-cm element. The source (located at the hole-coupling beam splitter) was placed in the focal plane, but off-axis in the horizontal direction by 35 cm. The parabola was, therefore, working in a 2.23° off-axis condition.

The satellite (Lageos) is supported in a fixture that allows it to rotate about the polar or equatorial axes built into the Lageos structure. The rotation axes can also be tilted relative to the optical axis and in a vertical plane by ±90°. This allows the satellite to be viewed from any combination of latitude and longitude. (See figure 5.)

The 60-cm reference flat shown in figure 24 is accurately aligned normal to the incident radiation, and is used for calibration of the spatial scale of the FFDP and its intensity calibration. The flat is aluminized and overcoated with SiO and has a reflectivity of 92 percent at 6328 Å. Its use is further described in a future section of this document.

The reflected FFDP from Lageos was imaged on the hole-coupling beam splitter by the 900-cm parabola. Because this scale was incompatible with the optical data digitizer, an 11:1 relay lens was used to lengthen the effective focal length to 100 meters.

The optical data digitizer (ODD) is basically a computer-controlled digital video camera that can be commanded by a computer to scan the image and store the intensity values for each coordinate location in digital form. Its characteristics are shown in figure 25. The ODD was controlled by a PDP-11/40 computer and was modified by incorporating an electromechanical shutter that could be computer controlled. Exposures were made at 2.5 ms to eliminate image motion. A narrow-band interference filter was used to eliminate stray room light, and neutral density filters were used for additional control over exposure.

Spatial Resolution

The goal of the optical systems used for the Lageos FFDP tests was to obtain a spatial resolution of 5 μr. The primary source of aberration was the 85-cm parabola used to collimate the radiation incident on the spacecraft. Because it was necessary to produce an obscuration-free beam, the parabola could not be used on-axis. It was therefore used 2.23° off-axis, which allowed the source to be 35-cm off-axis and prevented the source from obscuring the satellite. It is well known that the aberrations of a parabola off-axis are quite severe, and if it had been necessary to use the entire beam, the aberrations would have been intolerable. However, the retroreflective nature of the cube corners compensates for all aberrations of the collimator except those occurring within the aperture illuminating an individual cube corner. Therefore, the collimator effectively had an aperture of 3.81 cm, and with a focal length of 900 cm was working at f/236. In order to determine the image quality, a ray trace was done using the GOALS Program, which resulted in the data shown in figure 26. The geometrical ray trace/ray distribution in the system focal plane for perfect retroreflector is listed as follows:

Percent Total Rays	Diameter Microradians (μr)
10	1.2
20	2.0
30	2.4
40	3.4
50	4.6

Percent Total Rays	Diameter Microradians (μr)
60	5.8
70	6.0
80	7.2
90	8.6
100	10.0

These data are for the worst location in the collimator beam. Resolution was better by a factor of about 2 over most of the beam. Therefore, the spatial resolution was approximately the 5 μr desired.

Parallax

When an array of cube corners is observed in a collimator of the type used in this experiment, focusing of the system is quite critical. The focal range for an individual cube corner is quite large (141 mm), so that focusing of the system is unimportant from the individual cube corner standpoint, but, from the array standpoint, unless the focal plane relayed to the optical data digitizer corresponds to the plane of the source, severe parallax will occur. At the source plane, all images overlap as they would in the far field, but in front of this plane, the ray bundles from each cube corner converge on the source and diverge behind it. The method used in this experiment to assure that parallax does not occur is to move a single cube corner about the aperture of the parabola. If the image is observed to move in the final image plane, then parallax exists and must be corrected by moving the relay lens. Using this technique, parallax could be easily kept below 2 μr.

Beam Uniformity

The radiation from the lasers was spatially filtered by a Spectra Physics Model 331/332 spatial filter/beam expander to produce a 50-mm ($1/e^2$ intensity points) diameter collimated beam. After being condensed by a second Model 331 objective and passing through the hole-coupling beam splitter, it emerged as an f/3.6 cone which illuminated the 85-cm parabola. Because the focal length of the parabola was 900 cm, the cone was 250 cm across when it reached the parabola. Because only the central 30 cm of the beam-illuminating cube corners in Lageos are capable of producing reflection, we need worry only about the beam taper over the central 30 cm. After passing through the spatial filter, the beam intensity profile is Gaussian and described by the following equation

$$I/I_0 = e^{-2(r^2/a^2)} \tag{5}$$

where r is the radius of interest and a is the $1/e^2$ intensity radius. Since r is 15 cm (30 cm/2) and a is 125 cm (250 cm/2), the intensity at the edge of the 30-cm effective beam was theoretically 97.2 percent of the central intensity. Experimentally, the evaluation of the beam

EMR

Schlumberger

EMR PHOTOELECTRIC Model 658 A

optical data digitizer specification

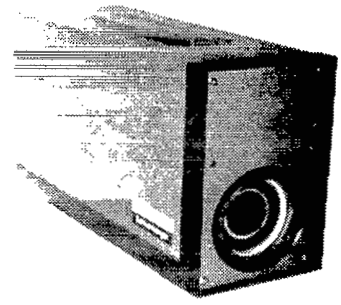

GENERAL

Until quite recently, visual data had to be manually or mechanically pre-processed before the computer could synthesize it into meaningful information. The new EMR Optical Data Digitizer has made this off-line pre-processing a thing of the past. With the O.D.D. the computer perceives visual data on-line as it determines what should be looked at and for how long.

By eliminating the pre-processing operation and by permitting the selection of pertinent input, the O.D.D. expands the service capability of the computer into visual applications whose scope is limited only by the imagination of the user and his software capabilities.

HOW THE O.D.D. WORKS

The Optical Data Digitizer creates the binary equivalent of a two-dimensional optical image and thus prepares it for immediate input for the computer. Having complete control over the O.D.D. scan along the X, Y coordinates enables the computer to select the size of each scanning step, choose the direction of the scan, determine the dwell time per element, all with random access capabilities. The computer based on predetermined instructions, can then perform computations and initiate procedures in accordance with the kind of data it receives. It can also perform arithmetic functions such as summing, averaging over several cycles, deconvolving, or formatting for tape entry.

To accommodate the wide range of applications for which the O.D.D. can be utilized, a choice of image sensors is available and includes the highly reliable EMR Image Dissector and a number of vidicon sensors (SEC, SIT/EBS, Sb_2S_3, PbO, or Si).

The mode of converting the optical image into its electronic equivalent varies with the sensor. Using the Image Dissector, conversion takes place by scanning an electronic image emitted by a target across an aperture. Vidicon sensors, on the other hand, perform this function by holding the corresponding charge pattern on a target for subsequent read-out by ane electron beam. The deflection field for either type of sensor is provided by a scanning-function driver which receives its analog voltage input from a scanning-function decoder. This permits the digital output of the computer to be used in controlling the scanning pattern within the sensor.

In the case of vidicon sensors, the electron charge-level output of the sensor is translated by the intensity-function detector into voltage or current levels suitable for input to the intensity-function encoder for A/D conversion. The resultant binary signal is stored and processed by the computer, which then prints out, displays, or formats for tape entry any pertinent information about the data determined by the software program.

Figure 25. Copies of EMR data sheets (1 of 4).

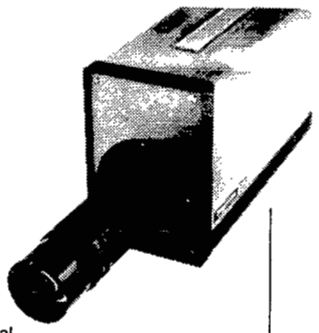

Model 658 A

ELECTRO-OPTICAL

Sensor:	EMR Model 575 Image Dissector.
Optics:	Specified or provided by customer.
Input Window:	7056 Glass flat, .080" (2.03mm) thick or fiber optic.
Input Image Size:	28 mm x 28 mm or any format less than 43 mm diagonal.
Recommended Sensor Illumination Range:	Five to 50 foot-candles.
Signal Transfer Function:	Unit gamma throughout range.
Uniformity:	±20% absolute, will not change faster than 2%/mm.
Elemental Exposure Time:	Controlled in software.
Sensor Modulation Transfer Function:	20 lp/mm @ 50% 40 lp/mm limiting } with 19 Micron aperture.
Maximum Readout Time:	Controlled in software.
Photocathode Dark Current:	10^3 electrons/sec/cm^2, nominal at 20°C.

ADDRESS & DATA

Commandable Data Points:	4096 X locations x 4096 Y locations max. .03% RMS data point repeatability. Randomly addressable.
Addressing Accuracy:	Error at any point in field: 3% of field (referred to optical input). .5% optional.
Addressing Time:	Depending upon address, 2 μs for 1% of field, 30 μs for full axis.
Speed:	Processing time per element is controlled in software. For small steps, 50 μs per element is typical.
Signal-to-noise Ratio:	Dependent upon number of quantum events per exposure time. Given by: $S/N = 1.22d\sqrt{E\Delta t}$ d = aperture dia. in mils E = face plate illumination in foot candles Δt = dwell time, μs
Encoder:	8 bit ADC standard, 4 μs conversion time. 10 & 12 bit optional, also 4 μs conversion time.

ENVIRONMENTAL

Operating Temperatures:	Specifications valid at ambient temperatures from 60-90°F (16-32°C).
Operating Humidity:	Less than 80% R.H.
Vibration:	MIL-STD-810B, Method 514, Procedure X "Shipment by Common Carrier" (5G)
Shock:	MIL-STD-810B, Method 516, Procedure V "Bench Handling" and Procedure VI "Rail Impact Test."
Storage Temperature:	32-131°F (0-55°C).

COMPUTER RELATED

Interface:	All interfacing is accomplished via the computer. No direct interface with the camera is required. Test connectors are provided for real time monitoring at the camera head.
Software Provided:	Camera control and camera scanning.
Peripherals:	Computer equipment may be interfaced normally. The camera interface card requires one slot.

SPURIOUS EMISSION: FCC Ruling (Part 15) "Unintended Radiation."

Figure 25. Copies of EMR data sheets (2 of 4).

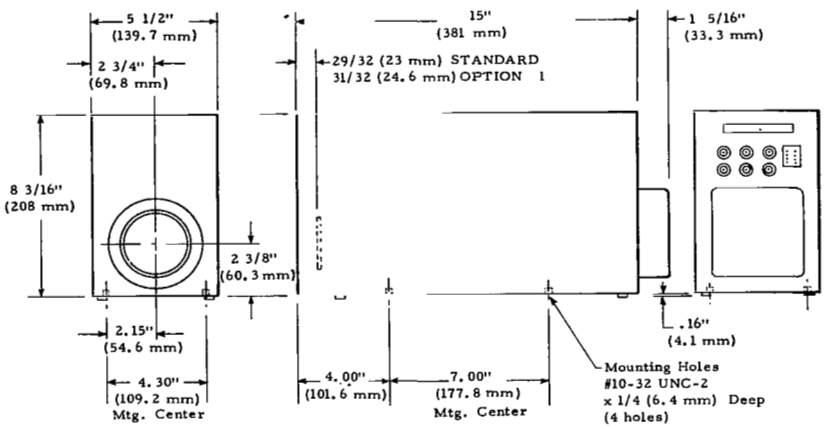

OUTLINE DRAWING

WEIGHT	20 lbs.
POWER	±15 V dc @ 2A +5 V dc @ 1A (Power supply optional)

NOTE 1 — Options:

Standard: Option 1 Precision deflection assembly, ±.5% geometry.
Option 2 Sample and hold (for dwell times less than 10 μs).
Option 3 10 bit ADC.
Option 4 12 bit ADC.
Option 5 Dynamic focus (for apertures less than 2 mil).
Option 6 Computer selected variable bandwith, 100 kHz, 10 kHz, 1 kHz, 100 Hz.

Speed:	Process times per element as short as 2 μs for small steps can be provided, if required.
Size:	For applications where computer size is objectionable, a control box with hard wired program can be provided, if required.
Power Supply:	A separate power supply Model 635A (635C rackmount) is available, operating from 115VAC 60Hz, same case size as 658A ODD.
Computer:	Unit can be supplied without computer or with alternate computer if required.
NOTE 2:	A special circuit is provided within the camera head to determine when the camera address has settled.
NOTE 3:	The use of a computer to set the scanning format allows the user an infinite number of variations which is obtainable in no other manner. These variations, of course, include direction of scan, size of scanning step, random access, and dwell time per element change as well as the ability to perform computations from the data as it is generated. This computation may take the form of averaging over several cycles in order to obtain accuracy, deconvolving, or performing arithmetic functions such as summing, etc. Only about 200 words are used in the scanning program. Therefore, many words are available for use by the customer in his programs.

Figure 25. Copies of EMR data sheets (3 of 4).

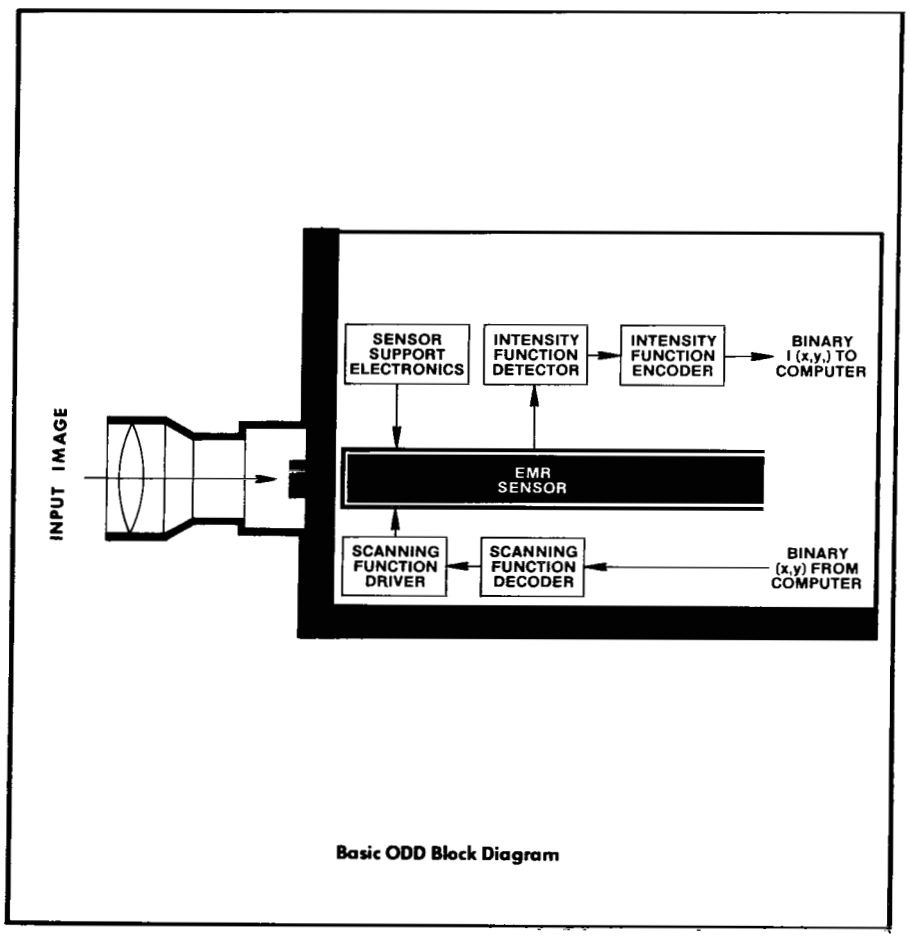

Figure 25. Copies of EMR data sheets (4 of 4).

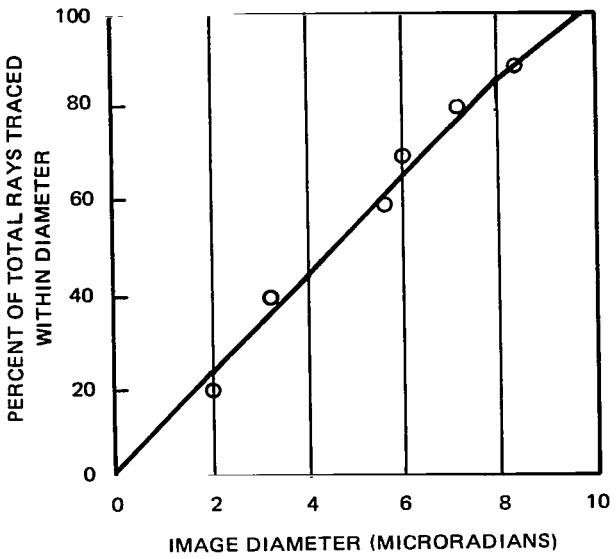

Figure 26. Geometrical ray trace/ray distribution in system focal plane for perfect retroreflector.

uniformity indicated no areas within the 85-cm aperture, which were less than 92 percent of the peak value.

Parameters

The FFDP of the Lageos is a function of wavelength, state of polarization, and aspect angle of the satellite. Therefore measurements were made at several wavelengths (4416 Å, 5320 Å, 6328 Å, and 10,640 Å) and several states of polarization (vertical, 45°, horizontal, and circular) to investigate the behavior of the satellite for these various conditions. Due to the symmetrical nature of the satellite, only slight changes in its FFDP with aspect angle were expected or noted. Therefore, an average FFDP was obtained for each wavelength and state of polarization by taking a FFDP at each of the 55 locations shown in the following list:

Latitude (Degrees)	Longitude (Degrees)
90	0
70	0, 60, 120, 180, 240, 300
60	0, 60, 120, 180, 240, 300
30	0, 30, 60, 90, 120, 150, 180, 210, 240, 270, 300, 330
0	0, 30, 60, 90, 120, 150, 180, 210, 240, 270, 300, 330
30	0, 30, 60, 90, 120, 150, 180, 210, 240, 270, 300, 330

Latitude (Degrees)	Longitude (Degrees)
60	0, 60, 120, 180, 240, 300
70	0, 60, 120, 180, 240, 300
90	0

The patterns were then summed and averaged in the PDP 11/40 computer to produce one average FFDP. This procedure effectively eliminated any statistical variations in the pattern due to coherence effects.

Scale Calibration

In order to establish the spatial scale of the FFDP on the final computer output, a special mask was constructed to cover the reference flat. This mask consisted of two parallel 1-mm by 10-cm slits spaced at a center-to-center distance of 63.28 mm. This double slit arrangement will give a Youngs interference pattern with maxima at

$$S = m\lambda/d \quad m = 0, 1, 2, \ldots \tag{6}$$

where d is the center-to-center separation of the slits and λ is the wavelength. Therefore at a wavelength of 6328 Å, the fringe spacing in the final image plane was 10 μr. By removing Lageos from the beam, exposures could be made of the flat covered with the mask, and images could be displayed on the computer output. The relay lens was then adjusted to give precisely the spatial scale required. This method has the advantage that no accurate knowledge of the focal lengths of the various optical elements, or the scaling in the ODD/PDP 11/40 is required. Scale calibration was set to within one image element (2 × 2 μr) at full scale, which made the spatial scale accurate to ±2 percent.

Calibration of Cross Section

Calibration of the FFDP in terms of intensity would be meaningless since it depends upon the irradiance at the satellite. Therefore, the FFDP's were calibrated in terms of lidar cross section, which fits directly into the radar-range equation and does not depend upon the parameters of the measuring system. The procedure of calibration was to expose the measuring system to the return from a known cross section. This produced an intensity that could be directly related to cross section. Once intensity was calibrated with respect to cross section, all intensity values could be converted by ratio to cross section.

The known target in this case was a 3.81-cm diameter flat, which was obtained by masking the 60-cm flat. For a flat, the peak cross section is

$$\sigma = \frac{4\pi A^2 \rho}{\lambda^2} \tag{7}$$

where A is the area of the flat, ρ is the reflectivity, and λ is the wavelength. The reflectivity of the flat was measured and found to be 0.924 at 6328 Å.

$$\sigma = 77.39 \times 10^6 \text{ m}^2 \text{ at } \lambda = 4416 \text{ Å}$$

$$\sigma = 53.33 \times 10^6 \text{ m}^2 \text{ at } \lambda = 5320 \text{ Å}$$

$$\sigma = 37.69 \times 10^6 \text{ m}^2 \text{ at } \lambda = 6328 \text{ Å}$$

$$\sigma = 13.33 \times 10^6 \text{ m}^2 \text{ at } \lambda = 10640 \text{ Å}$$

The above assumes constant reflectivity across the wavelength band.

Results

The following subroutines and figures present the results and explain their interpretation.

Far-Field Diffraction Patterns

Figure 27 shows a typical FFDP as presented by the PDP 11/40. At the top of the figure, the label indicates that this is an average FFDP (obtained by averaging FFDP's which were reasonably evenly distributed over the Lageos surface), that it is for a wavelength of 6328 Å, and that the polarization is vertical. The vertical scale of the FFDP is labeled along the left-hand border, and the horizontal scale along the bottom. The matrix of numbers displays the effective cross section of the satellite for each position in the far field. Each number gives the effective cross section for its location in the far field. The coding of the numbers (denoted as Z-axis scaling) is given at the bottom of the graph. In most cases, one unit in the graph corresponds to 2×10^6 m^2, 2 units to 4×10^6 m^2, 3 units to 6×10^6 m^2, etc. Due to the velocity aberration, the laser station will always lie in an annulus of 32.77 to 38.44 μr. A circle of 32 μr and a circle of 38 μr have been approximated by the lines shown on the matrix to approximate the area of interest. The blank area at the center of the graph is caused by the hole-coupling beam splitter. Because this area is of no practical use, the loss of these data is unimportant. Data beyond 38 μr in either X or Y directions have been cut off. When the cross sections were digitized, each value was assigned to the digit that was the next below its value. Therefore a 0.5 would show as 0, 1.3 as 1, 2.7 as 2, etc. Blank areas are to be interpreted as zeros. In cases where the cross section exceeds the range allowed by the coding scheme, an asterisk is shown.

At the bottom of the graph are shown the number of frames averaged and the date on which the data were taken are shown as well as a computer reference number.

Cross Section Versus Azimuth Curves

During testing, a pronounced polarization effect was noticed. This effect caused the intensities in the FFDP to vary with azimuth. Therefore, graphs presenting a running average for the values of cross section in the 32- to 38-μr annulus as a function of azimuth angle were made for each wavelength and type of polarization. The average was taken over an 18° sector of

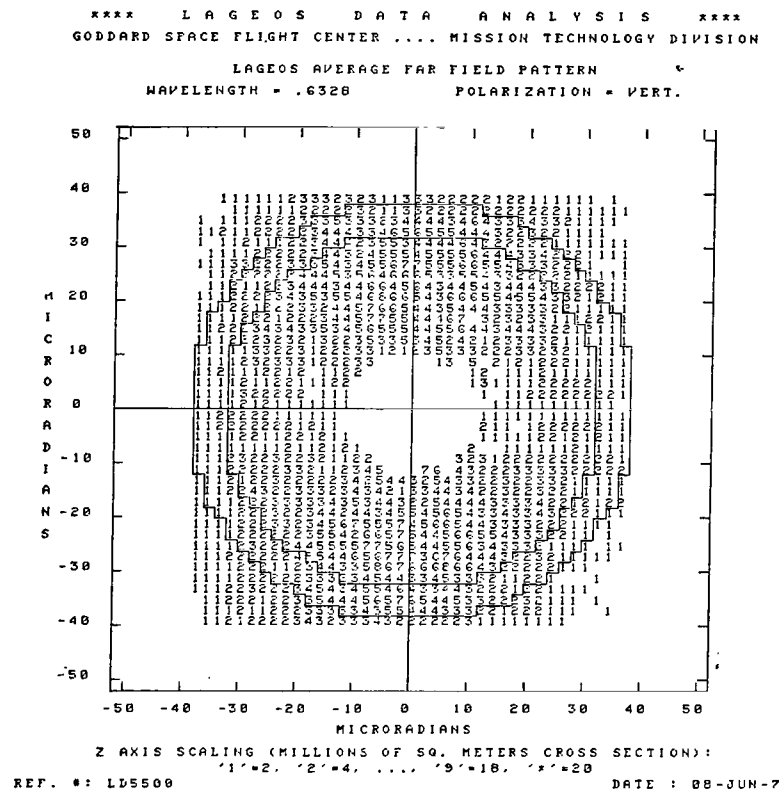

Figure 27. A typical FFDP presented by the PDP 11/40.

azimuth centered on the azimuth displayed in the graph. Most of these graphs show a pronounced variation of cross section with azimuths that lines up with the orientation of the polarization vector. Zero degrees corresponds to horizontal, with angles increasing counterclockwise. Figure 28 is an example of this type of curve.

Cross-Section Histograms

The probability density and cumulative density of the cross-section values in the 32 to 38 microradian annulus are shown in these graphs. Labeling of the axis is obvious. In addition, some statistical parameters of the cross section are shown (minimum, maximum, mean, median, and standard deviation). Figure 29 is an example of this type of curve.

Data Presentation

The results are shown in order of increasing wavelength (figures 30 through 53). For each wavelength and state of polarization, a FFDP graph, a cross-section versus azimuth, and a cross-section histogram are given in order. These are then followed by the new wavelength/polarization state. For convenience, table 4 presents a cross-reference of wavelength/polarization versus figure number.

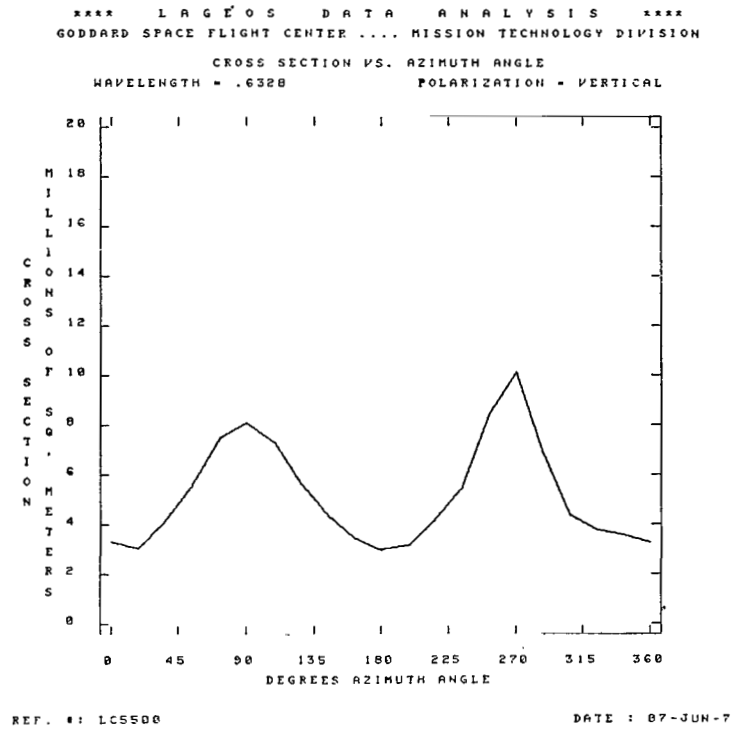

Figure 28. Cross section versus azimuth curve.

SUMMARY OF TEST RESULTS

Pulse Spreading

The pulse spreading introduced by Lageos at 0.53 μm has an average value of 125 ps FWHM (area weighted over the satellite surface). This result is derived for a system with a response of 205 ps and an average width (FWHM) of 240 ps. Results of the RETRO computer analysis (Appendix A) show that nearly all of the reflected energy comes from cube corners whose effective optical range is between 0.2427 and 0.2594 meter from the Lageos CG. This indicates that the maximum pulse spreading to be expected would be 111 ps, which is in close agreement with the 125-ps experimental results.

The results of analysis using the RETRO program show that the pulse spreading caused by Lageos is not a function of wavelength; that pulse spreading is not significantly affected by satellite orientation; and that exact pulse shapes from Lageos can be predicted for any given pulse length using the RETRO program.

The effects of the Lageos response upon the reflected pulse shape appear only in the trailing edge of the pulse and vary considerably with orientation of the spacecraft. For maximum accuracy with Lageos, ranging systems should be designed to detect the leading edge of the pulse.

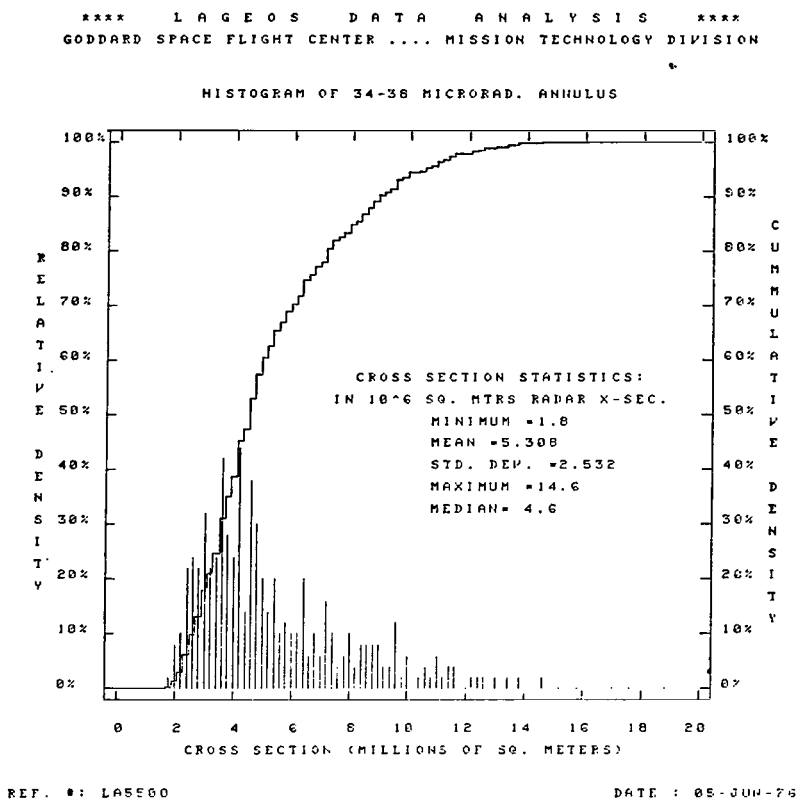

Figure 29. Cross-section histogram.

Further, the amount of pulse spreading is not significantly dependent on the location of the receiver in the far field.

Center-of-Gravity (CG) Correction

The CG correction has an area-weighted average of 251 mm for leading edge half-maximum detection with a standard deviation of 1.3 mm (5320 Å). The CG correction has an average value of 249 mm for peak detection with a standard deviation of 1.7 mm (5320 Å).

Computer analysis has been performed which correlates to measured values to within 2.5 mm. (See Appendix B.) Based upon this analysis, CG correction was found not to be a function of wavelength. No effects of polarization upon range correction were found during the test.

The effects of coherent interference upon received waveform have been analyzed by computer. Results show that the centroid of the pulse has a standard deviation of 1.15 cm in range, and that the probability distribution is skewed toward smaller range corrections. (See Appendix B.)

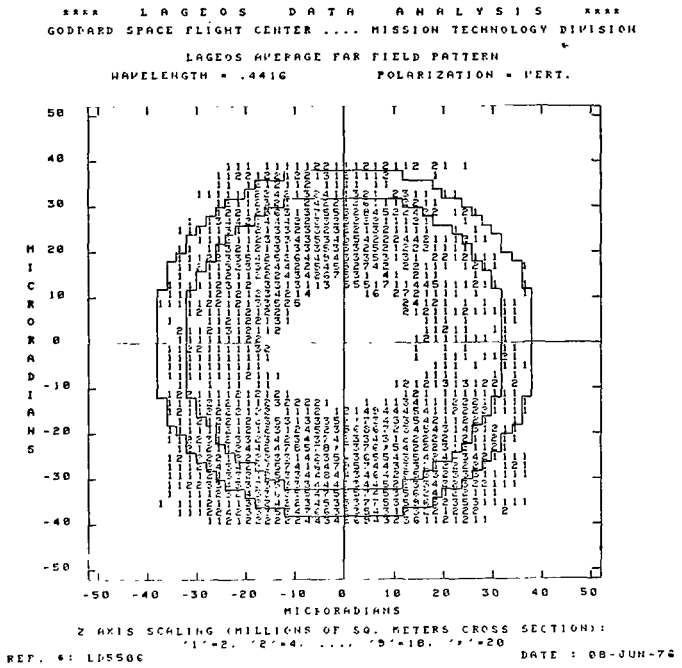

Figure 30.

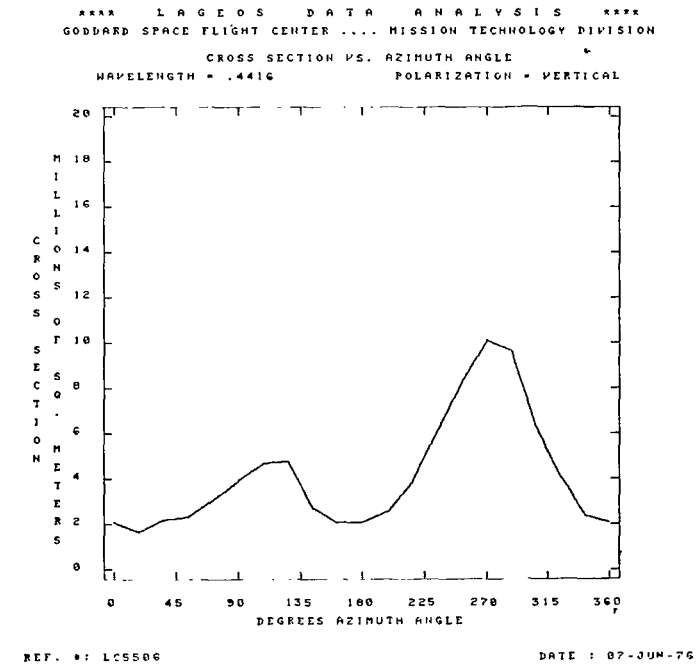

Figure 31.

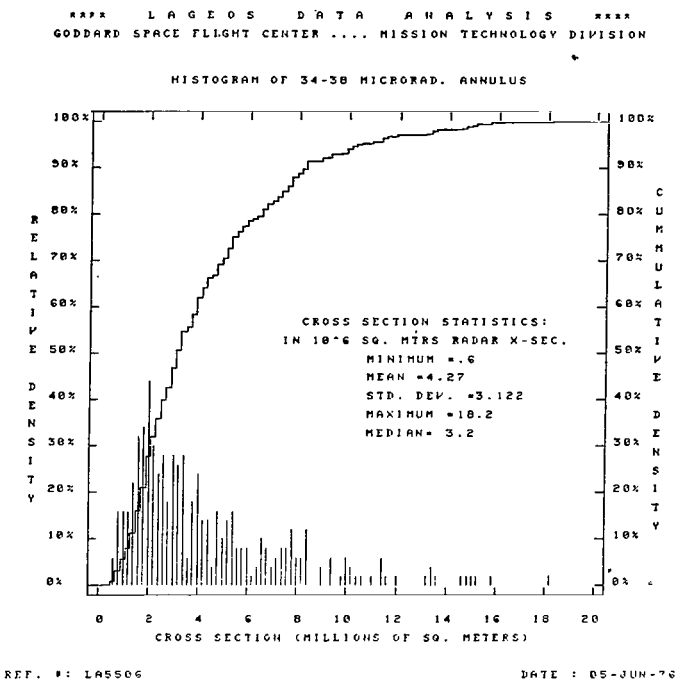

Figure 32.

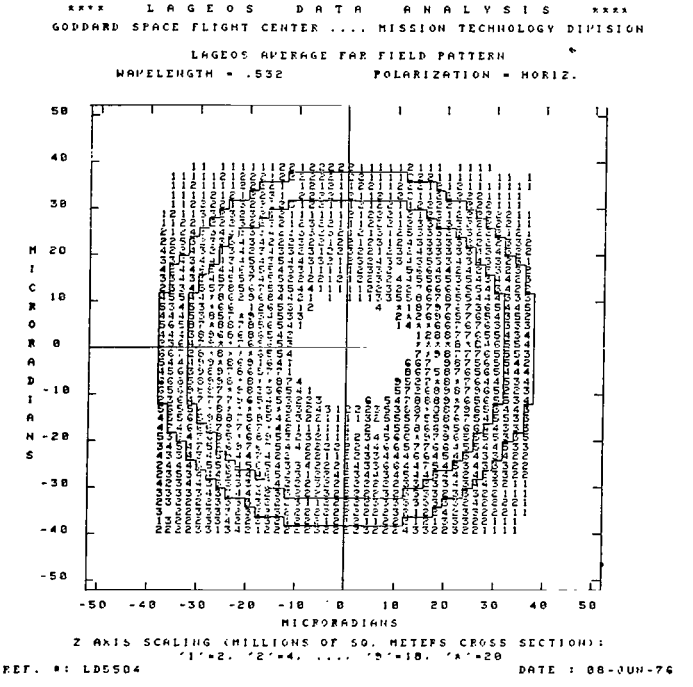

Figure 33.

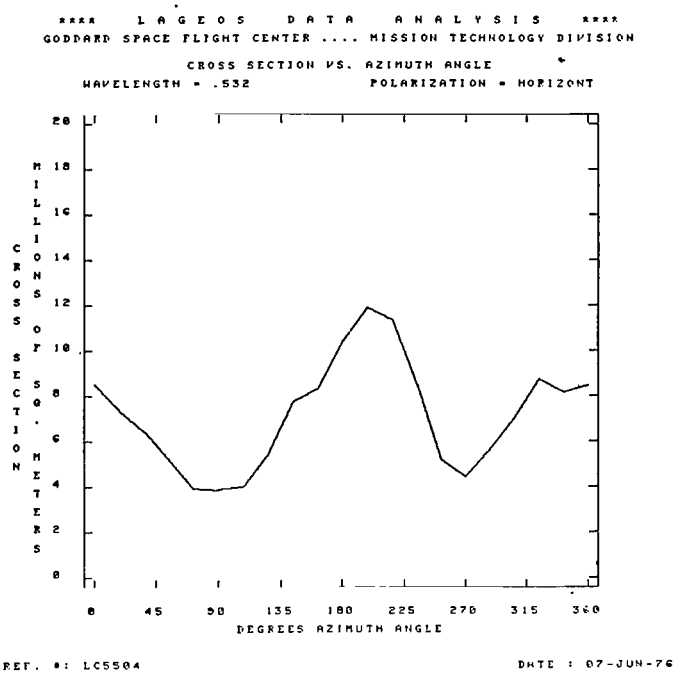

Figure 34.

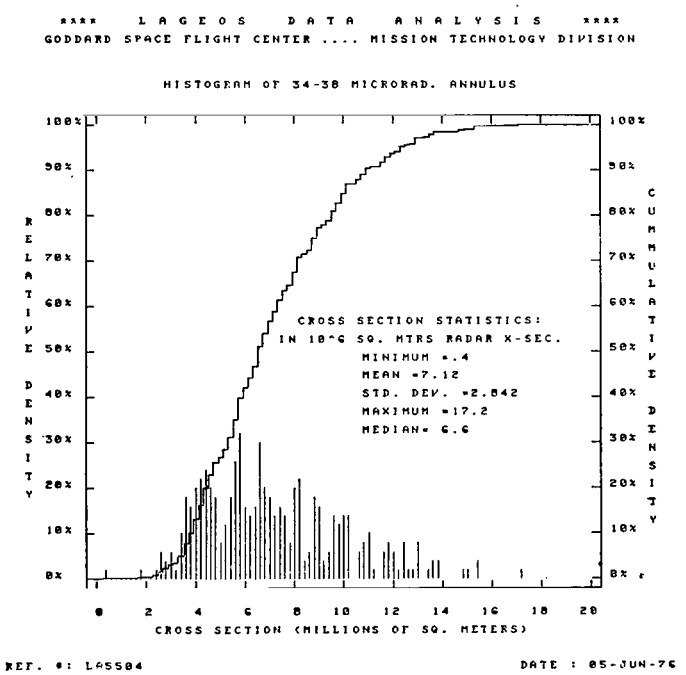

Figure 35.

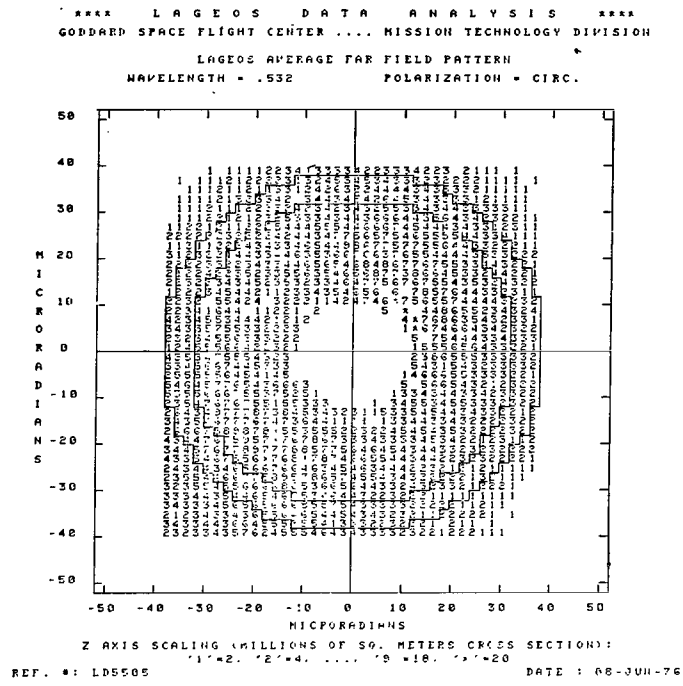

Figure 36.

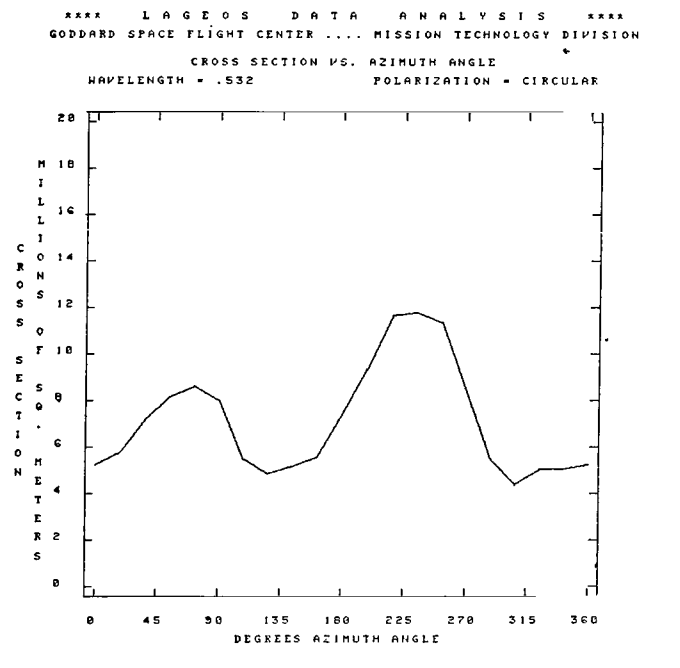

Figure 37.

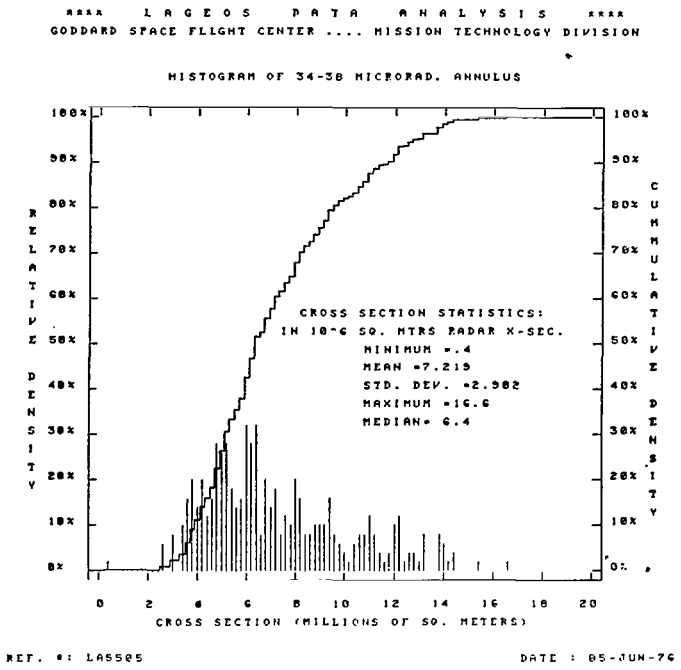

Figure 38.

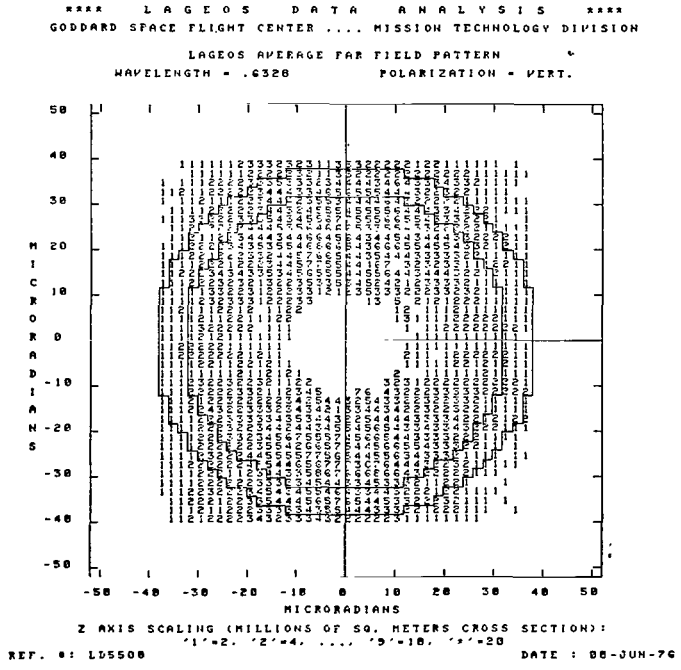

Figure 39.

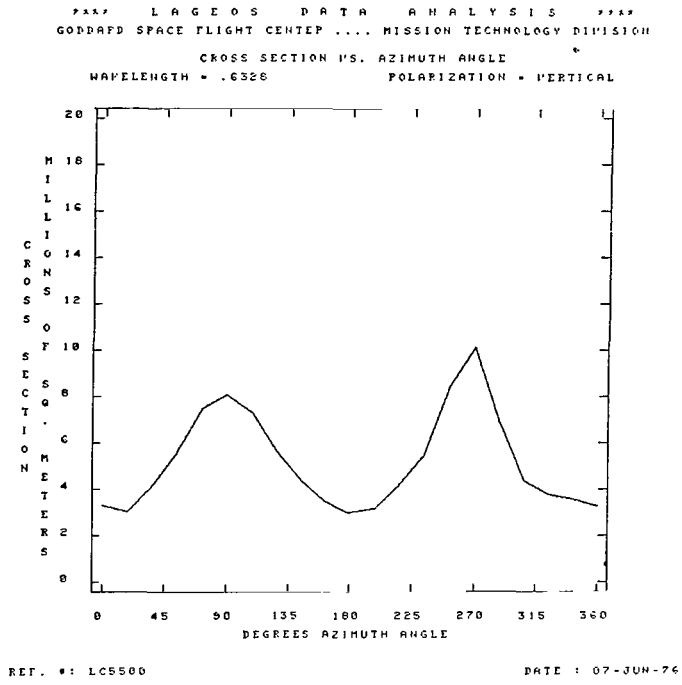

Figure 40.

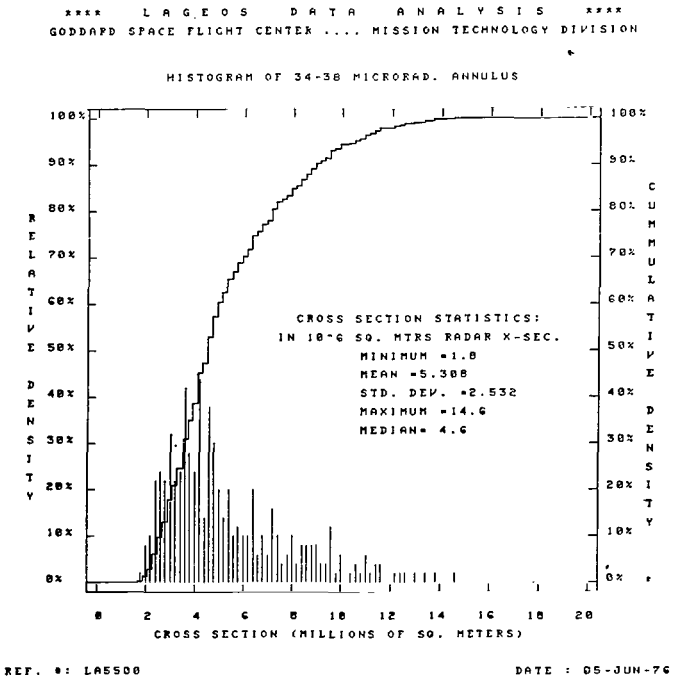

Figure 41.

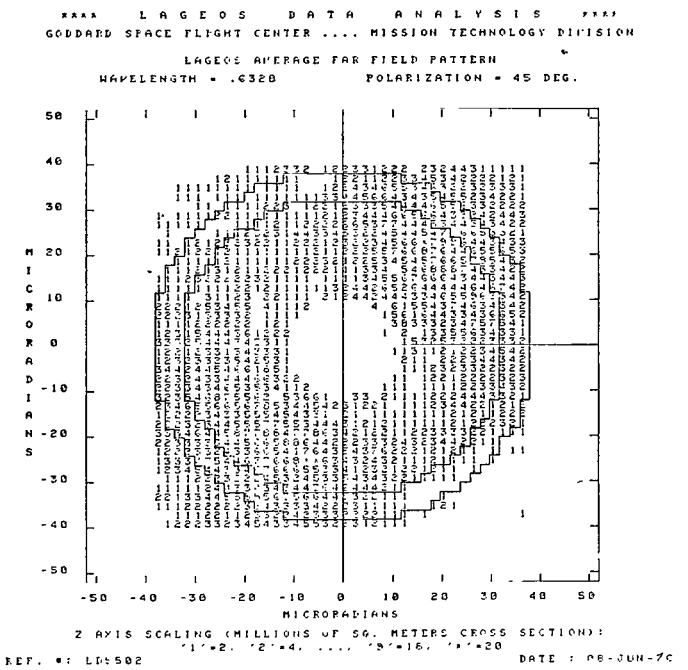

Figure 42.

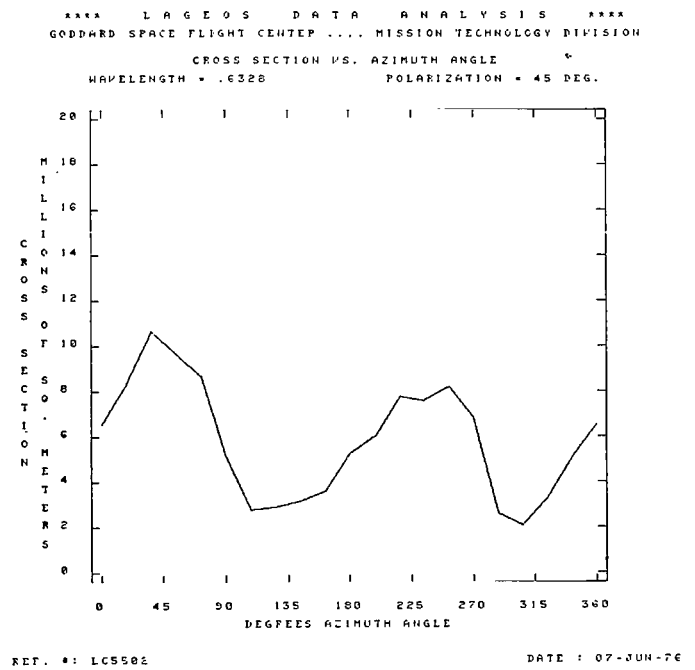

Figure 43.

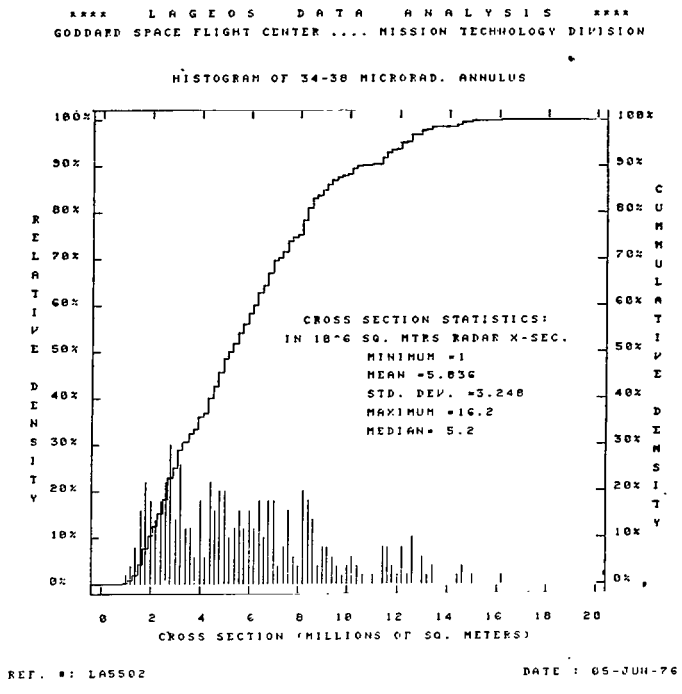

Figure 44.

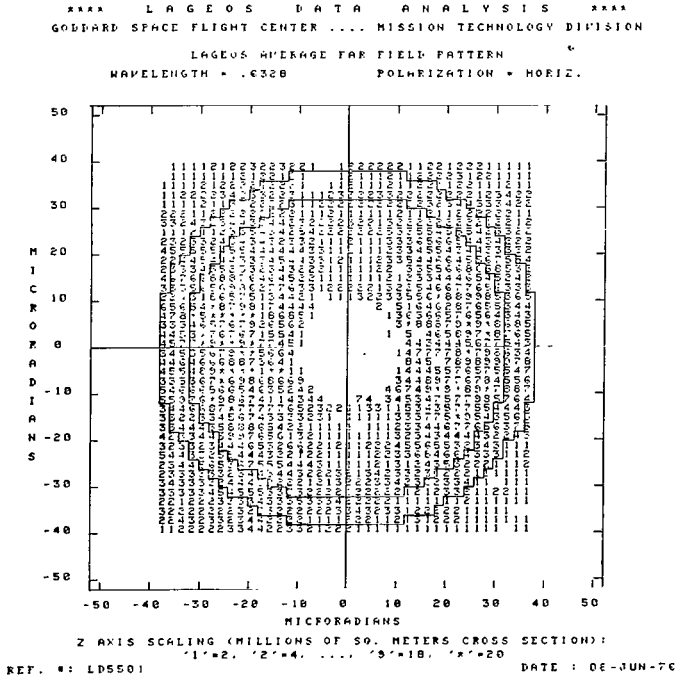

Figure 45.

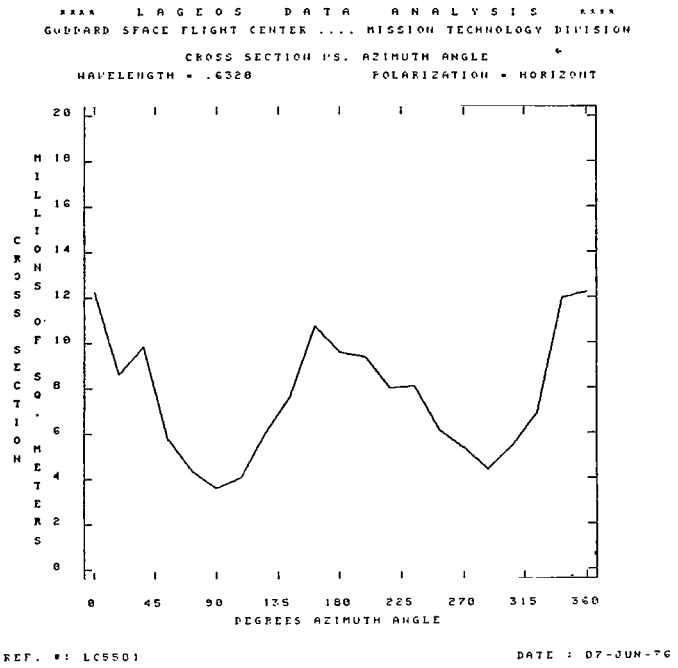

Figure 46.

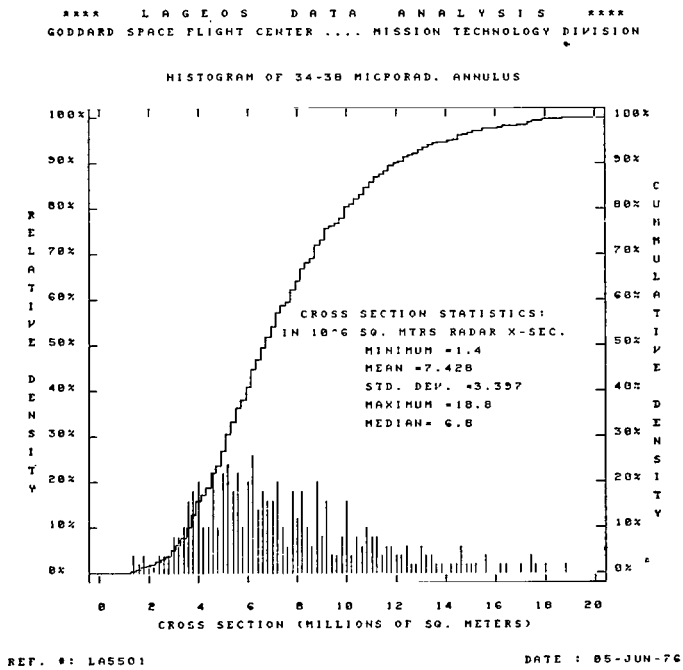

Figure 47.

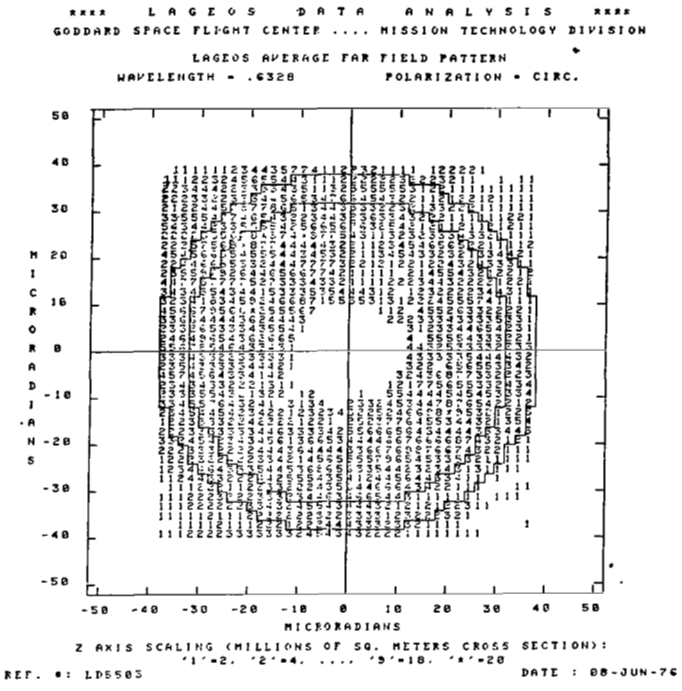

Figure 48.

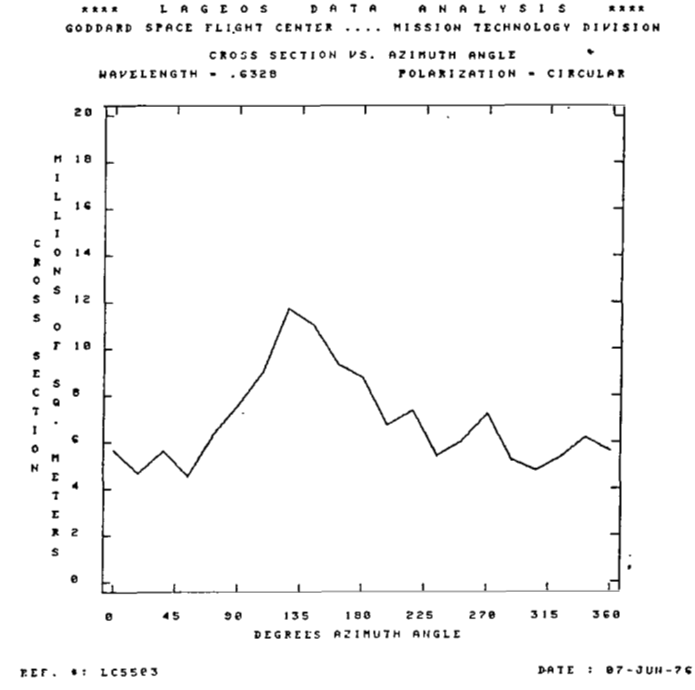

Figure 49.

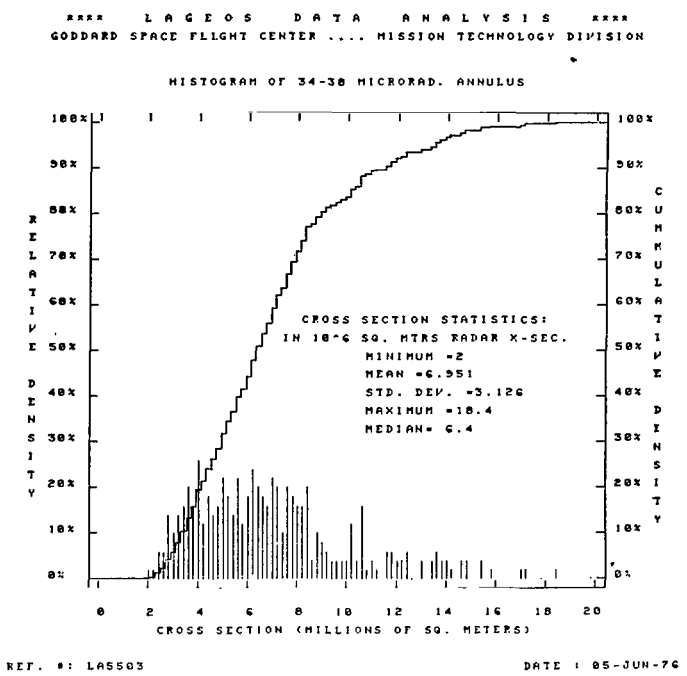

Figure 50.

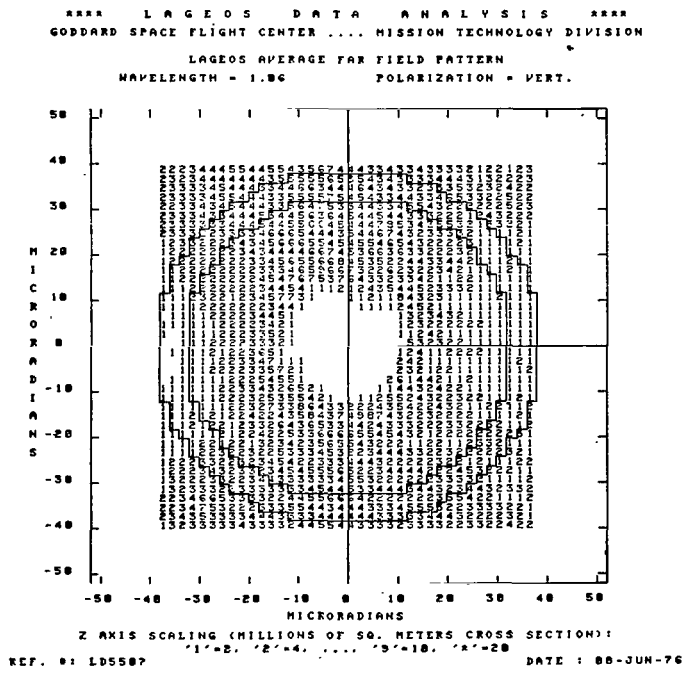

Figure 51.

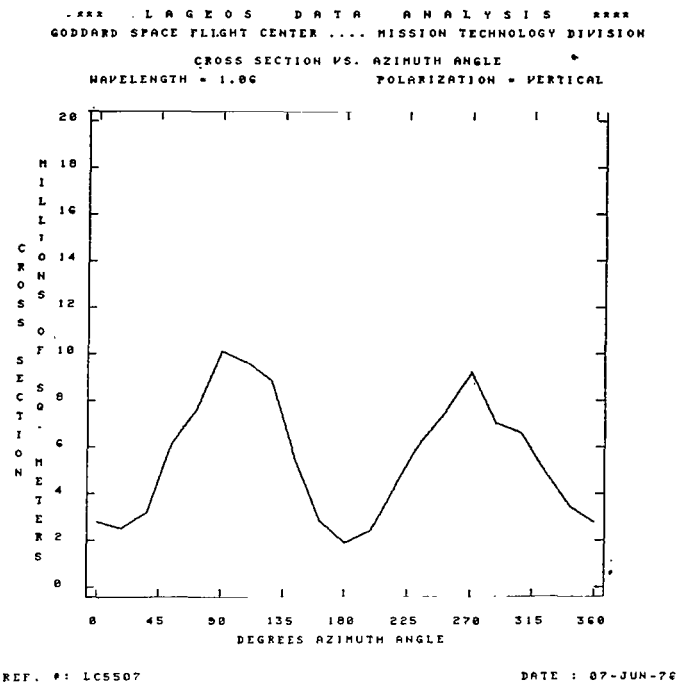

Figure 52.

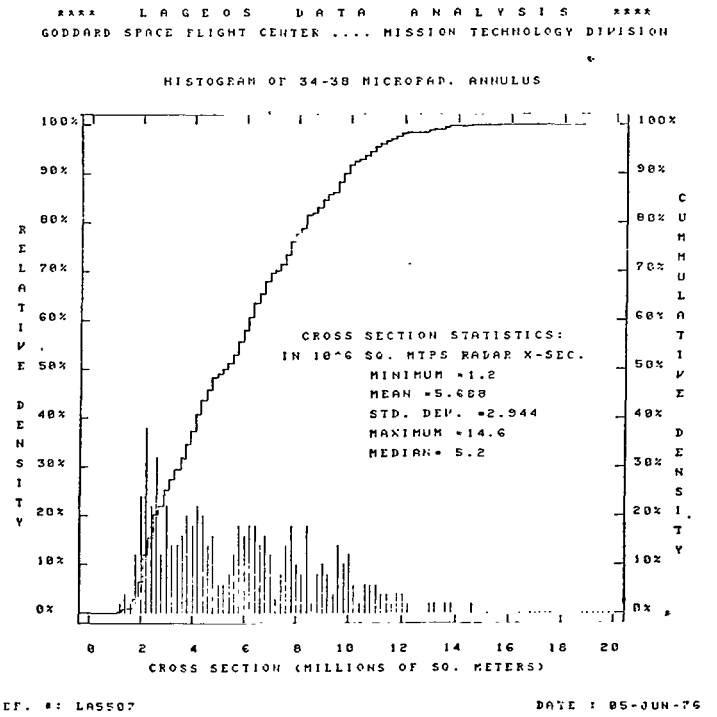

Figure 53.

Table 4
Index to Lidar Cross-Section Test Results

Wavelength (Angstroms)	Polarization	Figure Number		
		FFDP	Azimuth Curve	Histogram
4416	Vertical	3–9	3–10	3–11
5320	Horizontal	3–12	3–13	3–14
	Circular	3–15	3–16	3–17
6328	Vertical	3–18	3–19	3–20
	45 Degrees	3–21	3–22	3–23
	Horizontal	3–24	3–25	3–26
	Circular	3–27	3–28	3–29
10,640	Vertical	3–30	3–31	3–32

Cross Section

Maximum lidar cross section occurs at 5320 Å, with lower values at longer and shorter wavelengths. The area-weighted average cross section in the 34- to 38-μr annulus is listed as follows

Wavelength (Å)	Cross Section ($m^2 \times 10^6$)
4416	4.27
5320	7.12
6328	5.31
10,640	5.69

The far-field diffraction patterns (FFDP) show strong polarization-induced variations with azimuth. Testing and computer analysis proved that this effect was caused by the use of total internal reflection type cube corners. The variation in azimuth is approximately ±3 dB around the average for all wavelengths. The FFDP patterns measured during the tests and computer analysis indicate that the peak cross sections lie inside the 34- to 38-μr operational annulus at a radius of approximately 20 μr. (See graphs in the section "Lidar Cross-Section Tests" for details.)

ACKNOWLEDGMENTS

The Lageos test program reported in this document is the result of an intense joint effort of the Goddard Space Flight Center, the Bendix Corporation, and the Marshall Space Flight Center (MSFC) in the weeks immediately preceding launch. The authors wish to acknowledge and thank their coworkers at GSFC who made the success of these tests possible, in particular, the extraordinary efforts of Janis Bebris, Calvin Rossey, and Paul Weir throughout the preparation and implementation phases. The cooperation and steady assistance of Thomas

Zagwodzki, Don Premo, and Jack Coble is also gratefully acknowledged. The sometimes painful formalities of intercenter activities were minimized due to the efforts and continuous help of William Johnson of MSFC and Robert Spencer of the National Aeronautics and Space Administration Headquarters. The funding resources to carry out this work were supplied by Chris Stepanides, GSFC, whose early recognition of the importance of these tests was instrumental to their genesis. We are also most grateful for the performance and enthusiasm of the Bendix Corporation team led by John Bruger.

Theoretical analyses of the Lageos array by computer were performed with the assistance of the Computer Sciences Corporation (CSC). These analyses proved extremely useful in anticipating potential problem areas. In addition, CSC provided the technical documentation services for this report. Members of the CSC programming team to whom we are particularly indebted are John Kirk, Myrna Regardie, and John Zimmerman.

Goddard Space Flight Center
National Aeronautics and Space Administration
Greenbelt, Maryland July, 1977

REFERENCES

1. Siry, J. W., "The Lageos System," NASA/GSFC TM X-73072, December 1975.
2. McGunigal, T. E., W. J. Carrion, L. O. Caudill, C. R. Grant, T. S. Johnson, D. A. Premo, P. L. Spadin, and G. C. Winston, "Satellite Laser Ranging Work at the Goddard Space Flight Center," NASA/GSFC TM X-70948, July 1975.
3. Minott, P. O., "Measurement of the Lidar Cross Sections of Cube Corner Arrays for Laser Ranging of Satellites," NASA/GSFC TM X-70863, September 1974.
4. Zurasky, J. L., "Cube Corner Retroreflector Test and Analysis," *Applied Optics*, **15**(2), February 1976, pp. 445-452.
5. Minott, P. O., "Design of Retrodirector Arrays for Laser Ranging of Satellites," NASA/GSFC TM X-70657, March 1974.
6. David, I. B., "Communications Under the Poisson Regime," *IEEE Transactions on Information Theory*, **15**(1), January 1969, pp. 31-36.

APPENDIX A

ANALYSIS OF LAGEOS USING RETRO PROGRAM

An analysis of the Lageos array performance was done using the RETRO program, which was developed at GSFC for the analysis of cube corner arrays. The results of this analysis follow.

In the analysis procedure, cube corners that are beyond the angle at which total internal reflection occurs were assumed to have zero cross section. In actual test, it was found that due to Fresnel reflection these cube corners actually contributed to the cross section. For convenience, the analysis was done looking at the satellite from the south pole. This makes the cube corners lie in rings of equal incidence angle symmetrical about the pole, and facilities understanding how the array works. The analysis can be (and was) done at other angles, but these add no new information. On Unit 6, page 17,* the pole cube (No. 1) and six cube corners in a ring inclined at 10.1° contribute nearly all of the cross section (Nos. 2-7). The remainder of the cube corners are not effective. Since the optical positions of these six cube corners lie 255 mm from the CG, the CG correction is expected to be close to this value. An exact solution of the convolution of a 60-ps (FWHM) pulse is performed on Unit 11, page 2,* and confirms that the peak of the pulse indeed lies at 252.5 ± 2.5 mm, which is quite close to this row of six corners. The measured CG correction in this orientation was 250 mm, which is slightly less due to the contribution of cube corners operating in the Fresnel mode which are not included in the analysis.

On Unit 11, page 1,* a FFDP for the array is computed and displayed in the same format as used in the section, "Lidar Cross-Section Tests." A comparison of the calculated FFDP with the measured values shows a very close agreement. The peak cross section lies at the center, followed by a rapid drop, and then a secondary toroid surrounds the central maximum at a radius of approximately 20 to 25 μr. Cross section then rapidly falls off. A strong azimuthal asymmetry can be seen in both FFDP's caused by the use of total internal reflection type cube corners.

The cross section at the receiver position is indicated as 0.5† times the peak cross section, or approximately 13 million square meters, while the minimum value at the same radius is 0.2 times the peak cross section, or approximately 5.2 million square meters. The average value in the 34- to 38-μr annulus is approximately 70 percent higher than the measured value of 5.31 million square meters.

---

*Refers to the computer printout from the RETRO program (see pages A-3 through A-27).

†All values in the cross-section matrix are normalized to the peak value and have an implied decimal point in front of them.

The pulse shape (Unit 11, page 2)* shows a slight skewing towards the spacecraft CG, but the pulse width is only slightly larger than would be predicted from a point reflector.

Unit 11, page 3,* shows the effect of coherence upon the position of the centroids of individual pulses. As expected, the mode occurs at the peak of the predicted incoherent pulse, but the histogram is strongly skewed causing the average CG correction to be approximately 8 mm less than predicted by incoherent methods.

In summary, the calculations show very good correlation with measurement. Because of space limitations, only one sample of the many calculations made has been shown. However, on the basis of the results, it is believed that accurate prediction of Lageos performance can be made for system parameters not covered in the test program.

*Refers to the computer printout from the RETRO program (see pages A-3 through A-27).

RETROREFLECTOR ARRAY PERFORMANCE

MON NOV 29,1976

P. D. MINOTT CODE 722 GODDARD SPACE FLIGHT CENTER

PROGRAMMED BY

M. REGARDIE COMPUTER SCIENCES CORPORATION

J. KIRK COMPUTER SCIENCES CORPORATION

J. ZIMMERMAN COMPUTER SCIENCES CORPORATION

GIVEN VALUES

LASER INCIDENCE ANGLES		
POLAR ANGLE (THETA L)	0.0	DEGREES
AZIMUTH ANGLE (PHI L)	0.0	DEGREES
CUBE CORNER TYPE		
INDEX	1.4550	
ENTRANCE PUPIL		CIRCULAR
CONTROLLING DIMENSION		
DIAMETER	3.8100	CENTIMETERS
COATING CONSTANTS		
N	0.0	
K	0.0	
RHO	1.0000	
DIHEDRAL ANGLE OFFSET	1.2500	ARC-SECONDS
	1.2500	ARC-SECONDS
	1.2500	ARC-SECONDS

GIVEN VALUES

TRANSMITTER CHARACTERISTICS		
LASER WAVELENGTH	0.5320	MICROMETERS
GAUSSIAN PULSE (ONE STD. DEV.)	60.0000	PICOSECONDS
PULSE ENERGY	0.50	JOULES
TRANSMITTER DIVERGENCE	0.2500	MILLIRADIANS
TRANSMITTER OPTICAL EFFICIENCY	0.1100	
RECEIVER CHARACTERISTICS		
RECEIVER DIAMETER	0.51	METERS
RECEIVER OPTICAL EFFICIENCY	1.00	
PHOTOTUBE QUANTUM EFFICIENCY	0.025	
NUMBER OF PHOTOELECTRONS REQUIRED	10.00	
PATH CHARACTERISTICS		
SATELLITE APOGEE	5958.0000	KILOMETERS
SATELLITE PERIGEE	5854.0000	KILOMETERS
ALTITUDE USED IN MODEL CALCULATIONS	5900.0000	KILOMETERS
SATELLITE ZENITH ANGLE	0.0	DEGREES
SATELLITE VELOCITY VECTOR (OMEGA)	0.0	DEGREES

CALCULATED VALUES

TRANSMITTER CHARACTERISTICS		
PHOTON ENERGY	0.373D-18	JOULES
NUMBER OF PHOTONS/PULSE	0.1339D 19	
ANTENNA GAIN	0.5120D 0[illegible]	
STATION PARAMETER	0.4840D 24	SQUARE METERS
RECEIVER CHARACTERISTICS		
ANTENNA GAIN	0.9070D 13	
REQUIRED SIGNAL	0.1493D-15	JOULES
PATH CHARACTERISTICS		
RANGE	5900.0000	KILOMETERS
ATMOSPHERIC TRANSMISSION	0.7000	
PATH PARAMETER	0.2038D-30	METERS^{-4}
FAR FIELD COORDINATES		
POLAR ANGLE (PSI)	37.9915	MICRORADIANS
AZIMUTH ANGLE (ETA)	0.0	DEGREES
TARGET CROSS SECTION	13.4916	SQUARE METERS (IN MILLIONS)
SIGNAL		
PHOTOELECTRONS/PULSE	13.3	
MARGIN	1.33 1.24	DB

INTERFERENCE EFFECTS HISTOGRAM

LASER POLAR ANGLE 0.0 DEGREES
LASER AZIMUTH ANGLE 0.0 DEGREES

TIME (PICO SECONDS)	MIDPOINT DELTA R (METERS)		PERCENT PER BIN
-850.59	-0.1275	+	0.0
-883.94	-0.1325	+	0.0
-917.30	-0.1375	+	0.0
-950.66	-0.1425	+	0.0
-984.01	-0.1475	+	0.0
-1017.37	-0.1525	+	0.0
-1050.73	-0.1575	+	0.0
-1084.08	-0.1625	+	0.0
-1117.44	-0.1675	+	0.0
-1150.80	-0.1725	+	0.0
-1184.15	-0.1775	+	0.0
-1217.51	-0.1825	+	0.0
-1250.86	-0.1875	+	0.0
-1284.22	-0.1925	+	0.0
-1317.58	-0.1975	+	0.50
-1350.93	-0.2025	+	0.50
-1384.29	-0.2075	+	0.0
-1417.65	-0.2125	++	1.50
-1451.00	-0.2175	+++	3.00
-1484.36	-0.2225	+++	2.00
-1517.72	-0.2275	++++++	5.00
-1551.07	-0.2325	++++++++	7.00
-1584.43	-0.2375	+++++++++	8.00
-1617.79	-0.2425	++++++++	7.50
-1651.14	-0.2475	++++++++++++++++++++++	22.50
-1684.50	-0.2525	++++++++++++++++++++++++++++++++++	35.50
-1717.85	-0.2575	++++++++	7.00
-1751.21	-0.2625	+	0.0
-1784.57	-0.2675	+	0.0
-1817.92	-0.2725	+	0.0
-1851.28	-0.2775	+	0.0
-1884.64	-0.2825	+	0.0
-1917.99	-0.2875	+	0.0
-1951.35	-0.2925	+	0.0
		++	
		+ + + + + + + + + + +	100.00
		0 5 10 15 20 25 30 35 40 45 50	
		PROBABILITY DENSITY	

THE CENTROID IS -0.2443 METERS OR -1630.13 PICOSECONDS
THE STANDARD DEVIATION IS 0.0115 METERS
THE NUMBER OF SAMPLES = 200.0000

RESERVED FOR FUTURE USE

UNIT 6 PAGES 13-16

CUBE CORNER CROSS SECTIONS

CUBE CORNER	INCIDENCE ANGLE (DEGREES)	EFFECTIVE AREA ($METERS^2$)	GAIN	CROSS SECTION ($METERS^2 \times 10^6$)	DELTA R (METERS)	OPTICAL DELTA R (METERS)
1	0.0	0.11401D-02	0.24858D 10	2.8340	-0.2721	-0.2594
2	10.118	0.87776D-03	0.17098D 10	1.5008	-0.2678	-0.2550
3	10.118	0.87776D-03	0.31510D 10	2.7659	-0.2678	-0.2550
4	10.118	0.87776D-03	0.19294D 10	1.6936	-0.2678	-0.2550
5	10.118	0.87776D-03	0.10484D 10	0.9202	-0.2678	-0.2550
6	10.118	0.87776D-03	0.10484D 10	0.9202	-0.2678	-0.2550
7	10.118	0.87776D-03	0.19294D 10	1.6936	-0.2678	-0.2550
8	19.648	0.0	0.0	0.0	-0.2559	0.0
9	19.648	0.0	0.0	0.0	-0.2559	0.0
10	19.648	0.61803D-03	0.37583D 09	0.2323	-0.2559	-0.2427
11	19.648	0.0	0.0	0.0	-0.2559	0.0
12	19.648	0.0	0.0	0.0	-0.2559	0.0
13	19.648	0.0	0.0	0.0	-0.2559	0.0
14	19.648	0.61803D-03	0.28510D 09	0.1762	-0.2559	-0.2427
15	19.648	0.0	0.0	0.0	-0.2559	0.0
16	19.648	0.0	0.0	0.0	-0.2559	0.0
17	19.648	0.0	0.0	0.0	-0.2559	0.0
18	19.648	0.0	0.0	0.0	-0.2559	0.0
19	19.648	0.61803D-03	0.18002D 09	0.1113	-0.2559	-0.2427
20	29.579	0.0	0.0	0.0	-0.2366	0.0
21	29.579	0.0	0.0	0.0	-0.2366	0.0
22	29.579	0.0	0.0	0.0	-0.2366	0.0
23	29.579	0.0	0.0	0.0	-0.2366	0.0
24	29.579	0.0	0.0	0.0	-0.2366	0.0
25	29.579	0.0	0.0	0.0	-0.2366	0.0
26	29.579	0.0	0.0	0.0	-0.2366	0.0
27	29.579	0.0	0.0	0.0	-0.2366	0.0
28	29.579	0.0	0.0	0.0	-0.2366	0.0
29	29.579	0.0	0.0	0.0	-0.2366	0.0
30	29.579	0.0	0.0	0.0	-0.2366	0.0
31	29.579	0.0	0.0	0.0	-0.2366	0.0
32	29.579	0.0	0.0	0.0	-0.2366	0.0
33	29.579	0.0	0.0	0.0	-0.2366	0.0
34	29.579	0.0	0.0	0.0	-0.2366	0.0
35	29.579	0.37675D-03	0.97213D 09	0.3663	-0.2366	-0.2227
36	29.579	0.0	0.0	0.0	-0.2366	0.0
37	29.579	0.0	0.0	0.0	-0.2366	0.0
38	39.309	0.0	0.0	0.0	-0.2105	0.0
39	39.309	0.0	0.0	0.0	-0.2105	0.0
40	39.309	0.0	0.0	0.0	-0.2105	0.0
41	39.309	0.0	0.0	0.0	-0.2105	0.0
42	39.309	0.0	0.0	0.0	-0.2105	0.0
43	39.309	0.0	0.0	0.0	-0.2105	0.0
44	39.309	0.0	0.0	0.0	-0.2105	0.0
45	39.309	0.0	0.0	0.0	-0.2105	0.0
46	39.309	0.0	0.0	0.0	-0.2105	0.0
47	39.309	0.0	0.0	0.0	-0.2105	0.0
48	39.309	0.0	0.0	0.0	-0.2105	0.0
49	39.309	0.0	0.0	0.0	-0.2105	0.0
50	39.309	0.0	0.0	0.0	-0.2105	0.0

CUBE CORNER CROSS SECTIONS

CUBE CORNER	INCIDENCE ANGLE (DEGREES)	EFFECTIVE AREA ($METERS^2$)	GAIN	CROSS SECTION ($METERS^2 \times 10^6$)	DELTA R (METERS)	OPTICAL DELTA R (METERS)
51	39.309	0.0	0.0	0.0	-0.2105	0.0
52	39.309	0.0	0.0	0.0	-0.2105	0.0
53	39.309	0.178940-03	0.133390 10	0.2387	-0.2105	-0.1955
54	39.309	0.0	0.0	0.0	-0.2105	0.0
55	39.309	0.0	0.0	0.0	-0.2105	0.0
56	39.309	0.0	0.0	0.0	-0.2105	0.0
57	39.309	0.0	0.0	0.0	-0.2105	0.0
58	39.309	0.0	0.0	0.0	-0.2105	0.0
59	39.309	0.0	0.0	0.0	-0.2105	0.0
60	39.309	0.0	0.0	0.0	-0.2105	0.0
61	49.039	0.0	0.0	0.0	-0.1784	0.0
62	49.039	0.0	0.0	0.0	-0.1784	0.0
63	49.039	0.0	0.0	0.0	-0.1784	0.0
64	49.039	0.0	0.0	0.0	-0.1783	0.0
65	49.039	0.0	0.0	0.0	-0.1784	0.0
66	49.039	0.466330-04	0.414460 09	0.0193	-0.1784	-0.1619
67	49.039	0.0	0.0	0.0	-0.1783	0.0
68	49.039	0.0	0.0	0.0	-0.1783	0.0
69	49.039	0.0	0.0	0.0	-0.1784	0.0
70	49.039	0.0	0.0	0.0	-0.1783	0.0
71	49.039	0.0	0.0	0.0	-0.1783	0.0
72	49.039	0.0	0.0	0.0	-0.1783	0.0
73	49.039	0.0	0.0	0.0	-0.1783	0.0
74	49.039	0.0	0.0	0.0	-0.1783	0.0
75	49.039	0.0	0.0	0.0	-0.1783	0.0
76	49.039	0.0	0.0	0.0	-0.1783	0.0
77	49.039	0.0	0.0	0.0	-0.1784	0.0
78	49.039	0.0	0.0	0.0	-0.1784	0.0
79	49.039	0.0	0.0	0.0	-0.1783	0.0
80	49.039	0.466330-04	0.415460 09	0.0194	-0.1784	-0.1619
81	49.039	0.0	0.0	0.0	-0.1784	0.0
82	49.039	0.0	0.0	0.0	-0.1783	0.0
83	49.039	0.0	0.0	0.0	-0.1784	0.0
84	49.039	0.0	0.0	0.0	-0.1784	0.0
85	49.039	0.0	0.0	0.0	-0.1783	0.0
86	49.039	0.0	0.0	0.0	-0.1784	0.0
87	49.039	0.0	0.0	0.0	-0.1784	0.0
88	58.769	0.0	0.0	0.0	-0.1411	0.0
89	58.769	0.0	0.0	0.0	-0.1411	0.0
90	58.769	0.0	0.0	0.0	-0.1411	0.0
91	58.769	0.0	0.0	0.0	-0.1411	0.0
92	58.769	0.0	0.0	0.0	-0.1411	0.0
93	58.769	0.0	0.0	0.0	-0.1411	0.0
94	58.769	0.0	0.0	0.0	-0.1411	0.0
95	58.769	0.0	0.0	0.0	-0.1411	0.0
96	58.769	0.0	0.0	0.0	-0.1411	0.0
97	58.769	0.0	0.0	0.0	-0.1411	0.0
98	58.769	0.0	0.0	0.0	-0.1411	0.0
99	58.769	0.0	0.0	0.0	-0.1411	0.0
100	58.769	0.0	0.0	0.0	-0.1411	0.0

CUBE CORNER CROSS SECTIONS

CUBE CORNER	INCIDENCE ANGLE (DEGREES)	EFFECTIVE AREA ($METERS^2$)	GAIN	CROSS SECTION ($METERS^2 \times 10^6$)	DELTA R (METERS)	OPTICAL DELTA R (METERS)
101	58.769	0.0	0.0	0.0	-0.1411	0.0
102	58.769	0.0	0.0	0.0	-0.1411	0.0
103	58.769	0.0	0.0	0.0	-0.1411	0.0
104	58.769	0.0	0.0	0.0	-0.1411	0.0
105	58.769	0.0	0.0	0.0	-0.1411	0.0
106	58.769	0.0	0.0	0.0	-0.1411	0.0
107	58.769	0.0	0.0	0.0	-0.1411	0.0
108	58.769	0.0	0.0	0.0	-0.1411	0.0
109	58.769	0.0	0.0	0.0	-0.1411	0.0
110	58.769	0.0	0.0	0.0	-0.1411	0.0
111	58.769	0.0	0.0	0.0	-0.1411	0.0
112	58.769	0.0	0.0	0.0	-0.1411	0.0
113	58.769	0.0	0.0	0.0	-0.1411	0.0
114	58.769	0.0	0.0	0.0	-0.1411	0.0
115	58.769	0.0	0.0	0.0	-0.1411	0.0
116	58.769	0.0	0.0	0.0	-0.1411	0.0
117	58.769	0.0	0.0	0.0	-0.1411	0.0
118	58.769	0.0	0.0	0.0	-0.1411	0.0
119	67.018	0.0	0.0	0.0	-0.1062	0.0
120	67.018	0.0	0.0	0.0	-0.1062	0.0
121	67.018	0.0	0.0	0.0	-0.1062	0.0
122	67.018	0.0	0.0	0.0	-0.1062	0.0
123	67.018	0.0	0.0	0.0	-0.1062	0.0
124	67.018	0.0	0.0	0.0	-0.1062	0.0
125	67.018	0.0	0.0	0.0	-0.1062	0.0
126	67.018	0.0	0.0	0.0	-0.1062	0.0
127	67.018	0.0	0.0	0.0	-0.1062	0.0
128	67.018	0.0	0.0	0.0	-0.1062	0.0
129	67.018	0.0	0.0	0.0	-0.1062	0.0
130	67.018	0.0	0.0	0.0	-0.1062	0.0
131	67.018	0.0	0.0	0.0	-0.1062	0.0
132	67.018	0.0	0.0	0.0	-0.1062	0.0
133	67.018	0.0	0.0	0.0	-0.1062	0.0
134	67.018	0.0	0.0	0.0	-0.1062	0.0
135	67.018	0.0	0.0	0.0	-0.1062	0.0
136	67.018	0.0	0.0	0.0	-0.1062	0.0
137	67.018	0.0	0.0	0.0	-0.1062	0.0
138	67.018	0.0	0.0	0.0	-0.1062	0.0
139	67.018	0.0	0.0	0.0	-0.1062	0.0
140	67.018	0.0	0.0	0.0	-0.1062	0.0
141	67.018	0.0	0.0	0.0	-0.1062	0.0
142	67.018	0.0	0.0	0.0	-0.1062	0.0
143	67.018	0.0	0.0	0.0	-0.1062	0.0
144	67.018	0.0	0.0	0.0	-0.1062	0.0
145	67.018	0.0	0.0	0.0	-0.1062	0.0
146	67.018	0.0	0.0	0.0	-0.1062	0.0
147	67.018	0.0	0.0	0.0	-0.1062	0.0
148	67.018	0.0	0.0	0.0	-0.1062	0.0
149	67.018	0.0	0.0	0.0	-0.1062	0.0
150	76.748	0.0	0.0	0.0	-0.0624	0.0

CUBE CORNER CROSS SECTIONS

CUBE CORNER	INCIDENCE ANGLE (DEGREES)	EFFECTIVE AREA ($METERS^2$)	GAIN	CROSS SECTION ($METERS^2 \times 10^6$)	DELTA R (METERS)	OPTICAL DELTA R (METERS)
151	76.748	0.0	0.0	0.0	-0.0624	0.0
152	76.748	0.0	0.0	0.0	-0.0624	0.0
153	76.748	0.0	0.0	0.0	-0.0624	0.0
154	76.748	0.0	0.0	0.0	-0.0624	0.0
155	76.748	0.0	0.0	0.0	-0.0624	0.0
156	76.748	0.0	0.0	0.0	-0.0624	0.0
157	76.748	0.0	0.0	0.0	-0.0624	0.0
158	76.748	0.0	0.0	0.0	-0.0624	0.0
159	76.748	0.0	0.0	0.0	-0.0624	0.0
160	76.748	0.0	0.0	0.0	-0.0624	0.0
161	76.748	0.0	0.0	0.0	-0.0624	0.0
162	76.748	0.0	0.0	0.0	-0.0624	0.0
163	76.748	0.0	0.0	0.0	-0.0624	0.0
164	76.748	0.0	0.0	0.0	-0.0624	0.0
165	76.748	0.0	0.0	0.0	-0.0624	0.0
166	76.748	0.0	0.0	0.0	-0.0624	0.0
167	76.748	0.0	0.0	0.0	-0.0624	0.0
169	76.748	0.0	0.0	0.0	-0.0624	0.0
169	76.748	0.0	0.0	0.0	-0.0624	0.0
170	76.748	0.0	0.0	0.0	-0.0624	0.0
171	76.748	0.0	0.0	0.0	-0.0624	0.0
172	76.748	0.0	0.0	0.0	-0.0624	0.0
173	76.748	0.0	0.0	0.0	-0.0624	0.0
174	76.748	0.0	0.0	0.0	-0.0624	0.0
175	76.748	0.0	0.0	0.0	-0.0624	0.0
176	76.748	0.0	0.0	0.0	-0.0624	0.0
177	76.748	0.0	0.0	0.0	-0.0624	0.0
178	76.748	0.0	0.0	0.0	-0.0624	0.0
179	76.748	0.0	0.0	0.0	-0.0624	0.0
180	76.748	0.0	0.0	0.0	-0.0624	0.0
181	76.748	0.0	0.0	0.0	-0.0624	0.0
182	85.135	0.0	0.0	0.0	-0.0231	0.0
183	85.135	0.0	0.0	0.0	-0.0231	0.0
184	85.135	0.0	0.0	0.0	-0.0231	0.0
185	85.135	0.0	0.0	0.0	-0.0231	0.0
186	85.135	0.0	0.0	0.0	-0.0231	0.0
187	85.135	0.0	0.0	0.0	-0.0231	0.0
188	85.135	0.0	0.0	0.0	-0.0231	0.0
189	85.135	0.0	0.0	0.0	-0.0231	0.0
190	85.135	0.0	0.0	0.0	-0.0231	0.0
191	85.135	0.0	0.0	0.0	-0.0231	0.0
192	85.135	0.0	0.0	0.0	-0.0231	0.0
193	85.135	0.0	0.0	0.0	-0.0231	0.0
194	85.135	0.0	0.0	0.0	-0.0231	0.0
195	85.135	0.0	0.0	0.0	-0.0231	0.0
196	85.135	0.0	0.0	0.0	-0.0231	0.0
197	85.135	0.0	0.0	0.0	-0.0231	0.0
198	85.135	0.0	0.0	0.0	-0.0231	0.0
199	85.135	0.0	0.0	0.0	-0.0231	0.0
200	85.135	0.0	0.0	0.0	-0.0231	0.0

CUBE CORNER CROSS SECTIONS

CUBE CORNER	INCIDENCE ANGLE (DEGREES)	EFFECTIVE AREA ($METERS^2$)	GAIN	CROSS SECTION ($METERS^2 \times 10^6$)	DELTA R (METERS)	OPTICAL DELTA R (METERS)
201	85.135	0.0	0.0	0.0	-0.0231	0.0
202	85.135	0.0	0.0	0.0	-0.0231	0.0
203	85.135	0.0	0.0	0.0	-0.0231	0.0
204	85.135	0.0	0.0	0.0	-0.0231	0.0
205	85.135	0.0	0.0	0.0	-0.0231	0.0
206	85.135	0.0	0.0	0.0	-0.0231	0.0
207	85.135	0.0	0.0	0.0	-0.0231	0.0
208	85.135	0.0	0.0	0.0	-0.0231	0.0
209	85.135	0.0	0.0	0.0	-0.0231	0.0
210	85.135	0.0	0.0	0.0	-0.0231	0.0
211	85.135	0.0	0.0	0.0	-0.0231	0.0
212	85.135	0.0	0.0	0.0	-0.0231	0.0
213	85.135	0.0	0.0	0.0	-0.0231	0.0
214	94.865	0.0	0.0	0.0	-0.0231	0.0
215	94.865	0.0	0.0	0.0	-0.0231	0.0
216	94.865	0.0	0.0	0.0	-0.0231	0.0
217	94.865	0.0	0.0	0.0	-0.0231	0.0
218	94.865	0.0	0.0	0.0	-0.0231	0.0
219	94.865	0.0	0.0	0.0	-0.0231	0.0
220	94.865	0.0	0.0	0.0	-0.0231	0.0
221	94.865	0.0	0.0	0.0	-0.0231	0.0
222	94.865	0.0	0.0	0.0	-0.0231	0.0
223	94.865	0.0	0.0	0.0	-0.0231	0.0
224	94.865	0.0	0.0	0.0	-0.0231	0.0
225	94.865	0.0	0.0	0.0	-0.0231	0.0
226	94.865	0.0	0.0	0.0	-0.0231	0.0
227	94.865	0.0	0.0	0.0	-0.0231	0.0
228	94.865	0.0	0.0	0.0	-0.0231	0.0
229	94.865	0.0	0.0	0.0	-0.0231	0.0
230	94.865	0.0	0.0	0.0	-0.0231	0.0
231	94.865	0.0	0.0	0.0	-0.0231	0.0
232	94.865	0.0	0.0	0.0	-0.0231	0.0
233	94.865	0.0	0.0	0.0	-0.0231	0.0
234	94.865	0.0	0.0	0.0	-0.0231	0.0
235	94.865	0.0	0.0	0.0	-0.0231	0.0
236	94.865	0.0	0.0	0.0	-0.0231	0.0
237	94.865	0.0	0.0	0.0	-0.0231	0.0
238	94.865	0.0	0.0	0.0	-0.0231	0.0
239	94.865	0.0	0.0	0.0	-0.0231	0.0
240	94.865	0.0	0.0	0.0	-0.0231	0.0
241	94.865	0.0	0.0	0.0	-0.0231	0.0
242	94.865	0.0	0.0	0.0	-0.0231	0.0
243	94.865	0.0	0.0	0.0	-0.0231	0.0
244	94.865	0.0	0.0	0.0	-0.0231	0.0
245	94.865	0.0	0.0	0.0	-0.0231	0.0
246	103.252	0.0	0.0	0.0	-0.0624	0.0
247	103.252	0.0	0.0	0.0	-0.0624	0.0
248	103.252	0.0	0.0	0.0	-0.0624	0.0
249	103.252	0.0	0.0	0.0	-0.0624	0.0
250	103.252	0.0	0.0	0.0	-0.0624	0.0

CUBE CORNER CROSS SECTIONS

CUBE CORNER	INCIDENCE ANGLE (DEGREES)	EFFECTIVE AREA ($METERS^2$)	GAIN	CROSS SECTION ($METERS^2 \times 10^6$)	DELTA R (METERS)	OPTICAL DELTA R (METERS)
251	103.252	0.0	0.0	0.0	-0.0624	0.0
252	103.252	0.0	0.0	0.0	-0.0624	0.0
253	103.252	0.0	0.0	0.0	-0.0624	0.0
254	103.252	0.0	0.0	0.0	-0.0624	0.0
255	103.252	0.0	0.0	0.0	-0.0624	0.0
256	103.252	0.0	0.0	0.0	-0.0624	0.0
257	103.252	0.0	0.0	0.0	-0.0624	0.0
258	103.252	0.0	0.0	0.0	-0.0624	0.0
259	103.252	0.0	0.0	0.0	-0.0624	0.0
260	103.252	0.0	0.0	0.0	-0.0624	0.0
261	103.252	0.0	0.0	0.0	-0.0624	0.0
262	103.252	0.0	0.0	0.0	-0.0624	0.0
263	103.252	0.0	0.0	0.0	-0.0624	0.0
264	103.252	0.0	0.0	0.0	-0.0624	0.0
265	103.252	0.0	0.0	0.0	-0.0624	0.0
266	103.252	0.0	0.0	0.0	-0.0624	0.0
267	103.252	0.0	0.0	0.0	-0.0624	0.0
268	103.252	0.0	0.0	0.0	-0.0624	0.0
269	103.252	0.0	0.0	0.0	-0.0624	0.0
270	103.252	0.0	0.0	0.0	-0.0624	0.0
271	103.252	0.0	0.0	0.0	-0.0624	0.0
272	103.252	0.0	0.0	0.0	-0.0624	0.0
273	103.252	0.0	0.0	0.0	-0.0624	0.0
274	103.252	0.0	0.0	0.0	-0.0624	0.0
275	103.252	0.0	0.0	0.0	-0.0624	0.0
276	103.252	0.0	0.0	0.0	-0.0624	0.0
277	103.252	0.0	0.0	0.0	-0.0624	0.0
278	112.982	0.0	0.0	0.0	-0.1062	0.0
279	112.982	0.0	0.0	0.0	-0.1062	0.0
280	112.982	0.0	0.0	0.0	-0.1062	0.0
281	112.982	0.0	0.0	0.0	-0.1062	0.0
282	112.982	0.0	0.0	0.0	-0.1062	0.0
283	112.982	0.0	0.0	0.0	-0.1062	0.0
284	112.982	0.0	0.0	0.0	-0.1062	0.0
285	112.982	0.0	0.0	0.0	-0.1062	0.0
286	112.982	0.0	0.0	0.0	-0.1062	0.0
287	112.982	0.0	0.0	0.0	-0.1062	0.0
288	112.982	0.0	0.0	0.0	-0.1062	0.0
289	112.982	0.0	0.0	0.0	-0.1062	0.0
290	112.982	0.0	0.0	0.0	-0.1062	0.0
291	112.982	0.0	0.0	0.0	-0.1062	0.0
292	112.982	0.0	0.0	0.0	-0.1062	0.0
293	112.982	0.0	0.0	0.0	-0.1062	0.0
294	112.982	0.0	0.0	0.0	-0.1062	0.0
295	112.982	0.0	0.0	0.0	-0.1062	0.0
296	112.982	0.0	0.0	0.0	-0.1062	0.0
297	112.982	0.0	0.0	0.0	-0.1062	0.0
298	112.982	0.0	0.0	0.0	-0.1062	0.0
299	112.982	0.0	0.0	0.0	-0.1062	0.0
300	112.982	0.0	0.0	0.0	-0.1062	0.0

CUBE CORNER CROSS SECTIONS

CUBE CORNER	INCIDENCE ANGLE (DEGREES)	EFFECTIVE AREA ($METERS^2$)	GAIN	CROSS SECTION ($METERS^2 \times 10^6$)	DELTA R (METERS)	OPTICAL DELTA R (METERS)
301	112.982	0.0	0.0	0.0	-0.1062	0.0
302	112.982	0.0	0.0	0.0	-0.1062	0.0
303	112.982	0.0	0.0	0.0	-0.1062	0.0
304	112.982	0.0	0.0	0.0	-0.1062	0.0
305	112.982	0.0	0.0	0.0	-0.1062	0.0
306	112.982	0.0	0.0	0.0	-0.1062	0.0
307	112.982	0.0	0.0	0.0	-0.1062	0.0
308	112.982	0.0	0.0	0.0	-0.1062	0.0
309	121.231	0.0	0.0	0.0	-0.1411	0.0
310	121.231	0.0	0.0	0.0	-0.1411	0.0
311	121.231	0.0	0.0	0.0	-0.1411	0.0
312	121.231	0.0	0.0	0.0	-0.1411	0.0
313	121.231	0.0	0.0	0.0	-0.1411	0.0
314	121.231	0.0	0.0	0.0	-0.1411	0.0
315	121.231	0.0	0.0	0.0	-0.1411	0.0
316	121.231	0.0	0.0	0.0	-0.1411	0.0
317	121.231	0.0	0.0	0.0	-0.1411	0.0
318	121.231	0.0	0.0	0.0	-0.1411	0.0
319	121.231	0.0	0.0	0.0	-0.1411	0.0
320	121.231	0.0	0.0	0.0	-0.1411	0.0
321	121.231	0.0	0.0	0.0	-0.1411	0.0
322	121.231	0.0	0.0	0.0	-0.1411	0.0
323	121.231	0.0	0.0	0.0	-0.1411	0.0
324	121.231	0.0	0.0	0.0	-0.1411	0.0
325	121.231	0.0	0.0	0.0	-0.1411	0.0
326	121.231	0.0	0.0	0.0	-0.1411	0.0
327	121.231	0.0	0.0	0.0	-0.1411	0.0
328	121.231	0.0	0.0	0.0	-0.1411	0.0
329	121.231	0.0	0.0	0.0	-0.1411	0.0
330	121.231	0.0	0.0	0.0	-0.1411	0.0
331	121.231	0.0	0.0	0.0	-0.1411	0.0
332	121.231	0.0	0.0	0.0	-0.1411	0.0
333	121.231	0.0	0.0	0.0	-0.1411	0.0
334	121.231	0.0	0.0	0.0	-0.1411	0.0
335	121.231	0.0	0.0	0.0	-0.1411	0.0
336	121.231	0.0	0.0	0.0	-0.1411	0.0
337	121.231	0.0	0.0	0.0	-0.1411	0.0
338	121.231	0.0	0.0	0.0	-0.1411	0.0
339	121.231	0.0	0.0	0.0	-0.1411	0.0
340	130.961	0.0	0.0	0.0	-0.1784	0.0
341	130.961	0.0	0.0	0.0	-0.1784	0.0
342	130.961	0.0	0.0	0.0	-0.1784	0.0
343	130.961	0.0	0.0	0.0	-0.1783	0.0
344	130.961	0.0	0.0	0.0	-0.1784	0.0
345	130.961	0.0	0.0	0.0	-0.1784	0.0
346	130.961	0.0	0.0	0.0	-0.1783	0.0
347	130.961	0.0	0.0	0.0	-0.1783	0.0
348	130.961	0.0	0.0	0.0	-0.1784	0.0
349	130.961	0.0	0.0	0.0	-0.1783	0.0
350	130.961	0.0	0.0	0.0	-0.1783	0.0

CUBE CORNER CROSS SECTIONS

CUBE CORNER	INCIDENCE ANGLE (DEGREES)	EFFECTIVE AREA ($METERS^2$)	GAIN	CROSS SECTION ($METERS^2 \times 10^6$)	DELTA R (METERS)	OPTICAL DELTA R (METERS)
351	130.561	0.0	0.0	0.0	-0.1783	0.0
352	130.561	0.0	0.0	0.0	-0.1783	0.0
353	130.561	0.0	0.0	0.0	-0.1783	0.0
354	130.561	0.0	0.0	0.0	-0.1783	0.0
355	130.561	0.0	0.0	0.0	-0.1783	0.0
356	130.561	0.0	0.0	0.0	-0.1784	0.0
357	130.561	0.0	0.0	0.0	-0.1784	0.0
358	130.561	0.0	0.0	0.0	-0.1783	0.0
359	130.561	0.0	0.0	0.0	-0.1784	0.0
360	130.561	0.0	0.0	0.0	-0.1784	0.0
361	130.561	0.0	0.0	0.0	-0.1783	0.0
362	130.561	0.0	0.0	0.0	-0.1784	0.0
363	130.561	0.0	0.0	0.0	-0.1784	0.0
364	130.561	0.0	0.0	0.0	-0.1783	0.0
365	130.561	0.0	0.0	0.0	-0.1784	0.0
366	130.561	0.0	0.0	0.0	-0.1784	0.0
367	140.651	0.0	0.0	0.0	-0.2105	0.0
368	140.651	0.0	0.0	0.0	-0.2105	0.0
369	140.651	0.0	0.0	0.0	-0.2105	0.0
370	140.651	0.0	0.0	0.0	-0.2105	0.0
371	140.651	0.0	0.0	0.0	-0.2105	0.0
372	140.651	0.0	0.0	0.0	-0.2105	0.0
373	140.651	0.0	0.0	0.0	-0.2105	0.0
374	140.651	0.0	0.0	0.0	-0.2105	0.0
375	140.651	0.0	0.0	0.0	-0.2105	0.0
376	140.651	0.0	0.0	0.0	-0.2105	0.0
377	140.651	0.0	0.0	0.0	-0.2105	0.0
378	140.651	0.0	0.0	0.0	-0.2105	0.0
379	140.651	0.0	0.0	0.0	-0.2105	0.0
380	140.651	0.0	0.0	0.0	-0.2105	0.0
381	140.651	0.0	0.0	0.0	-0.2105	0.0
382	140.651	0.0	0.0	0.0	-0.2105	0.0
383	140.651	0.0	0.0	0.0	-0.2105	0.0
384	140.651	0.0	0.0	0.0	-0.2105	0.0
385	140.651	0.0	0.0	0.0	-0.2105	0.0
386	140.651	0.0	0.0	0.0	-0.2105	0.0
387	140.651	0.0	0.0	0.0	-0.2105	0.0
388	140.651	0.0	0.0	0.0	-0.2105	0.0
389	140.651	0.0	0.0	0.0	-0.2105	0.0
390	150.421	0.0	0.0	0.0	-0.2366	0.0
391	150.421	0.0	0.0	0.0	-0.2366	0.0
392	150.421	0.0	0.0	0.0	-0.2366	0.0
393	150.421	0.0	0.0	0.0	-0.2366	0.0
394	150.421	0.0	0.0	0.0	-0.2366	0.0
395	150.421	0.0	0.0	0.0	-0.2366	0.0
396	150.421	0.0	0.0	0.0	-0.2366	0.0
397	150.421	0.0	0.0	0.0	-0.2366	0.0
398	150.421	0.0	0.0	0.0	-0.2366	0.0
399	150.421	0.0	0.0	0.0	-0.2366	0.0
400	150.421	0.0	0.0	0.0	-0.2366	0.0

CUBE CORNER CROSS SECTIONS

CUBE CORNER	INCIDENCE ANGLE (DEGREES)	EFFECTIVE AREA ($METERS^2$)	GAIN	CROSS SECTION ($METERS^2 \times 10^6$)	DELTA R (METERS)	OPTICAL DELTA R (METERS)
401	15C.421	0.0	0.0	0.0	-0.2366	0.0
402	15C.421	0.0	0.0	0.0	-0.2366	0.0
403	15C.421	0.0	0.0	0.0	-0.2366	0.0
404	15C.421	0.0	0.0	0.0	-0.2366	0.0
405	15C.421	0.0	0.0	0.0	-0.2366	0.0
406	15C.421	0.0	0.0	0.0	-0.2366	0.0
407	15C.421	0.0	0.0	0.0	-0.2366	0.0
408	16C.151	0.0	0.0	0.0	-0.2559	0.0
409	16C.151	0.0	0.0	0.0	-0.2559	0.0
410	16C.151	0.0	0.0	0.0	-0.2559	0.0
411	16C.151	0.0	0.0	0.0	-0.2559	0.0
412	16C.151	0.0	0.0	0.0	-0.2559	0.0
413	16C.151	0.0	0.0	0.0	-0.2559	0.0
414	16C.151	0.0	0.0	0.0	-0.2559	0.0
415	16C.151	0.0	0.0	0.0	-0.2559	0.0
416	16C.151	0.0	0.0	0.0	-0.2559	0.0
417	16C.151	0.0	0.0	0.0	-0.2559	0.0
418	16C.151	0.0	0.0	0.0	-0.2559	0.0
419	16C.151	0.0	0.0	0.0	-0.2559	0.0
420	16S.881	0.0	0.0	0.0	-0.2678	0.0
421	16S.881	0.0	0.0	0.0	-0.2678	0.0
422	16S.881	0.0	0.0	0.0	-0.2678	0.0
423	16S.881	0.0	0.0	0.0	-0.2678	0.0
424	16S.881	0.0	0.0	0.0	-0.2678	0.0
425	16S.881	0.0	0.0	0.0	-0.2678	0.0
426	18C.CCC	0.0	0.0	0.0	-0.2721	0.0

THE SUM OF THE AREA= .H9097D-02
THE SUM OF THE CROSS SECTIONS= 13.4916 SQUARE METERS (IN MILLIONS)

CUBE CORNER COORDINATES

DISTANCES-METERS ANGLES-DEGREES

CUBE CORNER	CARTESIAN COORDINATES X	Y	Z	SPHERICAL COORDINATES R C	THETA C	PHI C	ORIENTATION ANGLES THETA N	PHI N	GAMMA
1	0.0	0.0	0.2721	0.2721	0.0	0.0	0.0	0.0	55.000
2	0.0478	0.0	0.2678	0.2721	10.118	0.0	10.118	0.0	91.000
3	0.0239	0.0414	0.2678	0.2721	10.118	60.000	10.118	60.000	65.000
4	-0.0239	0.0414	0.2678	0.2721	10.118	120.000	10.118	120.000	39.000
5	-0.0478	0.0000	0.2678	0.2721	10.118	180.000	10.118	180.000	13.000
6	-0.0239	-0.0414	0.2678	0.2721	10.118	240.000	10.118	240.000	107.000
7	0.0239	-0.0414	0.2678	0.2721	10.118	300.000	10.118	300.000	81.000
8	0.0924	0.0	0.2559	0.2721	19.848	0.0	19.848	0.0	43.000
9	0.0800	0.0462	0.2559	0.2721	19.848	30.000	19.848	30.000	17.000
10	0.0462	0.0800	0.2559	0.2721	19.848	60.000	19.848	60.000	111.000
11	0.0000	0.0924	0.2559	0.2721	19.848	90.000	19.848	90.000	85.000
12	-0.0462	0.0800	0.2559	0.2721	19.848	120.000	19.848	120.000	59.000
13	-0.0800	0.0462	0.2559	0.2721	19.848	150.000	19.848	150.000	33.000
14	-0.0924	0.0000	0.2559	0.2721	19.848	180.000	19.848	180.000	7.000
15	-0.0800	-0.0462	0.2559	0.2721	19.848	210.000	19.848	210.000	101.000
16	-0.0462	-0.0800	0.2559	0.2721	19.848	240.000	19.848	240.000	75.000
17	0.0000	-0.0924	0.2559	0.2721	19.848	270.000	19.848	270.000	49.000
18	0.0462	-0.0800	0.2559	0.2721	19.848	300.000	19.848	300.000	23.000
19	0.0800	-0.0462	0.2559	0.2721	19.848	330.000	19.848	330.000	117.000
20	0.1343	0.0	0.2366	0.2721	29.579	0.0	29.579	0.0	31.000
21	0.1262	0.0459	0.2366	0.2721	29.579	20.000	29.579	20.000	5.000
22	0.1029	0.0863	0.2366	0.2721	29.579	40.000	29.579	40.000	99.000
23	0.0671	0.1163	0.2366	0.2721	29.579	60.000	29.579	60.000	73.000
24	0.0233	0.1323	0.2366	0.2721	29.579	80.000	29.579	80.000	47.000
25	-0.0233	0.1323	0.2366	0.2721	29.579	100.000	29.579	100.000	21.000
26	-0.0671	0.1163	0.2366	0.2721	29.579	120.000	29.579	120.000	115.000
27	-0.1029	0.0863	0.2366	0.2721	29.579	140.000	29.579	140.000	89.000
28	-0.1262	0.0459	0.2366	0.2721	29.579	160.000	29.579	160.000	63.000
29	-0.1343	0.0000	0.2366	0.2721	29.579	180.000	29.579	180.000	37.000
30	-0.1262	-0.0459	0.2366	0.2721	29.579	200.000	29.579	200.000	11.000
31	-0.1029	-0.0863	0.2366	0.2721	29.579	220.000	29.579	220.000	105.000
32	-0.0671	-0.1163	0.2366	0.2721	29.579	240.000	29.579	240.000	79.000
33	-0.0233	-0.1323	0.2366	0.2721	29.579	260.000	29.579	260.000	53.000
34	0.0233	-0.1323	0.2366	0.2721	29.579	280.000	29.579	280.000	27.000
35	0.0671	-0.1163	0.2366	0.2721	29.579	300.000	29.579	300.000	1.000
36	0.1029	-0.0863	0.2366	0.2721	29.579	320.000	29.579	320.000	95.000
37	0.1262	-0.0459	0.2366	0.2721	29.579	340.000	29.579	340.000	69.000
38	0.1724	0.0	0.2105	0.2721	39.309	0.0	39.309	0.0	29.000
39	0.1660	0.0465	0.2105	0.2721	39.309	15.652	39.309	15.652	3.000
40	0.1473	0.0896	0.2105	0.2721	39.309	31.304	39.309	31.304	97.000
41	0.1170	0.1260	0.2105	0.2721	39.309	46.957	39.309	46.957	71.000
42	0.0793	0.1530	0.2105	0.2721	39.309	62.609	39.309	62.609	45.000
43	0.0351	0.1688	0.2105	0.2721	39.309	78.261	39.309	78.261	19.000
44	-0.0118	0.1720	0.2105	0.2721	39.309	93.913	39.309	93.913	113.000
45	-0.0577	0.1624	0.2105	0.2721	39.309	109.566	39.309	109.566	87.000
46	-0.0954	0.1408	0.2105	0.2721	39.309	125.218	39.309	125.218	61.000
47	-0.1237	0.1088	0.2105	0.2721	39.309	140.870	39.309	140.870	35.000
48	-0.1581	0.0687	0.2105	0.2721	39.309	156.522	39.309	156.522	9.000
49	-0.1708	0.0235	0.2105	0.2721	39.309	172.174	39.309	172.174	103.000
50	-0.1708	-0.0235	0.2105	0.2721	39.309	187.826	39.309	187.826	77.000

CUBE CORNER COORDINATES

DISTANCES-METERS ANGLES-DEGREES

CUBE CORNER	CARTESIAN COORDINATES X	Y	Z	SPHERICAL COORDINATES R C	THETA C	PHI C	ORIENTATION ANGLES THETA N	PHI N	GAMMA
51	-0.1561	-0.0687	0.2105	0.2721	39.309	203.479	39.309	203.479	51.000
52	-0.1337	-0.1088	0.2105	0.2721	39.309	219.131	39.309	219.131	25.000
53	-0.0994	-0.1408	0.2105	0.2721	39.309	234.783	39.309	234.783	119.000
54	-0.0577	-0.1624	0.2105	0.2721	39.309	250.435	39.309	250.435	93.000
55	-0.0118	-0.1720	0.2105	0.2721	39.309	266.087	39.309	266.087	67.000
56	0.0351	-0.1688	0.2105	0.2721	39.309	281.739	39.309	281.739	41.000
57	0.0793	-0.1530	0.2105	0.2721	39.309	297.392	39.309	297.392	15.000
58	0.1176	-0.1260	0.2105	0.2721	39.309	313.044	39.309	313.044	109.000
59	0.1473	-0.0896	0.2105	0.2721	39.309	328.696	39.309	328.696	83.000
60	0.1660	-0.0465	0.2105	0.2721	39.309	344.348	39.309	344.348	57.000
61	0.2055	0.0	0.1784	0.2721	49.039	0.0	49.039	0.0	11.000
62	0.1999	0.0474	0.1784	0.2721	49.039	13.333	49.039	13.333	105.000
63	0.1836	0.0922	0.1784	0.2721	49.039	26.667	49.039	26.667	79.000
64	0.1574	0.1321	0.1783	0.2721	49.039	40.000	49.039	40.000	53.000
65	0.1227	0.1648	0.1784	0.2721	49.039	53.333	49.039	53.333	27.000
66	0.0814	0.1887	0.1784	0.2721	49.039	66.666	49.039	66.666	1.000
67	0.0357	0.2023	0.1783	0.2721	49.039	80.000	49.039	80.000	95.000
68	-0.0119	0.2051	0.1783	0.2721	49.039	93.333	49.039	93.333	69.000
69	-0.0589	0.1968	0.1784	0.2721	49.039	106.666	49.039	106.666	43.000
70	-0.1027	0.1779	0.1783	0.2721	49.039	120.000	49.039	120.000	17.000
71	-0.1410	0.1494	0.1783	0.2721	49.039	133.333	49.039	133.333	111.000
72	-0.1716	0.1129	0.1783	0.2721	49.039	146.666	49.039	146.666	85.000
73	-0.1931	0.0703	0.1783	0.2721	49.039	160.000	49.039	160.000	59.000
74	-0.2041	0.0239	0.1783	0.2721	49.039	173.333	49.039	173.333	33.000
75	-0.2041	-0.0238	0.1783	0.2721	49.039	186.666	49.039	186.666	7.000
76	-0.1931	-0.0703	0.1783	0.2721	49.039	200.000	49.039	200.000	101.000
77	-0.1717	-0.1129	0.1784	0.2721	49.039	213.333	49.039	213.333	75.000
78	-0.1410	-0.1494	0.1784	0.2721	49.039	226.666	49.039	226.666	49.000
79	-0.1027	-0.1779	0.1783	0.2721	49.039	239.999	49.039	239.999	23.000
80	-0.0589	-0.1968	0.1784	0.2721	49.039	253.333	49.039	253.333	117.000
81	-0.0119	-0.2051	0.1784	0.2721	49.039	266.666	49.039	266.666	91.000
82	0.0357	-0.2023	0.1783	0.2721	49.039	279.999	49.039	279.999	65.000
83	0.0814	-0.1887	0.1784	0.2721	49.039	293.333	49.039	293.333	39.000
84	0.1227	-0.1648	0.1784	0.2721	49.039	306.666	49.039	306.666	13.000
85	0.1574	-0.1321	0.1783	0.2721	49.039	319.999	49.039	319.999	107.000
86	0.1836	-0.0922	0.1784	0.2721	49.039	333.333	49.039	333.333	81.000
87	0.1999	-0.0474	0.1784	0.2721	49.039	346.666	49.039	346.666	55.000
88	0.2326	0.0	0.1411	0.2721	58.769	0.0	58.769	0.0	97.000
89	0.2279	0.0468	0.1411	0.2721	58.769	11.613	58.769	11.613	71.000
90	0.2138	0.0917	0.1411	0.2721	58.769	23.226	58.769	23.226	45.000
91	0.1909	0.1329	0.1411	0.2721	58.769	34.839	58.769	34.839	19.000
92	0.1603	0.1686	0.1411	0.2721	58.769	46.451	58.769	46.451	113.000
93	0.1231	0.1974	0.1411	0.2721	58.769	58.065	58.769	58.065	87.000
94	0.0808	0.2182	0.1411	0.2721	58.769	69.677	58.769	69.677	61.000
95	0.0352	0.2300	0.1411	0.2721	58.769	81.290	58.769	81.290	35.000
96	-0.0118	0.2323	0.1411	0.2721	58.769	92.903	58.769	92.903	9.000
97	-0.0583	0.2252	0.1411	0.2721	58.769	104.516	58.769	104.516	103.000
98	-0.1025	0.2089	0.1411	0.2721	58.769	116.129	58.769	116.129	77.000
99	-0.1424	0.1840	0.1411	0.2721	58.769	127.742	58.769	127.742	51.000
100	-0.1765	0.1515	0.1411	0.2721	58.769	139.355	58.769	139.355	25.000

CUBE CORNER COORDINATES

DISTANCES-METERS ANGLES-DEGREES

CUBE CORNER	CARTESIAN COORDINATES X	Y	Z	SPHERICAL COORDINATES R C	THETA C	PHI C	ORIENTATION ANGLES THETA N	PHI N	GAMMA
101	-0.2034	0.1129	0.1411	0.2721	58.769	150.968	58.769	150.968	119.000
102	-0.2220	0.0696	0.1411	0.2721	58.769	162.581	58.769	162.581	93.000
103	-0.2314	0.0235	0.1411	0.2721	58.769	174.193	58.769	174.193	67.000
104	-0.2314	-0.0235	0.1411	0.2721	58.769	185.806	58.769	185.806	41.000
105	-0.2220	-0.0696	0.1411	0.2721	58.769	197.419	58.769	197.419	15.000
106	-0.2034	-0.1129	0.1411	0.2721	58.769	209.032	58.769	209.032	169.000
107	-0.1765	-0.1515	0.1411	0.2721	58.769	220.645	58.769	220.645	83.000
108	-0.1424	-0.1840	0.1411	0.2721	58.769	232.258	58.769	232.258	57.000
109	-0.1025	-0.2089	0.1411	0.2721	58.769	243.871	58.769	243.871	31.000
110	-0.0583	-0.2252	0.1411	0.2721	58.769	255.484	58.769	255.484	5.000
111	-0.0118	-0.2323	0.1411	0.2721	58.769	267.097	58.769	267.097	99.000
112	0.0352	-0.2300	0.1411	0.2721	58.769	278.710	58.769	278.710	73.000
113	0.0808	-0.2182	0.1411	0.2721	58.769	290.322	58.769	290.322	47.000
114	0.1231	-0.1974	0.1411	0.2721	58.769	301.936	58.769	301.936	21.000
115	0.1603	-0.1686	0.1411	0.2721	58.769	313.548	58.769	313.548	115.000
116	0.1909	-0.1329	0.1411	0.2721	58.769	325.161	58.769	325.161	89.000
117	0.2138	-0.0917	0.1411	0.2721	58.769	336.774	58.769	336.774	63.000
118	0.2279	-0.0469	0.1411	0.2721	58.769	348.387	58.769	348.387	37.000
119	0.2492	0.0253	0.1062	0.2721	67.018	5.806	67.018	5.806	63.000
120	0.2350	0.0750	0.1062	0.2721	67.018	17.420	67.018	17.420	37.000
121	0.2190	0.1216	0.1062	0.2721	67.018	29.032	67.018	29.032	11.000
122	0.1900	0.1632	0.1062	0.2721	67.018	40.645	67.018	40.645	105.000
123	0.1533	0.1981	0.1062	0.2721	67.018	52.258	67.018	52.258	79.000
124	0.1103	0.2249	0.1062	0.2721	67.018	63.871	67.018	63.871	53.000
125	0.0628	0.2425	0.1062	0.2721	67.018	75.484	67.018	75.484	27.000
126	0.0127	0.2502	0.1062	0.2721	67.018	87.097	67.018	87.097	1.000
127	-0.0379	0.2476	0.1062	0.2721	67.018	98.710	67.018	98.710	95.000
128	-0.0870	0.2349	0.1062	0.2721	67.018	110.322	67.018	110.322	69.000
129	-0.1325	0.2126	0.1062	0.2721	67.018	121.936	67.018	121.936	43.000
130	-0.1726	0.1815	0.1062	0.2721	67.018	133.548	67.018	133.548	17.000
131	-0.2056	0.1431	0.1062	0.2721	67.018	145.161	67.018	145.161	111.000
132	-0.2302	0.0988	0.1062	0.2721	67.018	156.774	67.018	156.774	85.000
133	-0.2453	0.0504	0.1062	0.2721	67.018	168.387	67.018	168.387	59.000
134	-0.2505	0.0000	0.1062	0.2721	67.018	180.000	67.018	180.000	33.000
135	-0.2453	-0.0504	0.1062	0.2721	67.018	191.613	67.018	191.613	7.000
136	-0.2302	-0.0988	0.1062	0.2721	67.018	203.226	67.018	203.226	101.000
137	-0.2056	-0.1431	0.1062	0.2721	67.018	214.839	67.018	214.839	75.000
138	-0.1726	-0.1815	0.1062	0.2721	67.018	226.452	67.018	226.452	49.000
139	-0.1325	-0.2126	0.1062	0.2721	67.018	238.065	67.018	238.065	23.000
140	-0.0870	-0.2349	0.1062	0.2721	67.018	249.677	67.018	249.677	117.000
141	-0.0379	-0.2476	0.1062	0.2721	67.018	261.291	67.018	261.291	91.000
142	0.0127	-0.2502	0.1062	0.2721	67.018	272.903	67.018	272.903	65.000
143	0.0628	-0.2425	0.1062	0.2721	67.018	284.516	67.018	284.516	39.000
144	0.1103	-0.2249	0.1062	0.2721	67.018	296.129	67.018	296.129	13.000
145	0.1533	-0.1981	0.1062	0.2721	67.018	307.742	67.018	307.742	107.000
146	0.1900	-0.1632	0.1062	0.2721	67.018	319.355	67.018	319.355	81.000
147	0.2190	-0.1216	0.1062	0.2721	67.018	330.968	67.018	330.968	55.000
148	0.2350	-0.0750	0.1062	0.2721	67.018	342.581	67.018	342.581	29.000
149	0.2492	-0.0253	0.1062	0.2721	67.018	354.193	67.018	354.193	3.000
150	0.2648	0.0	0.0624	0.2721	76.748	0.0	76.748	0.0	55.000

CUBE CORNER COORDINATES

DISTANCES-METERS ANGLES-DEGREES

CUBE CORNER	CARTESIAN COORDINATES X	Y	Z	SPHERICAL COORDINATES R	THETA C	PHI C	ORIENTATION ANGLES THETA N	PHI N	GAMMA
151	0.2557	0.0517	0.0624	0.2721	76.748	11.250	76.748	11.250	29.000
152	0.2447	0.1013	0.0624	0.2721	76.748	22.500	76.748	22.500	3.000
153	0.2202	0.1471	0.0624	0.2721	76.748	33.750	76.748	33.750	97.000
154	0.1873	0.1873	0.0624	0.2721	76.748	45.000	76.748	45.000	71.000
155	0.1471	0.2202	0.0624	0.2721	76.748	56.250	76.748	56.250	45.000
156	0.1013	0.2447	0.0624	0.2721	76.748	67.500	76.748	67.500	19.000
157	0.0517	0.2597	0.0624	0.2721	76.748	78.750	76.748	78.750	113.000
158	-0.0000	0.2648	0.0624	0.2721	76.748	90.000	76.748	90.000	87.000
159	-0.0517	0.2597	0.0624	0.2721	76.748	101.250	76.748	101.250	61.000
160	-0.1013	0.2447	0.0624	0.2721	76.748	112.500	76.748	112.500	35.000
161	-0.1471	0.2202	0.0624	0.2721	76.748	123.750	76.748	123.750	9.000
162	-0.1873	0.1873	0.0624	0.2721	76.748	135.000	76.748	135.000	103.000
163	-0.2202	0.1471	0.0624	0.2721	76.748	146.250	76.748	146.250	77.000
164	-0.2447	0.1013	0.0624	0.2721	76.748	157.500	76.748	157.500	51.000
165	-0.2597	0.0517	0.0624	0.2721	76.748	168.750	76.748	168.750	25.000
166	-0.2648	0.0000	0.0624	0.2721	76.748	180.000	76.748	180.000	119.000
167	-0.2597	-0.0517	0.0624	0.2721	76.748	191.250	76.748	191.250	93.000
168	-0.2447	-0.1013	0.0624	0.2721	76.748	202.500	76.748	202.500	67.000
169	-0.2202	-0.1471	0.0624	0.2721	76.748	213.750	76.748	213.750	41.000
170	-0.1873	-0.1873	0.0624	0.2721	76.748	225.000	76.748	225.000	15.000
171	-0.1471	-0.2202	0.0624	0.2721	76.748	236.250	76.748	236.250	109.000
172	-0.1013	-0.2447	0.0624	0.2721	76.748	247.500	76.748	247.500	83.000
173	-0.0517	-0.2597	0.0624	0.2721	76.748	258.750	76.748	258.750	57.000
174	0.0000	-0.2648	0.0624	0.2721	76.748	270.000	76.748	270.000	31.000
175	0.0517	-0.2597	0.0624	0.2721	76.748	281.250	76.748	281.250	5.000
176	0.1013	-0.2447	0.0624	0.2721	76.748	292.500	76.748	292.500	99.000
177	0.1471	-0.2202	0.0624	0.2721	76.748	303.750	76.748	303.750	73.000
178	0.1873	-0.1873	0.0624	0.2721	76.748	315.000	76.748	315.000	47.000
179	0.2202	-0.1471	0.0624	0.2721	76.748	326.250	76.748	326.250	21.000
180	0.2447	-0.1013	0.0624	0.2721	76.748	337.500	76.748	337.500	115.000
181	0.2597	-0.0517	0.0624	0.2721	76.748	348.750	76.748	348.750	89.000
182	0.2056	0.0266	0.0231	0.2721	85.135	5.625	85.135	5.625	47.000
183	0.2594	0.0787	0.0231	0.2721	85.135	16.875	85.135	16.875	21.000
184	0.2391	0.1278	0.0231	0.2721	85.135	28.125	85.135	28.125	115.000
185	0.2056	0.1720	0.0231	0.2721	85.135	39.375	85.135	39.375	89.000
186	0.1720	0.2096	0.0231	0.2721	85.135	50.625	85.135	50.625	63.000
187	0.1278	0.2391	0.0231	0.2721	85.135	61.875	85.135	61.875	37.000
188	0.0787	0.2594	0.0231	0.2721	85.135	73.125	85.135	73.125	11.000
189	0.0266	0.2698	0.0231	0.2721	85.135	84.375	85.135	84.375	105.000
190	-0.0266	0.2698	0.0231	0.2721	85.135	95.625	85.135	95.625	79.000
191	-0.0787	0.2594	0.0231	0.2721	85.135	106.875	85.135	106.875	53.000
192	-0.1278	0.2391	0.0231	0.2721	85.135	118.125	85.135	118.125	27.000
193	-0.1720	0.2096	0.0231	0.2721	85.135	129.375	85.135	129.375	1.000
194	-0.2056	0.1720	0.0231	0.2721	85.135	140.625	85.135	140.625	95.000
195	-0.2391	0.1278	0.0231	0.2721	85.135	151.875	85.135	151.875	69.000
196	-0.2594	0.0787	0.0231	0.2721	85.135	163.125	85.135	163.125	43.000
197	-0.2698	0.0266	0.0231	0.2721	85.135	174.375	85.135	174.375	17.000
198	-0.2698	-0.0266	0.0231	0.2721	85.135	185.625	85.135	185.625	111.000
199	-0.2594	-0.0787	0.0231	0.2721	85.135	196.875	85.135	196.875	85.000
200	-0.2391	-0.1278	0.0231	0.2721	85.135	208.125	85.135	208.125	59.000

CUBE CORNER COORDINATES

DISTANCES-METERS ANGLES-DEGREES

CUBE CORNER	CARTESIAN COORDINATES X	Y	Z	SPHERICAL COORDINATES R	THETA	PHI	ORIENTATION ANGLES THETA	PHI	GAMMA
				C	C	C	N	N	
201	-0.2356	-0.1720	0.0231	0.2721	85.135	219.375	85.135	219.375	33.000
202	-0.1720	-0.2096	0.0231	0.2721	85.135	230.625	85.135	230.625	7.000
203	-0.1278	-0.2391	0.0231	0.2721	85.135	241.875	85.135	241.875	101.000
204	-0.0787	-0.2594	0.0231	0.2721	85.135	253.125	85.135	253.125	75.000
205	-0.0266	-0.2698	0.0231	0.2721	85.135	264.375	85.135	264.375	49.000
206	0.0266	-0.2698	0.0231	0.2721	85.135	275.625	85.135	275.625	23.000
207	0.0787	-0.2594	0.0231	0.2721	85.135	286.875	85.135	286.875	117.000
208	0.1278	-0.2391	0.0231	0.2721	85.135	298.125	85.135	298.125	91.000
209	0.1720	-0.2096	0.0231	0.2721	85.135	309.375	85.135	309.375	65.000
210	0.2096	-0.1720	0.0231	0.2721	85.135	320.625	85.135	320.625	39.000
211	0.2391	-0.1278	0.0231	0.2721	85.135	331.875	85.135	331.875	13.000
212	0.2594	-0.0787	0.0231	0.2721	85.135	343.125	85.135	343.125	107.000
213	0.2698	-0.0266	0.0231	0.2721	85.135	354.375	85.135	354.375	81.000
214	0.2698	0.0266	-0.0231	0.2721	94.865	5.625	94.865	5.625	94.000
215	0.2594	0.0787	-0.0231	0.2721	94.865	16.875	94.865	16.875	68.000
216	0.2391	0.1278	-0.0231	0.2721	94.865	28.125	94.865	28.125	42.000
217	0.2096	0.1720	-0.0231	0.2721	94.865	39.375	94.865	39.375	16.000
218	0.1720	0.2096	-0.0231	0.2721	94.865	50.625	94.865	50.625	110.000
219	0.1278	0.2391	-0.0231	0.2721	94.865	61.875	94.865	61.875	84.000
220	0.0787	0.2594	-0.0231	0.2721	94.865	73.125	94.865	73.125	58.000
221	0.0266	0.2698	-0.0231	0.2721	94.865	84.375	94.865	84.375	32.000
222	-0.0266	0.2698	-0.0231	0.2721	94.865	95.625	94.865	95.625	6.000
223	-0.0787	0.2594	-0.0231	0.2721	94.865	106.875	94.865	106.875	100.000
224	-0.1278	-0.2391	-0.0231	0.2721	94.865	118.125	94.865	118.125	74.000
225	-0.1720	0.2096	-0.0231	0.2721	94.865	129.375	94.865	129.375	48.000
226	-0.2096	0.1720	-0.0231	0.2721	94.865	140.625	94.865	140.625	22.000
227	-0.2391	0.1278	-0.0231	0.2721	94.865	151.875	94.865	151.875	116.000
228	-0.2594	0.0787	-0.0231	0.2721	94.865	163.125	94.865	163.125	90.000
229	-0.2698	0.0266	-0.0231	0.2721	94.865	174.375	94.865	174.375	64.000
230	-0.2698	-0.0266	-0.0231	0.2721	94.865	185.625	94.865	185.625	38.000
231	-0.2594	-0.0787	-0.0231	0.2721	94.865	196.875	94.865	196.875	12.000
232	-0.2391	-0.1278	-0.0231	0.2721	94.865	208.125	94.865	208.125	106.000
233	-0.2096	-0.1720	-0.0231	0.2721	94.865	219.375	94.865	219.375	80.000
234	-0.1720	-0.2096	-0.0231	0.2721	94.865	230.625	94.865	230.625	54.000
235	-0.1278	-0.2391	-0.0231	0.2721	94.865	241.875	94.865	241.875	28.000
236	-0.0787	-0.2594	-0.0231	0.2721	94.865	253.125	94.865	253.125	2.000
237	-0.0266	-0.2698	-0.0231	0.2721	94.865	264.375	94.865	264.375	96.000
238	0.0266	-0.2698	-0.0231	0.2721	94.865	275.625	94.865	275.625	70.000
239	0.0787	-0.2594	-0.0231	0.2721	94.865	286.875	94.865	286.875	44.000
240	0.1278	-0.2391	-0.0231	0.2721	94.865	298.125	94.865	298.125	18.000
241	0.1720	-0.2096	-0.0231	0.2721	94.865	309.375	94.865	309.375	112.000
242	0.2096	-0.1720	-0.0231	0.2721	94.865	320.625	94.865	320.625	86.000
243	0.2391	-0.1278	-0.0231	0.2721	94.865	331.875	94.865	331.875	60.000
244	0.2594	-0.0787	-0.0231	0.2721	94.865	343.125	94.865	343.125	34.000
245	0.2698	-0.0266	-0.0231	0.2721	94.865	354.375	94.865	354.375	8.000
246	0.2648	0.0	-0.0624	0.2721	103.252	0.0	103.252	0.0	102.000
247	0.2597	0.0517	-0.0624	0.2721	103.252	11.250	103.252	11.250	76.000
248	0.2447	0.1013	-0.0624	0.2721	103.252	22.500	103.252	22.500	50.000
249	0.2202	0.1471	-0.0624	0.2721	103.252	33.750	103.252	33.750	24.000
250	0.1873	0.1873	-0.0624	0.2721	103.252	45.000	103.252	45.000	118.000

CUBE CORNER COORDINATES

DISTANCES-METERS ANGLES-DEGREES

CUBE CORNER	CARTESIAN COORDINATES X	Y	Z	SPHERICAL COORDINATES R	THETA	PHI	ORIENTATION ANGLES THETA	PHI	GAMMA
				C	C	C	N	N	
251	0.1471	0.2202	-0.0624	0.2721	103.252	56.250	103.252	56.250	92.000
252	0.1013	0.2447	-0.0624	0.2721	103.252	67.500	103.252	67.500	66.000
253	0.0517	0.2597	-0.0624	0.2721	103.252	78.750	103.252	78.750	40.000
254	-0.0000	0.2648	-0.0624	0.2721	103.252	90.000	103.252	90.000	14.000
255	-0.0517	0.2597	-0.0624	0.2721	103.252	101.250	103.252	101.250	108.000
256	-0.1013	0.2447	-0.0624	0.2721	103.252	112.500	103.252	112.500	82.000
257	-0.1471	0.2202	-0.0624	0.2721	103.252	123.750	103.252	123.750	56.000
258	-0.1873	0.1873	-0.0624	0.2721	103.252	135.000	103.252	135.000	30.000
259	-0.2202	0.1471	-0.0624	0.2721	103.252	146.250	103.252	146.250	4.000
260	-0.2447	0.1013	-0.0624	0.2721	103.252	157.500	103.252	157.500	98.000
261	-0.2597	0.0517	-0.0624	0.2721	103.252	168.750	103.252	168.750	72.000
262	-0.2648	0.0000	-0.0624	0.2721	103.252	180.000	103.252	180.000	46.000
263	-0.2597	-0.0517	-0.0624	0.2721	103.252	191.250	103.252	191.250	20.000
264	-0.2447	-0.1013	-0.0624	0.2721	103.252	202.500	103.252	202.500	114.000
265	-0.2202	-0.1471	-0.0624	0.2721	103.252	213.750	103.252	213.750	88.000
266	-0.1873	-0.1873	-0.0624	0.2721	103.252	225.000	103.252	225.000	62.000
267	-0.1471	-0.2202	-0.0624	0.2721	103.252	236.250	103.252	236.250	36.000
268	-0.1013	-0.2447	-0.0624	0.2721	103.252	247.500	103.252	247.500	10.000
269	-0.0517	-0.2597	-0.0624	0.2721	103.252	258.750	103.252	258.750	104.000
270	0.0000	-0.2648	-0.0624	0.2721	103.252	270.000	103.252	270.000	78.000
271	0.0517	-0.2597	-0.0624	0.2721	103.252	281.250	103.252	281.250	52.000
272	0.1013	-0.2447	-0.0624	0.2721	103.252	292.500	103.252	292.500	26.000
273	0.1471	-0.2202	-0.0624	0.2721	103.252	303.750	103.252	303.750	120.000
274	0.1873	-0.1873	-0.0624	0.2721	103.252	315.000	103.252	315.000	94.000
275	0.2202	-0.1471	-0.0624	0.2721	103.252	326.250	103.252	326.250	68.000
276	0.2447	-0.1013	-0.0624	0.2721	103.252	337.500	103.252	337.500	42.000
277	0.2597	-0.0517	-0.0624	0.2721	103.252	348.750	103.252	348.750	16.000
278	0.2492	0.0253	-0.1062	0.2721	112.982	5.806	112.982	5.806	110.000
279	0.2390	0.0750	-0.1062	0.2721	112.982	17.420	112.982	17.420	84.000
280	0.2190	0.1216	-0.1062	0.2721	112.982	29.032	112.982	29.032	58.000
281	0.1901	0.1632	-0.1062	0.2721	112.982	40.645	112.982	40.645	32.000
282	0.1535	0.1981	-0.1062	0.2721	112.982	52.258	112.982	52.258	6.000
283	0.1101	0.2249	-0.1062	0.2721	112.982	63.871	112.982	63.871	100.000
284	0.0628	0.2425	-0.1062	0.2721	112.982	75.484	112.982	75.484	74.000
285	0.0127	0.2502	-0.1062	0.2721	112.982	87.097	112.982	87.097	48.000
286	-0.0379	0.2476	-0.1062	0.2721	112.982	98.710	112.982	98.710	22.000
287	-0.0870	0.2349	-0.1062	0.2721	112.982	110.322	112.982	110.322	116.000
288	-0.1325	0.2126	-0.1062	0.2721	112.982	121.936	112.982	121.936	90.000
289	-0.1726	0.1815	-0.1062	0.2721	112.982	133.548	112.982	133.548	64.000
290	-0.2056	0.1431	-0.1062	0.2721	112.982	145.161	112.982	145.161	38.000
291	-0.2302	0.0988	-0.1062	0.2721	112.982	156.774	112.982	156.774	12.000
292	-0.2453	0.0504	-0.1062	0.2721	112.982	168.387	112.982	168.387	106.000
293	-0.2505	0.0000	-0.1062	0.2721	112.982	180.000	112.982	180.000	80.000
294	-0.2453	-0.0504	-0.1062	0.2721	112.982	191.613	112.982	191.613	54.000
295	-0.2302	-0.0988	-0.1062	0.2721	112.982	203.226	112.982	203.226	28.000
296	-0.2056	-0.1431	-0.1062	0.2721	112.982	214.839	112.982	214.839	2.000
297	-0.1726	-0.1815	-0.1062	0.2721	112.982	226.452	112.982	226.452	96.000
298	-0.1325	-0.2126	-0.1062	0.2721	112.982	238.065	112.982	238.065	70.000
299	-0.0870	-0.2349	-0.1062	0.2721	112.982	249.677	112.982	249.677	44.000
300	-0.0379	-0.2476	-0.1062	0.2721	112.982	261.291	112.982	261.291	18.000

CUBE CORNER COORDINATES

DISTANCES-METERS ANGLES-DEGREES

CUBE CORNER	CARTESIAN COORDINATES X	Y	Z	SPHERICAL COORDINATES R	THETA	PHI	ORIENTATION ANGLES THETA	PHI	GAMMA
				C	C	C	N	N	
301	0.0127	-0.2502	-0.1062	0.2721	112.982	272.903	112.982	272.903	112.000
302	0.0628	-0.2425	-0.1062	0.2721	112.982	284.516	112.982	284.516	86.000
303	0.1103	-0.2249	-0.1062	0.2721	112.982	296.129	112.982	296.129	60.000
304	0.1531	-0.1981	-0.1062	0.2721	112.982	307.742	112.982	307.742	34.000
305	0.1900	-0.1632	-0.1062	0.2721	112.982	319.355	112.982	319.355	8.000
306	0.2190	-0.1216	-0.1062	0.2721	112.982	330.968	112.982	330.968	102.000
307	0.2390	-0.0750	-0.1062	0.2721	112.982	342.581	112.982	342.581	76.000
308	0.2492	-0.0253	-0.1062	0.2721	112.982	354.193	112.982	354.193	50.000
309	0.2326	0.0	-0.1411	0.2721	121.231	0.0	121.231	0.0	24.000
310	0.2279	0.0468	-0.1411	0.2721	121.231	11.613	121.231	11.613	118.000
311	0.2138	0.0917	-0.1411	0.2721	121.231	23.226	121.231	23.226	92.000
312	0.1909	0.1329	-0.1411	0.2721	121.231	34.839	121.231	34.839	66.000
313	0.1603	0.1686	-0.1411	0.2721	121.231	46.451	121.231	46.451	40.000
314	0.1231	0.1974	-0.1411	0.2721	121.231	58.065	121.231	58.065	14.000
315	0.0808	0.2182	-0.1411	0.2721	121.231	69.677	121.231	69.677	108.000
316	0.0352	0.2300	-0.1411	0.2721	121.231	81.290	121.231	81.290	82.000
317	-0.0118	0.2323	-0.1411	0.2721	121.231	92.903	121.231	92.903	56.000
318	-0.0583	0.2252	-0.1411	0.2721	121.231	104.516	121.231	104.516	30.000
319	-0.1025	0.2089	-0.1411	0.2721	121.231	116.129	121.231	116.129	4.000
320	-0.1424	0.1840	-0.1411	0.2721	121.231	127.742	121.231	127.742	98.000
321	-0.1765	0.1515	-0.1411	0.2721	121.231	139.355	121.231	139.355	72.000
322	-0.2034	0.1129	-0.1411	0.2721	121.231	150.968	121.231	150.968	46.000
323	-0.2220	0.0696	-0.1411	0.2721	121.231	162.581	121.231	162.581	20.000
324	-0.2314	0.0235	-0.1411	0.2721	121.231	174.193	121.231	174.193	114.000
325	-0.2314	-0.0235	-0.1411	0.2721	121.231	185.806	121.231	185.806	88.000
326	-0.2220	-0.0696	-0.1411	0.2721	121.231	197.419	121.231	197.419	62.000
327	-0.2034	-0.1129	-0.1411	0.2721	121.231	209.032	121.231	209.032	36.000
328	-0.1765	-0.1515	-0.1411	0.2721	121.231	220.645	121.231	220.645	10.000
329	-0.1424	-0.1840	-0.1411	0.2721	121.231	232.258	121.231	232.258	104.000
330	-0.1025	-0.2089	-0.1411	0.2721	121.231	243.871	121.231	243.871	78.000
331	-0.0583	-0.2252	-0.1411	0.2721	121.231	255.484	121.231	255.484	52.000
332	-0.0118	-0.2323	-0.1411	0.2721	121.231	267.097	121.231	267.097	26.000
333	0.0352	-0.2300	-0.1411	0.2721	121.231	278.710	121.231	278.710	120.000
334	0.0808	-0.2182	-0.1411	0.2721	121.231	290.322	121.231	290.322	94.000
335	0.1231	-0.1974	-0.1411	0.2721	121.231	301.936	121.231	301.936	68.000
336	0.1603	-0.1686	-0.1411	0.2721	121.231	313.548	121.231	313.548	42.000
337	0.1909	-0.1329	-0.1411	0.2721	121.231	325.161	121.231	325.161	16.000
338	0.2138	-0.0917	-0.1411	0.2721	121.231	336.774	121.231	336.774	110.000
339	0.2279	-0.0468	-0.1411	0.2721	121.231	348.387	121.231	348.387	84.000
340	0.2085	0.0	-0.1784	0.2721	130.961	0.0	130.961	0.0	58.000
341	0.1999	0.0474	-0.1784	0.2721	130.961	13.333	130.961	13.333	32.000
342	0.1836	0.0922	-0.1784	0.2721	130.961	26.667	130.961	26.667	6.000
343	0.1574	0.1321	-0.1783	0.2721	130.961	40.000	130.961	40.000	100.000
344	0.1227	0.1648	-0.1784	0.2721	130.961	53.333	130.961	53.333	74.000
345	0.0814	0.1887	-0.1784	0.2721	130.961	66.666	130.961	66.666	48.000
346	0.0357	0.2023	-0.1783	0.2721	130.961	80.000	130.961	80.000	22.000
347	-0.0119	0.2051	-0.1783	0.2721	130.961	93.333	130.961	93.333	116.000
348	-0.0589	0.1968	-0.1784	0.2721	130.961	106.666	130.961	106.666	90.000
349	-0.1027	0.1779	-0.1783	0.2721	130.961	120.000	130.961	120.000	64.000
350	-0.1410	0.1494	-0.1783	0.2721	130.961	133.333	130.961	133.333	38.000

CUBE CORNER COORDINATES

DISTANCES-METERS ANGLES-DEGREES

CUBE CORNER	CARTESIAN COORDINATES X	Y	Z	SPHERICAL COORDINATES R	THETA	PHI	ORIENTATION ANGLES THETA	PHI	GAMMA
				C	C	C	N	N	
351	-0.1716	0.1129	-0.1783	0.2721	130.961	146.666	130.961	146.666	12.000
352	-0.1931	0.0703	-0.1783	0.2721	130.961	160.000	130.961	160.000	106.000
353	-0.2041	0.0239	-0.1783	0.2721	130.961	173.333	130.961	173.333	80.000
354	-0.2041	-0.0238	-0.1783	0.2721	130.961	186.666	130.961	186.666	54.000
355	-0.1931	-0.0703	-0.1783	0.2721	130.961	200.000	130.961	200.000	28.000
356	-0.1717	-0.1129	-0.1784	0.2721	130.961	213.333	130.961	213.333	2.000
357	-0.1410	-0.1494	-0.1784	0.2721	130.961	226.666	130.961	226.666	96.000
358	-0.1027	-0.1779	-0.1783	0.2721	130.961	239.999	130.961	239.999	70.000
359	-0.0589	-0.1968	-0.1784	0.2721	130.961	253.333	130.961	253.333	44.000
360	-0.0119	-0.2051	-0.1784	0.2721	130.961	266.666	130.961	266.666	18.000
361	0.0357	-0.2023	-0.1783	0.2721	130.961	279.999	130.961	279.999	112.000
362	0.0814	-0.1887	-0.1784	0.2721	130.961	293.333	130.961	293.333	86.000
363	0.1227	-0.1648	-0.1784	0.2721	130.961	306.666	130.961	306.666	60.000
364	0.1574	-0.1321	-0.1783	0.2721	130.961	319.999	130.961	319.999	34.000
365	0.1836	-0.0922	-0.1784	0.2721	130.961	333.333	130.961	333.333	8.000
366	0.1999	-0.0478	-0.1784	0.2721	130.961	346.666	130.961	346.666	102.000
367	0.1724	0.0	-0.2105	0.2721	140.691	0.0	140.691	0.0	76.000
368	0.1660	0.0465	-0.2105	0.2721	140.691	15.652	140.691	15.652	50.000
369	0.1473	0.0896	-0.2105	0.2721	140.691	31.304	140.691	31.304	24.000
370	0.1176	0.1260	-0.2105	0.2721	140.691	46.957	140.691	46.957	118.000
371	0.0793	0.1530	-0.2105	0.2721	140.691	62.609	140.691	62.609	92.000
372	0.0351	0.1688	-0.2105	0.2721	140.691	78.261	140.691	78.261	66.000
373	-0.0118	0.1720	-0.2105	0.2721	140.691	93.913	140.691	93.913	40.000
374	-0.0577	0.1624	-0.2105	0.2721	140.691	109.566	140.691	109.566	14.000
375	-0.0994	0.1408	-0.2105	0.2721	140.691	125.218	140.691	125.218	108.000
376	-0.1337	0.1088	-0.2105	0.2721	140.691	140.870	140.691	140.870	82.000
377	-0.1581	0.0687	-0.2105	0.2721	140.691	156.522	140.691	156.522	56.000
378	-0.1708	0.0235	-0.2105	0.2721	140.691	172.174	140.691	172.174	30.000
379	-0.1708	-0.0235	-0.2105	0.2721	140.691	187.826	140.691	187.826	4.000
380	-0.1581	-0.0687	-0.2105	0.2721	140.691	203.479	140.691	203.479	98.000
381	-0.1337	-0.1088	-0.2105	0.2721	140.691	219.131	140.691	219.131	72.000
382	-0.0994	-0.1408	-0.2105	0.2721	140.691	234.783	140.691	234.783	46.000
383	-0.0577	-0.1624	-0.2105	0.2721	140.691	250.435	140.691	250.435	20.000
384	-0.0118	-0.1720	-0.2105	0.2721	140.691	266.087	140.691	266.087	114.000
385	0.0351	-0.1688	-0.2105	0.2721	140.691	281.739	140.691	281.739	88.000
386	0.0793	-0.1530	-0.2105	0.2721	140.691	297.392	140.691	297.392	62.000
387	0.1176	-0.1260	-0.2105	0.2721	140.691	313.044	140.691	313.044	36.000
388	0.1473	-0.0896	-0.2105	0.2721	140.691	328.696	140.691	328.696	10.000
389	0.1660	-0.0465	-0.2105	0.2721	140.691	344.348	140.691	344.348	104.000
390	0.1343	0.0	-0.2366	0.2721	150.421	0.0	150.421	0.0	78.000
391	0.1262	0.0459	-0.2366	0.2721	150.421	20.000	150.421	20.000	52.000
392	0.1029	0.0863	-0.2366	0.2721	150.421	40.000	150.421	40.000	26.000
393	0.0671	0.1163	-0.2366	0.2721	150.421	60.000	150.421	60.000	120.000
394	0.0223	0.1323	-0.2366	0.2721	150.421	80.000	150.421	80.000	94.000
395	-0.0253	0.1323	-0.2366	0.2721	150.421	100.000	150.421	100.000	68.000
396	-0.0671	0.1163	-0.2366	0.2721	150.421	120.000	150.421	120.000	42.000
397	-0.1029	0.0863	-0.2366	0.2721	150.421	140.000	150.421	140.000	16.000
398	-0.1262	0.0459	-0.2366	0.2721	150.421	160.000	150.421	160.000	110.000
399	-0.1343	0.0000	-0.2366	0.2721	150.421	180.000	150.421	180.000	84.000
400	-0.1262	-0.0459	-0.2366	0.2721	150.421	200.000	150.421	200.000	58.000

CUBE CORNER COORDINATES'

DISTANCES-METERS ANGLES-DEGREES

CUBE CORNER	CARTESIAN COORDINATES X	Y	Z	SPHERICAL COORDINATES R C	THETA C	PHI C	ORIENTATION ANGLES THETA N	PHI N	GAMMA N
401	-0.1029	-0.0863	-0.2366	0.2721	150.421	220.000	150.421	220.000	32.000
402	-0.0671	-0.1163	-0.2366	0.2721	150.421	240.000	150.421	240.000	6.000
403	-0.0233	-0.1323	-0.2366	0.2721	150.421	260.000	150.421	260.000	100.000
404	0.0233	-0.1323	-0.2366	0.2721	150.421	280.000	150.421	280.000	74.000
405	0.0671	-0.1163	-0.2366	0.2721	150.421	300.000	150.421	300.000	48.000
406	0.1029	-0.0863	-0.2366	0.2721	150.421	320.000	150.421	320.000	22.000
407	0.1262	-0.0459	-0.2366	0.2721	150.421	340.000	150.421	340.000	116.000
408	0.0924	0.0	-0.2559	0.2721	160.151	0.0	160.151	0.0	90.000
409	0.0800	0.0462	-0.2559	0.2721	160.151	30.000	160.151	30.000	64.000
410	0.0462	0.0800	-0.2559	0.2721	160.151	60.000	160.151	60.000	38.000
411	0.0000	0.0924	-0.2559	0.2721	160.151	90.000	160.151	90.000	12.000
412	-0.0462	0.0800	-0.2559	0.2721	160.151	120.000	160.151	120.000	106.000
413	-0.0800	0.0462	-0.2559	0.2721	160.151	150.000	160.151	150.000	80.000
414	-0.0924	0.0000	-0.2559	0.2721	160.151	180.000	160.151	180.000	54.000
415	-0.0800	-0.0462	-0.2559	0.2721	160.151	210.000	160.151	210.000	28.000
416	-0.0462	-0.0800	-0.2559	0.2721	160.151	240.000	160.151	240.000	-2.000
417	0.0000	-0.0924	-0.2559	0.2721	160.151	270.000	160.151	270.000	96.000
418	0.0462	-0.0800	-0.2559	0.2721	160.151	300.000	160.151	300.000	70.000
419	0.0800	-0.0462	-0.2559	0.2721	160.151	330.000	160.151	330.000	44.000
420	0.0478	0.0	-0.2678	0.2721	169.881	0.0	169.881	0.0	18.000
421	0.0239	0.0414	-0.2678	0.2721	169.881	60.000	169.881	60.000	112.000
422	-0.0239	0.0414	-0.2678	0.2721	169.881	120.000	169.881	120.000	86.000
423	-0.0478	0.0000	-0.2678	0.2721	169.881	180.000	169.881	180.000	60.000
424	-0.0239	-0.0414	-0.2678	0.2721	169.881	240.000	169.881	240.000	34.000
425	0.0239	-0.0414	-0.2678	0.2721	169.881	300.000	169.881	300.000	8.000
426	0.0000	0.0	-0.2721	0.2721	180.000	0.0	180.000	0.0	102.000

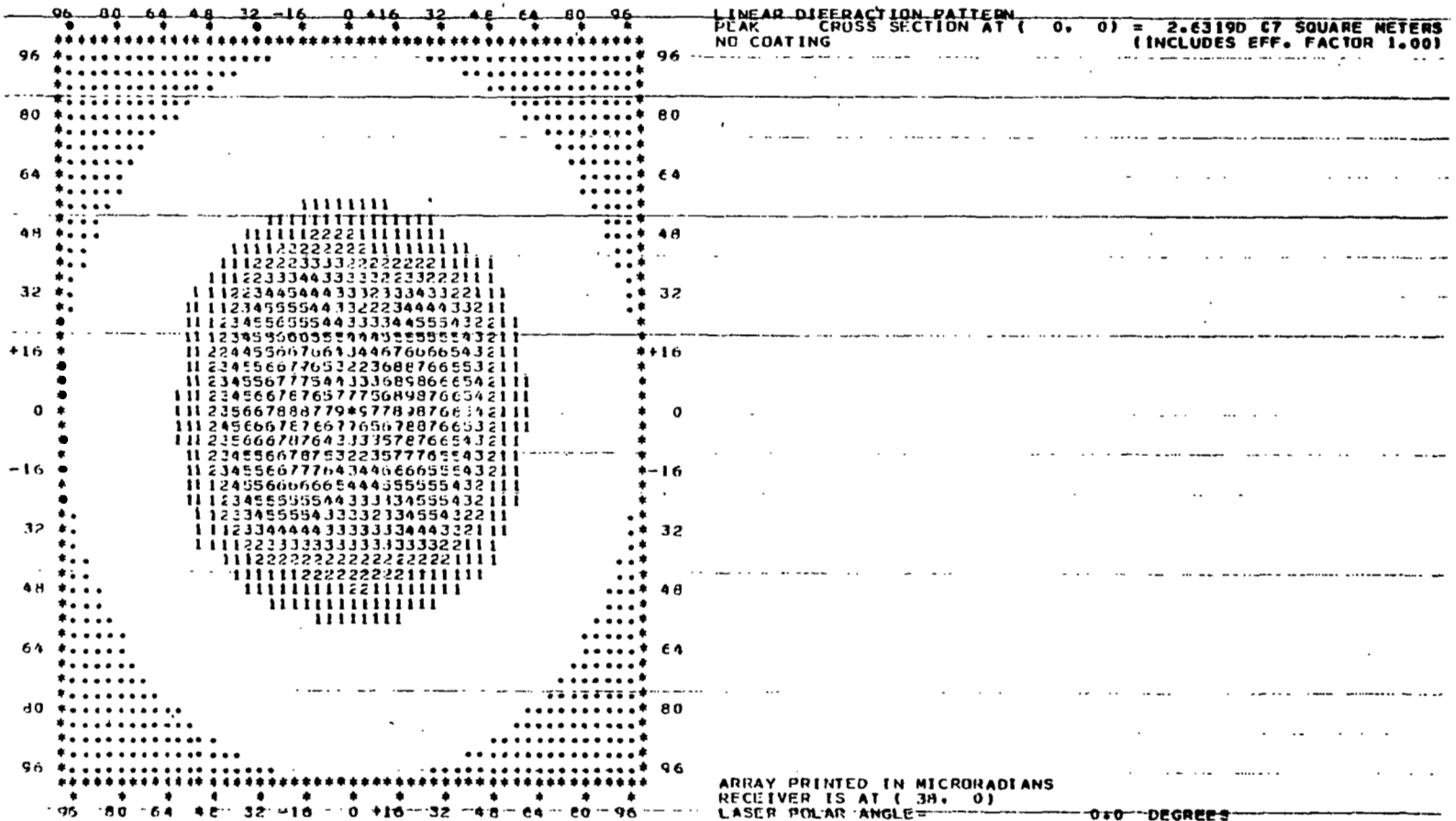
LINEAR DIFFRACTION PATTERN
PEAK CROSS SECTION AT (0. 0) = 2.6319D C7 SQUARE METERS
NO COATING
(INCLUDES EFF. FACTOR 1.00)
ARRAY PRINTED IN MICRORADIANS
RECEIVER IS AT (38. 0)
LASER POLAR ANGLE= 0.0 DEGREES
LASER AZIMUTH ANGLE= 0.0 DEGREES
LASER PLANE OF POLARIZATION= 0.0 DEGREES

IMPULSE RESPONSE HISTOGRAM

LASER POLAR ANGLE 0.0 DEGREES
LASER AZIMUTH ANGLE 0.0 DEGREES
ZENITH ANGLE 0.0 DEGREES

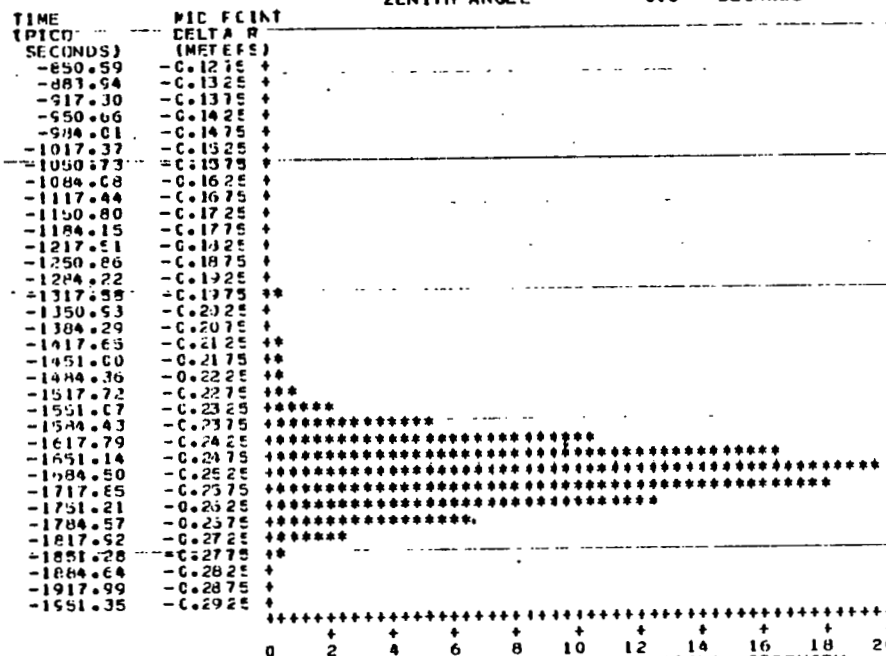

TIME (PICO SECONDS)	MIC POINT DELTA R (METERS)	PERCENT PHOTOELECTRONS	AVERAGE PHOTOELECTRONS PER BIN
-850.59	-0.1215	0.00	0.51821D-05
-883.94	-0.1325	0.00	0.36814D-04
-917.30	-0.1375	0.00	0.19331D-03
-950.66	-0.1425	0.01	0.75052D-03
-984.01	-0.1475	0.02	0.21548D-02
-1017.37	-0.1525	0.03	0.45762D-02
-1050.73	-0.1575	0.05	0.71902D-02
-1084.08	-0.1625	0.06	0.83907D-02
-1117.44	-0.1675	0.06	0.74172D-02
-1150.80	-0.1725	0.04	0.57685D-02
-1184.15	-0.1775	0.05	0.67836D-02
-1217.51	-0.1825	0.11	0.14040D-01
-1250.86	-0.1875	0.21	0.28466D-01
-1284.22	-0.1925	0.34	0.44730D-01
-1317.58	-0.1975	0.40	0.53387D-01
-1350.93	-0.2025	0.39	0.51448D-01
-1384.29	-0.2075	0.37	0.48686D-01
-1417.65	-0.2125	0.43	0.57091D-01
-1451.00	-0.2175	0.58	0.76540D-01
-1484.36	-0.2225	0.75	0.99785D-01
-1517.72	-0.2275	1.11	0.14733D 00
-1551.07	-0.2325	2.28	0.30307D 00
-1584.43	-0.2375	5.26	0.70053D 00
-1617.79	-0.2425	10.52	0.13998D 01
-1651.14	-0.2475	16.51	0.21974D 01
-1684.50	-0.2525	19.83	0.26389D 01
-1717.85	-0.2575	18.07	0.24050D 01
-1751.21	-0.2625	12.47	0.16592D 01
-1784.57	-0.2675	6.51	0.86632D 00
-1817.92	-0.2725	2.57	0.34240D 00
-1851.28	-0.2775	0.77	0.10245D 00
-1884.64	-0.2825	0.17	0.23187D-01
-1917.99	-0.2875	0.03	0.39671D-02
-1951.35	-0.2925	0.00	0.37947D-03
			0.13307D 02

PERCENT OF TOTAL RETURN SIGNAL STRENGTH

THE 10 - 90 PERCENT RISE TIME IS 109.64 PICOSECONDS
THE 90 - 10 PERCENT FALL TIME IS 121.88 PICOSECONDS
THE 50 - 50 PERCENT TIME INTERVAL IS 151.55 PICOSECONDS

THE CENTROID IS -0.2511 METERS OR -1675.29 PICOSECONDS
THE PEAK VALUE IS 0.52778D 03 PHOTOELECTRONS PER CENTIMETER

APPENDIX B

A SECOND METHOD OF MEASURING THE RANGE CORRECTION

The Lageos array is composed of 426 cube corners, four of which are germanium and have no effects upon the visible laser reflections. The velocity aberration deflects the reflected beam by 32.77 to 38.34 μr, and therefore the individual cube corners were designed with a 6.1-μr (1.25 arc-seconds) dihedral offset to compensate for the velocity aberration. The far-field pattern of each cube corner is a function of incidence angle (i), azimuth of the polarization vector (γ), wavelength (λ), and position in the far-field pattern (described by the polar coordinates ψ and η). If this functional dependence is known, the reflected pulse shape, the range correction, and the cross section can easily be computed by summing the contribution of each cube corner.

Unfortunately, such calculations can only be considered as a starting point because the actual "as produced" cube corners rarely conform to the specifications to the accuracy required for the calculations to be precise. However, such calculations are quite instructive in understanding the behavior of the array, and therefore a simple analysis of the array will be performed for one specific orientation.

To compute the return from an array of retroreflectors, the calculation starts with the individual cube corners. Their position and orientation on the satellite must be defined first. In the case of Lageos, if the cube corner location in polar coordinates is defined, the problem is greatly simplified because the radius for all cube corners is constant, and the position angles for each cube corner are identical to its orientation angles. This problem can be further simplified if a laser incidence direction is assumed in the south pole to north pole direction. In this case, the cube corners lie in several rings which are centered on the polar axis, and all the cube corners within a given ring have the same axial distance from the source.

The key to solving the problem is to determine the cross section of the individual cube corners as a function of angle of incidence and far-field coordinates. To do this, Lageos was placed in the FFDP test setup and this function was determined experimentally by recording the FFDP of each row individually. These FFDP's are shown in figures B-1 through B-5. On the basis of the analysis of these FFDP's, empirical equations for the cross section in the 32.77- to 38.34-μr annulus were developed and are shown with other pertinent parameters in table B-1. The rows are numbered from the south pole (row 0) backward toward the spacecraft CG. The number of cube corners in each row is shown in the second column. In the third column, the incidence angle is listed. In the fourth column is given the optical distance from the spacecraft CG which is computed by the formula:

$$Z = R_0 \cos i - L\sqrt{n^2 - \sin^2 i} \qquad \text{(B-1)}$$

Table B-1
Model of Lageos Cross-Section Parameters
Based Upon Row-by-Row FFDP Tests in
Polar Orientation (Viewing South Pole)*

Row	Number	Inclination Angle	Z	Cross Section†/ Computer Calculation
0	1	0	0.2567	$[1 + \cos(2\eta)]$
1	6	10.12	0.2533	$0.44\,[1 + 0.67\cos(2\eta)]$
2	12	19.85	0.2410	$0.24\,[1 + 0.33\cos(2\eta)]$
3	18	29.58	0.2210	$0.057\,[1 + 0.\cos(2\eta)]$

Total Cross Section† = $7.55 + 3.72\cos(2\eta)$

*For 32.77- to 38.34-μr Annulus in FFDP.

†In Millions of Square Meters with the Far-field Azimuth, η, Relative to the Polarization Vector in Degrees.

where R_0 is the radial location of the front face of the cube corner (298.07 mm), L is the depth of the cube corner (27.8 mm), and n is the refractive index (1.455). The last column lists the effective cross section of each cube corner in the row as a function of position in the far field. The quantity η is the azimuth angle with respect to the polarization vector. Cross sections are evaluated for the 32.77- to 38.34-μr annulus. With the data in table B-1, it is a simple matter to convolve each cube corner with the laser pulse and obtain a return pulse for each cube corner, the strength of which depends upon the orientation and polarization, and the position of which depends on its Z-position. This has been done for a 62.3-ps FWHM pulse (approximately the same as that used in the target-signature testing), and the results are shown in figure B-6. This figure shows the signal strength normalized to the peak value as a function of time referenced to the time at which a pulse would return from a point reflector at the spacecraft CG. As can be seen, due to the very short pulse length, the individual rows produce separate peaks. The first peak represents row 0 and row 1 because these rows are separated by only 4.3 mm (28.7 ps). However, the second row is 12.2 mm (82.0 ps) from the first row, and is therefore shown clearly as a separate peak. The third row is even further separated from the second (20.0 mm (133.3 ps)) and therefore also shows as a separate pulse. The rows beyond third row are at too steep an angle to produce any return. One thing is quite clear: as the far-field observation point azimuth moves farther away from the polarization azimuth, the energy in the reflected pulse decreases (energy in the pulse is proportional to the area under the curve). Further, the energy lost comes from the leading edge of the pulse. This causes the peak to shift backward towards the spacecraft CG as the cross polarization condition is reached. Figures B-7 and B-8 show the same type of curves for 125 and 250 ps, respectively. The range corrections derived from these curves are shown in table B-2.

Table B-2
Peak Detection Range Corrections

Azimuth Angle	Range Corrections (ps) for Pulse Widths*			Range Corrections (mm) for Pulse Widths*		
	62.5	125	250	62.5	125	250
0°	-1690	-1670	-1660	-253.5	-250.5	-249.0
45°	-1690	-1650	-1650	-253.5	-247.5	-247.5
90°	-1610	-1620	-1610	-241.5	-243.0	-241.5

*Pulse widths are defined by ps (FHWM) units.

To compare these calculations with data taken in the target signature tests, figure B-9 was made taking the photomultiplier tube response into account. The laser pulse has a Gaussian profile and a FWHM of 62.5 ps, and the photomultiplier has a 10- to 90-percent rise time of 150 ps. When these are combined (assuming a Gaussian photomultiplier impulse response), an effective Gaussian impulse response with a standard deviation of 92 ps (217-ps FWHM) is obtained. Due to the broadening of the pulse by the photomultiplier, all indication of the separate rows is lost. However, the polarization effects are still quite evident, amounting to a shift of approximately 6 mm for peak detection. If the detector uses 50-percent peak on the leading edge as a criteria, the shift increases only slightly to 6.5 mm.

It should also be noted that the range correction is a function of pulse length. When the laser pulse is convolved with the satellite response because of the skewness of the satellite response curve, the peak of the return pulse shifts towards the spacecraft CG. Figure B-9 shows the effect for the 0° polarization conditions for pulse lengths varying from 62.5 to 1000 ps. Table B-3 shows the positions of the peaks for the various pulse lengths.

In summary, on the basis of analysis derived from actual experimental FFDP, the range correction varies by as much as 8.5 mm with polarization and by up to 8.1 mm with pulse length. The actual value derived from target signature tests (249 ± 1.7 mm; see figure 18) agrees extremely well with the results from FFDP tests (figure B-10 and table B-4). In comparing these results, it should be kept in mind that the tests were taken over the entire annulus and represent an average range correction. Table B-4 lists the range correction as a function of far-field azimuth. When this table is weighted according to the relative intensity of the various far-field positions, an average range correction of 247.0 mm is obtained. The final result is that for all polarizations and pulse lengths, the range correction is 249^{+0}_{-16} mm for peak detection.

An analysis of figure B-10 also shows that the expected pulse width is 261-ps FWHM and appears to be in close agreement with the results. The slight increase of 21 ps (8 percent) over the experimentally measured value is probably due to the fact that the analysis was done for one special orientation, and errors in estimating the pulse width and photomultiplier rise time.

Table B-3
Range Correction as a Function of Pulse Length

Pulse Width (ps FWHM)	Range Correction	
	(ps)	(mm)
62.5	-1692	-253.8
125	-1654	-248.1
290	-1646	-246.9
500	-1640	-246.0
1000	-1638	-245.7

Table B-4
Peak Detection Range Correction
(Photomultiplier Response Included)

Azimuth Angle	Range Corrections for Pulse Width 62.5×10^{-12} sec (FWHM)	
	(ps)	(mm)
0°	-1660	-249.0
45°	-1650	-247.5
90°	-1620	-243.0

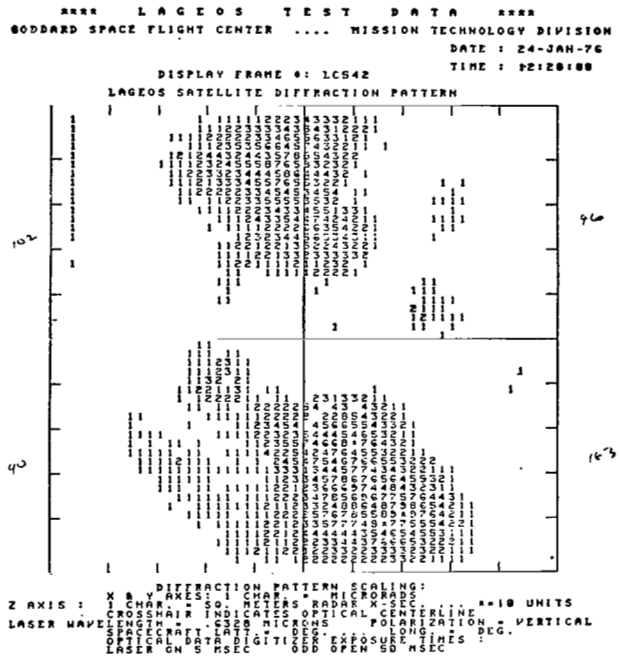

Figure B-1. FFDP of the Lageos Satellite's south pole (laser type: neutral density = 0.3).

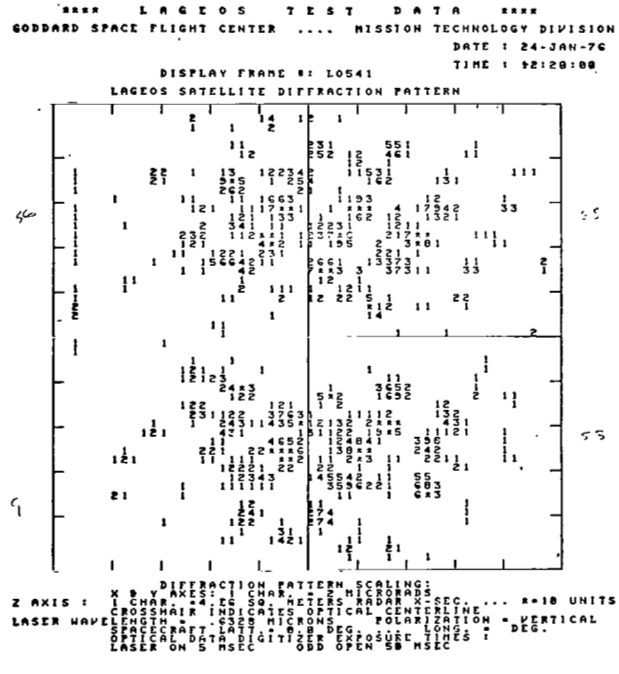

Figure B-2. FFDE of first row from south pole (laser type: neutral density = 1.0, incidence angle = 10.1°).

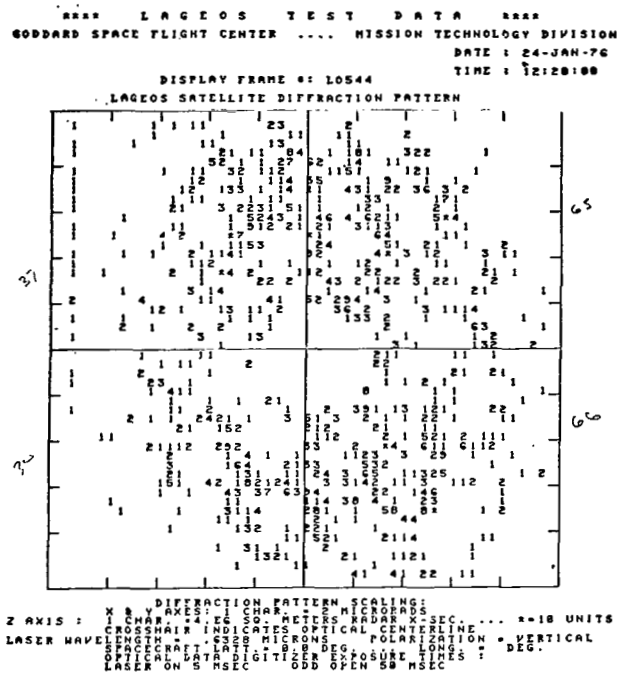

Figure B-3. FFDP of second row from south pole (laser type: neutral density = 1.0, incidence angle = 19.8°).

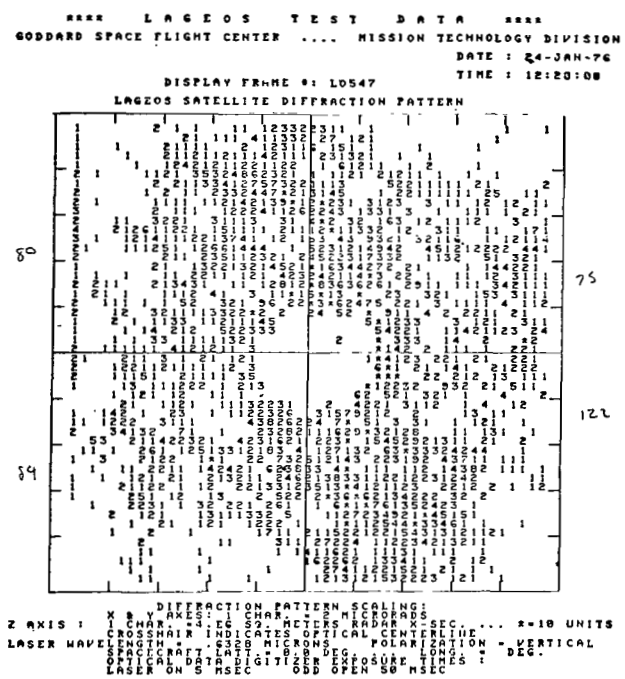

Figure B-4. FFDP of third row from south pole (laser type: neutral density = 0.3).

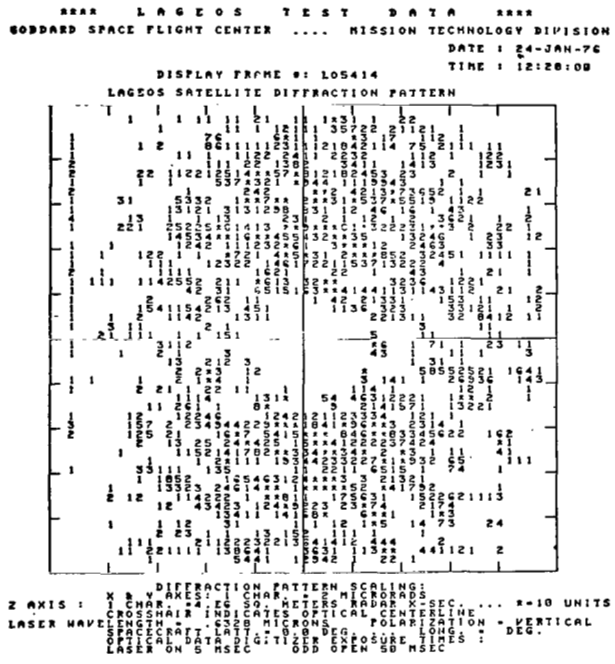

Figure B-5. FFDP of full satellite illumination from south pole (laser type: neutral density = 1.0).

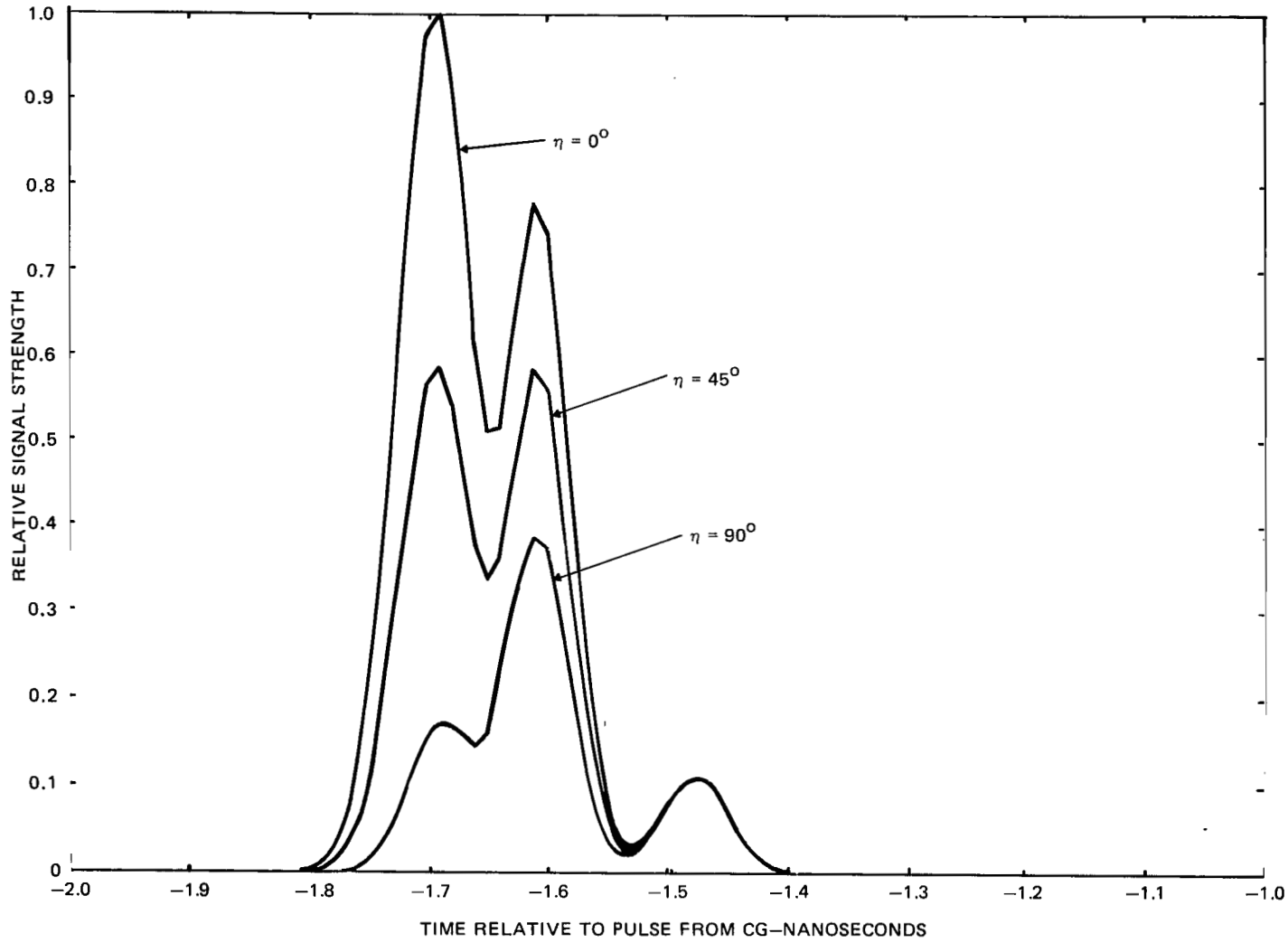

Figure B-6. Pulse return curves for 62.3 ps.

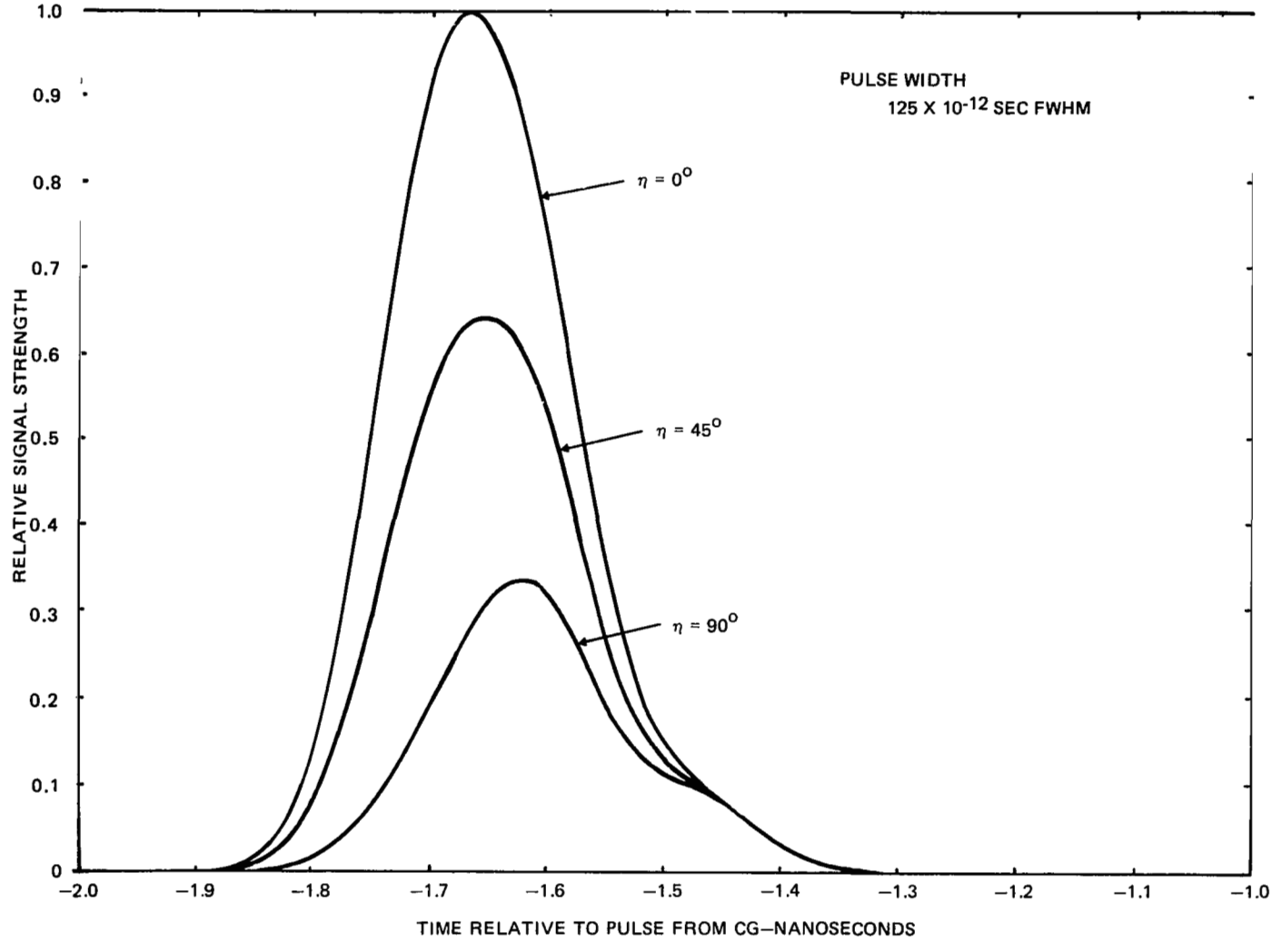

Figure B-7. Pulse return curves for 125 ps.

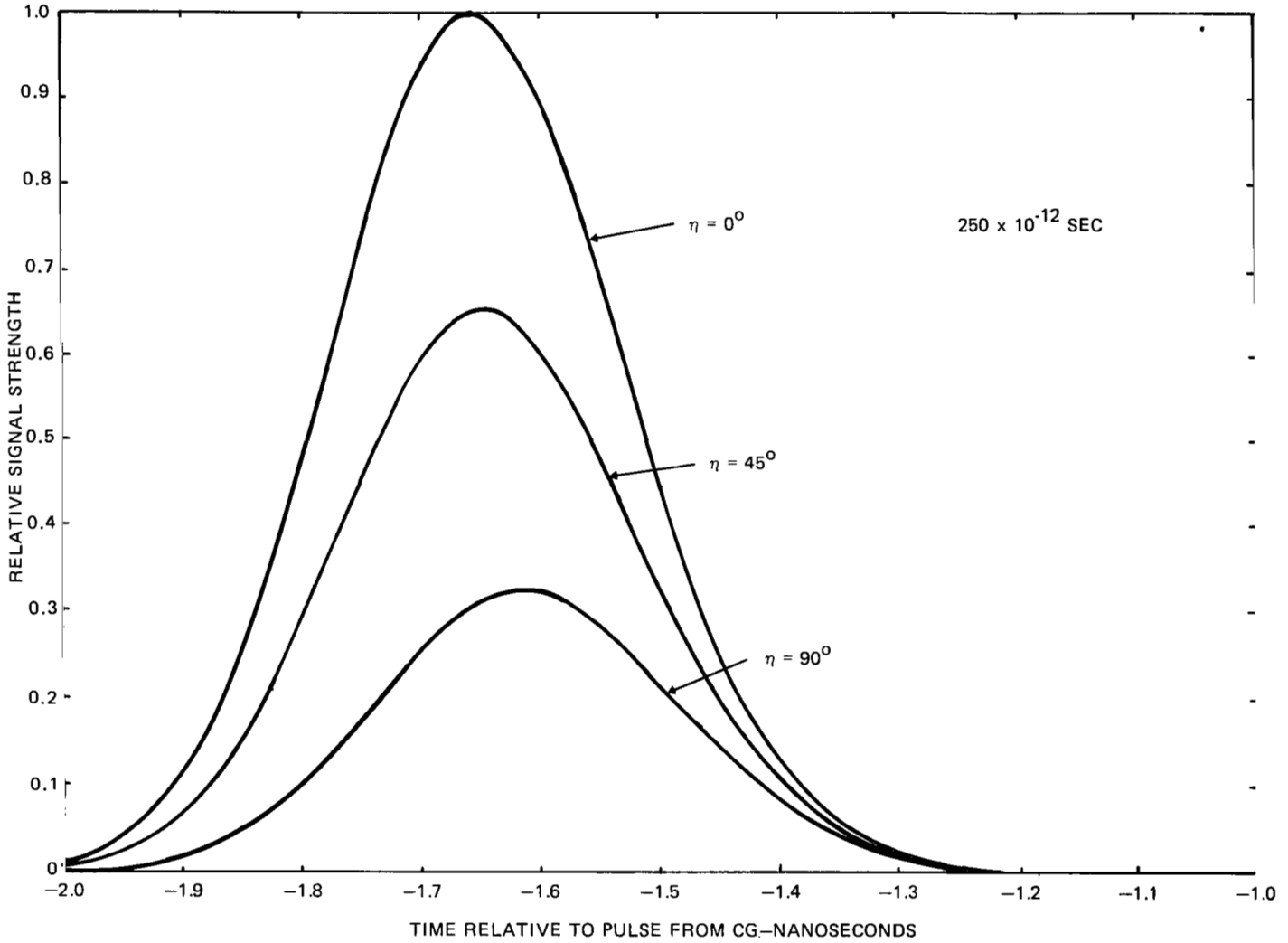

Figure B-8. Pulse return curves for 250 ps.

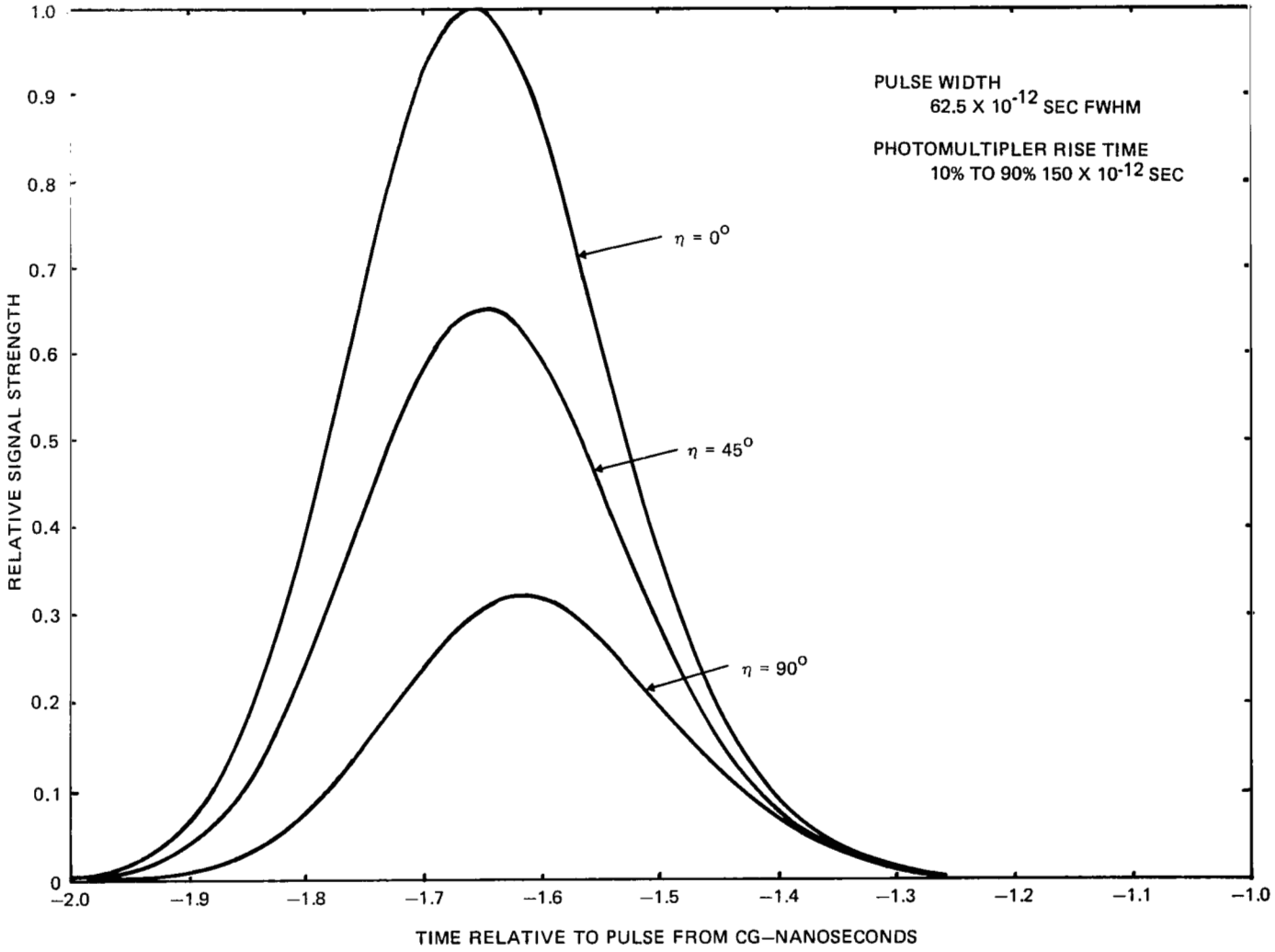

Figure B-9. Pulse return curve for 62.5 to 1000 ps with 0° polarization.

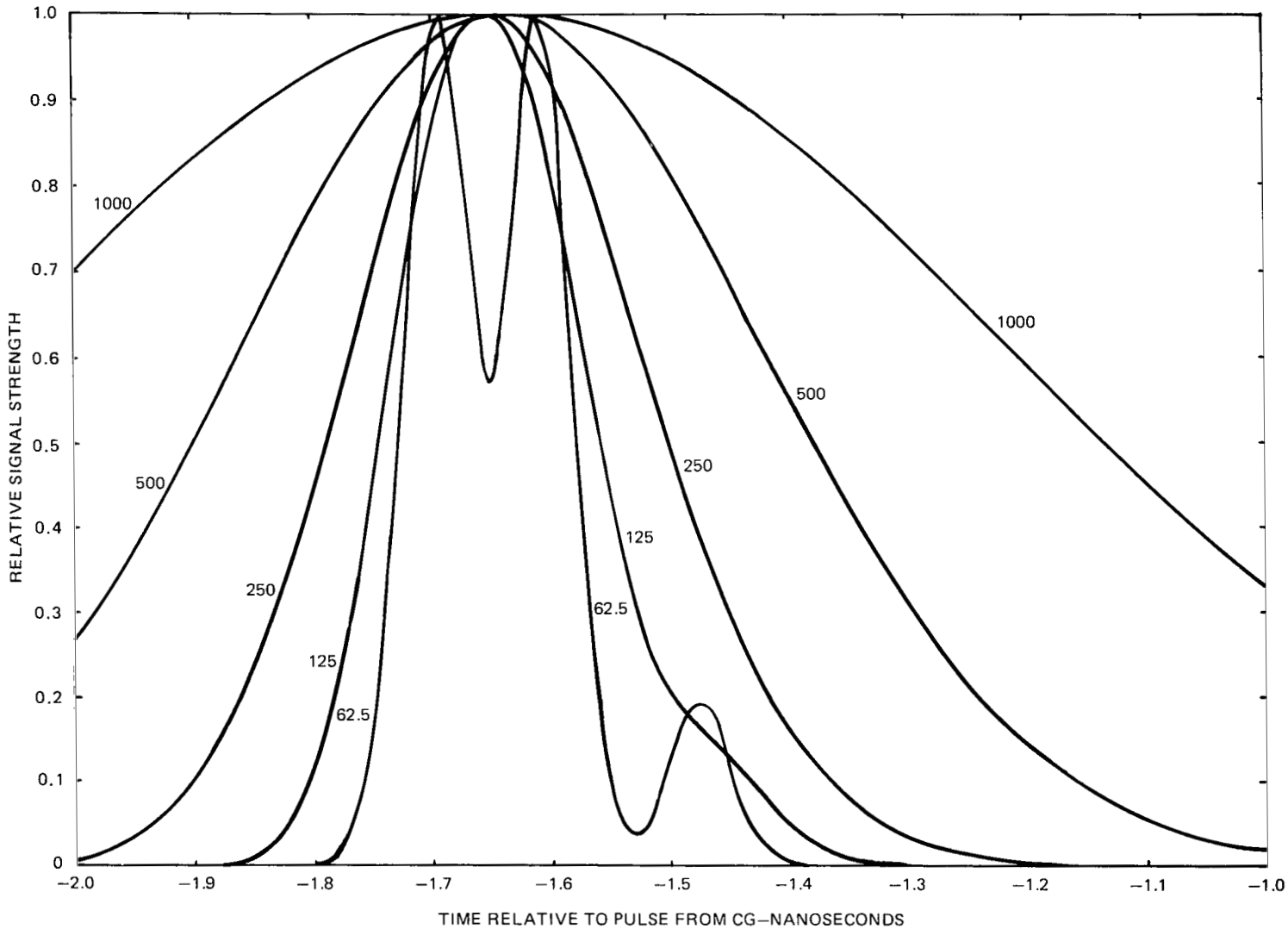

Figure B-10. Pulse return curve for 62.5 ps with photomultiplier tube response.

1. Report No.	2. Government Accession No.	3. Recipient's Catalog No.
TP-1062		

4. Title and Subtitle
Prelaunch Testing of the Laser Geodynamic Satellite (LAGEOS)

5. Report Date
October 1977

6. Performing Organization Code
723

7. Author(s)
M.W.Fitzmaurice, P.O.Minott, J.B.Abshire, H.E.Rowe

8. Performing Organization Report No.
G-7702 F-16

9. Performing Organization Name and Address
Goddard Space Flight Center
Greenbelt, Maryland 20771

10. Work Unit No.
506-20-33

11. Contract or Grant No.

12. Sponsoring Agency Name and Address
National Aeronautics and Space Administration
Washington, D.C. 20546

13. Type of Report and Period Covered
Technical Paper

14. Sponsoring Agency Code

15. Supplementary Notes

16. Abstract

The LAGEOS was extensively tested optically at GSFC during January 1976 prior to launch in May 1976. This document describes the measurement techniques used and presents the resulting data.

Principal emphasis was placed on pulse spreading characteristics, range correction for center of mass tracking, and pulse distortion due to coherent effects. A mode-locked frequency doubled Nd:YAG laser with a pulse width of about 60 ps [full width at half-maximum (FWHM)] was used as the ranging transmitter and a crossfield photomultiplier was used in the receiver. High-speed sampling electronics were employed to increase receiver bandwidth. LAGEOS-reflected pulses typically had a width of 250 ps (FWHM) with a variability in the range correction of less than 2 mm rms. Pulse distortion due to coherent effects was inferred from average waveforms and appears to introduce less than ± 50 ps jitter in the location of the pulse peak. Analytic results on this effect based on computer simulations are also presented. Theoretical and experimental data on the lidar cross section were developed in order to predict the strength of lidar echoes from the satellite. Cross section was measured using a large-aperture laser collimating system to illuminate the LAGEOS. Reflected radiation far-field patterns were measured using the collimator in an autocollimating mode. Data were collected with an optical data digitzer and displayed as a three-dimensional plot of intensity versus the two far-field coordinates. Measurements were made at several wavelengths, for several types of polarizations, and as a function of satellite orientation. Theoretical predictions of the corresponding far-field patterns were computed and are shown to be in close agreement with experimental results. Several unusual polarization effects caused by the use of total internal reflection cube corners were noted and confirmed by computer analysis. Velocity aberration compensation methods used for LAGEOS are discussed. The array was found to have slightly lower cross section than expected, and possible causes for this difference are suggested.

17. Key Words (Selected by Author(s))	18. Distribution Statement
Laser ranging, Satellites, Optical retroreflectors, Crustal motions	Unclassifed–Unlimited

19. Security Classif. (of this report)	20. Security Classif. (of this page)	21. No. of Pages	22. Price*
Unclassified	Unclassified	96	$5.00

*For sale by the National Technical Information Service, Springfield, Virginia 22161.

NASA-Langley, 1977

National Aeronautics and
Space Administration

Washington, D.C.
20546

Official Business
Penalty for Private Use, $300

THIRD-CLASS BULK RATE

Postage and Fees Paid
National Aeronautics and
Space Administration
NASA-451

12 1 1U,D, 091977 S00903DS
DEPT OF THE AIR FORCE
AF WEAPONS LABORATORY
ATTN: TECHNICAL LIBRARY (SUL)
KIRTLAND AFB NM 87117

NASA

Undeliverable (Section 158
Postal Manual) Do Not Return

S